universität wien

DIPLOMARBEIT/DIPLOMA THESIS

Titel der Diplomarbeit / Title of the Diploma Thesis

„In vivo optical imaging based characterization of siRNA/SSO therapeutics and transgenic mice“

verfasst von / submitted by

Karla-Nikita Singeorzan

angestrebter akademischer Grad / in partial fulfilment of the requirements for the degree of

Magistra der Pharmazie (Mag.pharm.)

Wien, 2020 / Vienna, 2020

Studienkennzahl lt. Studienblatt / degree programme code as it appears on the student record sheet:	A 449
Studienrichtung lt. Studienblatt / degree programme as it appears on the student record sheet:	Diplomstudium Pharmazie
Betreut von / Supervisor:	Univ.-Prof. Dipl.-Ing. Dr. Manfred Ogris
Mitbetreut von / Co-Supervisor:	Dr. Haider Sami

ACKNOWELDGEMENT

Vorerst möchte ich mich herzlichst bei Herrn Univ.-Prof. Dipl.-Ing. Dr. Manfred Ogris bedanken, der die Durchführung meiner Diplomarbeit am ‚Laboratory of Macromolecular Cancer Therapeutics' (MMCT) ermöglicht hat.

Ein großer Dank gebührt meinem Betreuer Dr. Haider Sami, der mir kontinuierlich mit Rat und Tat, Geduld und Positivität während meiner Arbeit zur Seite stand.

Meinen Diplomarbeitskollegen am MMCT möchte ich auch einen Dank aussprechen, diese haben die Zeit während der Arbeit unvergesslich gemacht und sind mittlerweile lieb gewonnene Freunde.

Zu guter Letzt möchte ich mich an meine Mutter, Oma und Wahloma Margarete wenden. Ihr habt mir alles ermöglicht und wart immer eine riesen Stütze in meinem Leben, dafür bin ich euch auf ewig dankbar.

TABLE OF CONTENT:

1 ABSTRACT

Nucleic acids and their synthetic oligonucleotide analogs, such as small interfering RNA (siRNA) and splice switching oligonucleotides (SSO), are highly attractive and promising constituents for developing therapeutics for a vast range of treatments. This thesis focuses on nucleic acid-based therapeutics and their in vivo studies in transgenic and non-transgenic mice by fluorescence-based imaging (FLI) and bioluminescence imaging (BLI).

The first part of this thesis examines the biodistribution behavior of intravenously applied siRNA labeled with the near infrared emitting dye AF750 (AF750- siRNA) by FLI. Renal excretion of AF750- siRNA was observed within the investigated time frame. The AF750-siRNA treated group revealed FLI signals in bladder and kidney area and also shows reproducibility among the group. These findings were validated by ex vivo organ imaging, as the same organs showed signals in the treated group.

Splice switching oligonucleotides can correct aberrant splicing and redirect the splicing machinery resulting in transcription of the functional protein. The second project investigated systemically administered splice switching oligonucleotides (SSO) based polyplexes within transgenic reporter mice (Luc 705 Split-Luc mice), which carry an interrupted firefly luciferase reporter gene. The interruption is achieved via a mutated human beta-globin intron 2 which includes an aberrant splice site at nucleotide 705. The applied SSO should restore an aberrant splicing outcome resulting in luciferase expression trackable by BLI. Moreover, localizing successful SSO induced splice correction was aimed at. The Luc-SSO polyplex treated group did not demonstrate any clear results within in vivo whole-body imaging experiments. However, the findings obtained in ex vivo organ imaging revealed reproducible luciferase detection in lung and bladder area of animals treated with Luc-SSO based polyplexes in comparison to Non-coding-SSO based polyplexes.

Third, reporter gene activity was measured by BLI in a lung-specific mouse model, which had the luciferase reporter gene coupled to the SpC-promoter, which is exclusively localized in alveolar type II cells of lungs.

Lastly, another side project studied growth of implanted B16F10 melanoma cells in Tg Thy 1.2-Luc mice. Melanoma cell adhesion to activated human endothelial cells leading to migration and invasion into peripheral tissue is linked to Thy-1, a cell surface protein. Monitoring the role and interplay of Thy-1 in implanted B16F10 melanoma cells was part of this project. The investigation process was monitored by BLI, as the luciferase reporter gene was coupled to the Thy-1 promoter. Therefore, localization of growth and metastatic potential could be visualized, and the concerning organs linked to a signal movement were from lungs to liver.

2 ZUSAMMENFASSUNG

Nukleinsäuren und ihre dazugehörig synthetischen Oligonukleotid-Analoga, wie small interfering RNA (siRNA) und splice switching Oligonukleotide (SSO), drängen immer mehr in die Rolle der Hauptakteure der Forschung. Sie bilden eine Klasse von Kandidaten, welche das Potenzial besitzt eine Vielfalt von unterschiedlichen genetischen Erkrankungen zu therapieren. Deren große Bedeutung kommt zu tragen, da die am Markt zugelassenen „small molecule“ Substanzen nur eine limitierte Anzahl von zellulären Proteinen spezifisch beeinflussen können. Der Hauptteil dieser Diplomarbeit befasst sich mit Nukleinsäure-basierten Therapeutika, welche zur Entwicklung von personalisierter Gentherapeutika herangezogen werden können. Die Untersuchungen wurden mit Hilfe von Fluoreszenz-basiertem Imaging (FLI) und Biolumineszenz-basiertem Imaging (BLI) in vivo und ex vivo durchgeführt.

Die siRNA ermöglicht die Suppression eines beliebigen Onkogens auf Basis ihrer Fähigkeit des „Gene-Silencings“. Dies erfolgt durch das komplementäre Paaren der siRNA an die gewünschte mRNA Abfolge der Target-Sequenz. Dennoch sind Modifikationen der synthetisch hergestellten siRNA limitiert, da sie in weiterer Folge noch kompatibel für die nachgeschalteten Enzyme bleiben muss, um einen Erfolg zu erzielen. Es ist jedoch bekannt, dass die Nieren und die Leber primäre Zielorgane der Biodistributionskette sind. Ein Teil der vorliegenden Diplomarbeit untersucht das Biodistributionsverhalten von systemisch applizierter siRNA, welche an ein Fluorophor, AF750, gekoppelt worden ist. Dies ermöglicht das „live“ Tracking des Moleküls mittels FLI in vivo. Die Ergebnisse der behandelten Gruppe zeigen Reproduzierbarkeit untereinander, da wiederholt klare Signale in Nieren und Blase beobachten wurden. Somit konnte die renale Exkretion der AF750 gekoppelten siRNA Moleküle gezeigt werden.

Splice Switching Oligonukleotide (SSO), besitzen die Fähigkeit, abweichende Splicing-Seiten zu korrigieren und somit die Splicing-Maschinerie auf den richtigen Weg zu leiten um ein funktionales Protein aus der erhaltenen mRNA zu translatieren. Ein weiteres Projekt befasst sich in dieser Diplomarbeit mit der Lokalisation und

Funktionalität von systemisch injizierten SSO. Die Ergebnisse einer erfolgreichen Splicing Korrektur und der damit gekoppelte Erhalt eines funktionalen Reportergenes, der Luciferase, wurde mittels BLI untersucht. Die erfolgreiche Splicing Korrektur resultiert in einer Erhöhung der Signalintensität im BLI. Obwohl mittels in vivo BLI keine ersichtliche Signalintensitäts-Zunahme und somit erfolgreiche Splice-Korrektur beobachten werden konnte, waren die Ergebnisse im ex vivo BLI erfolgreich. Letzteres konnte Signale in der Lunge und Blase der behandelten Gruppe nachweisen. Daraus lässt sich auf eine erfolgreiche Splice-Korrektur und somit die SSO Lokalisation in der Lunge und Blase schlussfolgern.

Mit Hilfe der BLI Methode wurde in einem weiteren Project die Luciferase Reportergen-Aktivität in einem transgenen Maus-Model untersucht. Der verwendete transgene Stamm trägt das Reportergen Luciferase,welches unter Kontrolle des in Typ II Pneumocyten der Lunge aktivierten SpC-Promotor exprimiert wird. Die vorliegenden Ergebnisse wiesen eine Aktivität des Promoters sowohl in der Lunge als auch im Hautgewebe nach.

Das letzte Projekt dieser Diplomarbeit befasst sich mit dem metastatischen Potenzial von B16F10 Melanom Zellen, einem Modell für aggressiven Melanom Zellen, welche in der Entwicklung von Chemotherapeutika gegen Hautkrebs verwendet werden. Darüber hinaus wurde die Rolle von Thy-1.2 in der Extravasation und folgendlich Metastase der systemisch applizierten B16F10 Zellen näher untersucht. Thy-1.2. ist ein Zelloberflächen-Protein, welches mit der Adhäsion der Melanom Zellen an aktivierte humane Endothelzellen assoziiert wird. In diesem Experiment wurden Transgene Thy-1.2 Mäuse verwendet, die das Luciferase-Reportergen an den Thy-1.2 Promotor gekoppelt hatten. Somit konnte nach Injektion der Melanom Zellen mittels BLI die Thy-1.2 Aktivität untersucht werden und so auf ein mögliches metastatisches Potenzial rückgeschlossen werden. Jedoch war das Ergebnis nicht eindeutig, da es unklar war ob die in vivo BLI Signale in Lunge zur Leber durch Metastasierung oder nur durch den Blutfluss beeinflusst wurde.

3 INTRODUCTION

3.1 In vivo imaging of biological processes in vivo

Molecular imaging enables a wide range of characterization, quantification and visualization of several events at cellular and subcellular stages in living subjects [1] by providing a non-invasive way of gene and protein function evaluation. Therefore, studying the interplay of proteins and signal transmission of human diseases in animal models can be understood more clearly. Moreover, pathogenesis can be investigated at a molecular level. [2] Beside single photon emission computed tomography, positron emission tomography, magnetic resonance imaging, computed tomography (CT), and ultrasound, which are already clinically applied on humans, fluorescence imaging (FLI) and bioluminescence imaging (BLI) are two supplemental preclinical methods for imaging small living animals. [3]

Compared to the other modalities, which are mentioned above, these two methods are highly attractive due to their low-costs, ease of use and rapidity and result in a suitable way of usage for preclinical in vivo investigations. [4]

Both imaging techniques, BLI and FLI detect the emission of light signals from small living animals with the help of a sensitive charge coupled device (CCD) camera including a range from visible to near infrared (NIR) light spectrum. [2] [5]

The biological use of BLI and FLI have different purpose as their usage of energy source in order to obtain the production of a light signal differs. Following table shows a general comparison of both imaging methods BLI and FLI. [5]

	Bioluminiscence	Fluorescence
Imaging mechanism and energy source	Firefly luciferase enzyme metabolizing D-luciferin substrate in presence of ATP and oxygen	Excitation of fluorophores by energy of an external light source
Interpretation	High sensitivity and specificity	High versatile and flexible
Biological readouts and applications	Measurement of cell location, viability and growth	1. Vascular agents for imaging of vascularity 2. Targeted agents for binding to specific biomarkers 3. Activatable fluorescent agents which change enzyme-mediated from non-fluorescent to fluorescent
Experimental considerations	Requires genetic modification to obtain luciferase expression	Requires FLI of control animals, which receive same fluorophore to detect background fluorescence of the agent

Table 1 Comparison of bioluminescence and fluorescence imaging. Source modified from Tseng et al, 2015 [5]

3.1.1 Fluorescence imaging for real-time tracking of biological processes

FLI is an imaging method based on using molecules, called fluorophores. An external light source excites the fluorophores, these absorb the energy and subsequently emit photons on another wavelength. [6], [7] Fluorescence happens when electrons are elevated to a higher based excitation state by an external radiant source. Afterwards there is an energy collapse, the process of relapse of the electron into its ground state. When falling back into their ground state, a measurable emission of photons, which correlates with the absorbed energy, in another wavelength occurs. Thus, it incorporates the fact, that emitted light has a longer wavelength than the absorbed one. [8] A wide range of various fluorophores which have specific excitation and

emission profiles [5] are available for in vivo fluorescence based imaging which enables tracking of the conjugated substance of interest. [9] There are already a broad range of emission and excitation filters which can be adapted to the above-mentioned fluorophores disposing individual optical properties. These filters are required to capture the light including the range of visible spectrum to the near infrared spectrum. [5]

Another method of using FLI is the possibility of using the fluorescent agents as specific reporter genes, such as green fluorescent protein (GFP) in order to investigate a molecular event. [9] There has already been an extensive usage of GFP as a reporter gene, with the aim of studying protein localization and subcellular processes as gene expression. [4] Further, it has been playing an important role in investigating various processes of infections and tumor growth, its metastasis and treatment. [4] But not only deployment of GFP as a reporter gene was in past commonly used, also usage as a fluorophore itself played a crucial role. [4] The GFP gene origins from a jellyfish species, called *Aequorea victoria* living in the Pacific Ocean. The excitation wavelength of GFP is approximately 470 nm and it emits light in a wavelength of 510 nm. [4]

In contrast to GFP, fluorophores which are based on near infrared dyes have an emission spectrum of 650-900 nm. They endure a higher penetration of photons as well into, as out of the tissue. Therefore, they lead to an ameliorated visualization of signals that are deeper within the tissue. [4]

Fluorophores which emit light in the near infrared spectrum (NIR) are convenient molecules for fluorescence-based in vivo imaging due to their low scattering effects and a high tissue penetration. [6]

One of the projects which will be introduced in this thesis uses Alexa Fluor 750 as a fluorophore. This is a NIR dye which can be excited at 633 nm till a maximum of 749 nm and emits light in a longer wavelength, emission maximum 775 nm. This is well suited for imaging in tissues with background autofluorescence. [10]

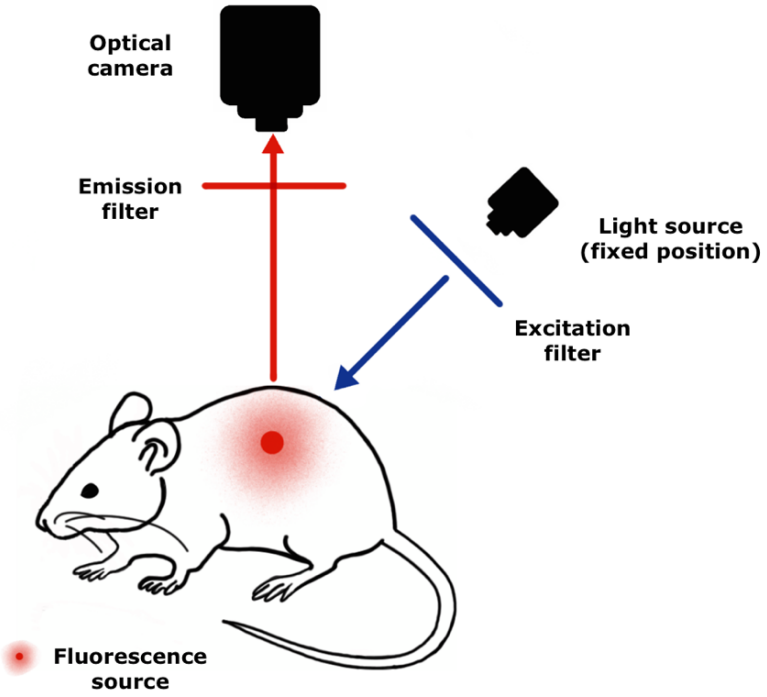

Figure 1 Scheme of 2D FLI Illustration of essential components required for FLI. Excitation light source is placed above the animal including appropriate filters. Additionally, located also above the animal the optical camera with the corresponding filters set before the lens to capture emitted light signals deriving from the fluorophore.

The figure above is an illustration of the main principle of 2D epifluorescence imaging where the placement for both, camera and light source is located above the animal. In order to prohibit background noise [9] and obtain an ideal fluorescence signal [5] a specific excitation and emission filter [5] [9] is needed. The selection of the filters, excitation and emission, is chosen in dependence of the spectral properties of the used fluorophore/imaging agent. For receiving a 2D image the excitation light irradiates the whole surface of the animal whilst the CCD camera collects the emitted signal and directly detects them. [5]

3.1.2 Benefits and limitations of FLI

FLI includes various benefits whilst using it for investigations: Utilizing fluorophores based on their main function of emitting light at a longer wavelength after excitation enables no additional need of substrates. This facilitates the working flow and prevents potential unwanted reactions which may disturb and distract from observing the main molecular pathway. Further, due to specific adaption of excitation and emission ranges

a big platform of various reagents with different spectral properties is available. Therefore, using more than one fluorophore with different spectral properties, enables tracking and detection of more than one process at the same time and in the same experimental animal. In addition, the equal emission signal from the fluorophore, used to monitor a molecular event can be subsequently used for ex vivo validation. Furthermore, fluorescent agents which do not require generating experimental models which express specific reporter genes in order to obtain the wanted signals for tracking, are a huge advantage because faster evaluation and preclinical research is possible. [9]

Nevertheless, all those advantages are accompanied by disadvantages, which have to be kept in mind: there is a need for an external light source to excite the imaging agent, this can be attenuated by image depth. [9] All cells dispose endogenous molecules which may lead to an increased or reduced imaging contrast caused by autofluorescence. This has to be taken in consideration when performing in vivo FLI. Autofluorescence contributes background fluorescence in the image and is caused by light absorption of tissue due to some parts of the body like blood or hair which possess the same excitation and emission properties as the used fluorophore.[8]

3.1.3 Bioluminescence imaging for tracking biological processes

Bioluminescence imaging (BLI) permits studying different biological processes at a molecular dimension by using mice or pathogens which have been previously generated and modified with the aim of expressing the enzyme luciferase. Especially in transgenic mice, this non-invasive optical imaging method has been used for expression studies and in vivo gene transfer. It is remarkable that in the previous years the number of BLI studies has exponentially increased and has become more crucial in preclinical investigations. [11]

The principle of BLI is based on visualizing light which is generated by the enzyme luciferase in a living organism. [5] The light production is referred to the luciferase due to metabolization of its substrate luciferin. [9] Luciferase enzymes have been

discovered in marine species and insects for example; *Gaussia princeps* (Gluc; Gaussia luciferase), *Renilla Reniformis* (Rluc; Renila luciferase), *Photinus pyralis* (Fluc; Firefly luciferase) and *Pyrophorus plagiophtalamus* (CBR; Click beetle luciferase). [1] As shown in figure 2, CBR and the most commonly used luciferase Fluc emit light by catalyzing oxidation of their substrate D-luciferin to oxyluciferin [1] in the presence of ATP and oxygen. This reaction is chemical highly efficient, because nearly all the energy put into the reaction can be subsequently converted to light which can be then measured. Thus, it is an extremely sensitive method which is very suitable for a reporter assay/ in general preclinical investigations observing several biochemical events even on nuclear levels. [12] Gluc and Rluc do not require ATP as a co-substrate, they use coelenterazine and oxygen as a substrate. [1] Another group of luciferases, called lux, is also available but not suitable for BLI imaging experiments due to low signal intensity and toxicity of its needed substrates. [1]

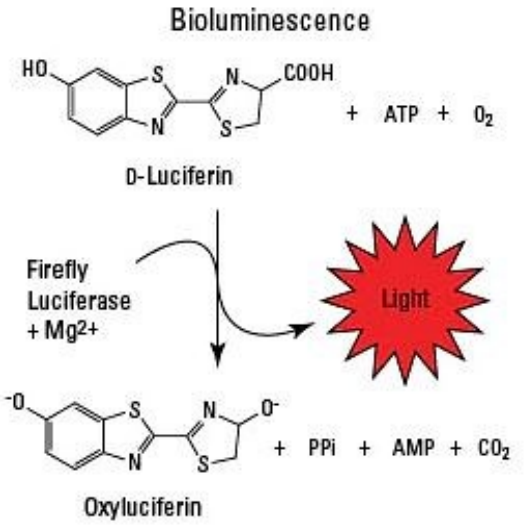

Figure 2 Chemical reaction of D-lucifern to oxyluciferin, Source: Luciferase Reporters https://www.thermofisher.com/at/en/home/life-science/protein-biology/protein-biology-learning-center/protein-biology-resource-library/pierce-protein-methods/luciferase-reporters.html

Investigating BLI imaging events require a luciferase expressing gene, which can either be integrated into cells, viruses or into the whole animal. This is done by using molecular biology techniques. [5] Constitutively active promoters are used to express luciferases which allow an in vivo monitoring of survival and growth of the transplanted cells, like stem cells or cancer cells. Therefore, the DNA coding sequence

for luciferase has been identified more precisely and its expression sequence in mammalian cell has been optimized and ameliorated.
Investigating luciferase signals in animals are not only offering a signal intensity and spatial distribution measurement, but also monitoring migration of several cells for e.g. neuronal stem-cells or T-cell trafficking. Additionally, introducing luciferase genes into pathogens allow evaluation of pathologic pathways or its respond to a treatment. [1]

Furthermore, monitoring the activity of gene expression is also possible by using the reporter gene. Therefore, the luciferase gene is directly positioned by the promoter element from the gene of interest or placed downstream of a coding sequence which corresponds to a selected transcription factor. As soon as the wanted relevant genes are transcribed, similarly the reporter is transcribed considering duration and relative amount of luciferase expression should correlate with the gene of interest. [1] Depending on the aims of the investigations, various models of transgenic animals are available. These differ in their transgenic expression properties, provided by the reporter gene which is bound to the promoter of the gene of interest. In chapter “3.5.- Transgenic mice models as a versatile tool in research for human diseases” examples for thesis relevant transgenic mouse models will be explained more clearly.

In figure 3, 2D BLI imaging is illustrated. This mode has the CCD camera placement above the mouse, which detects emitted light from the animal surface. A very low background signal offers the possibility of imaging in 2D BLI mode without any emission filter which maximizes the imaging sensitivity. This refers to the fact, that mammalian tissue does not emit photons, that would lead to a background noise signal. [5]

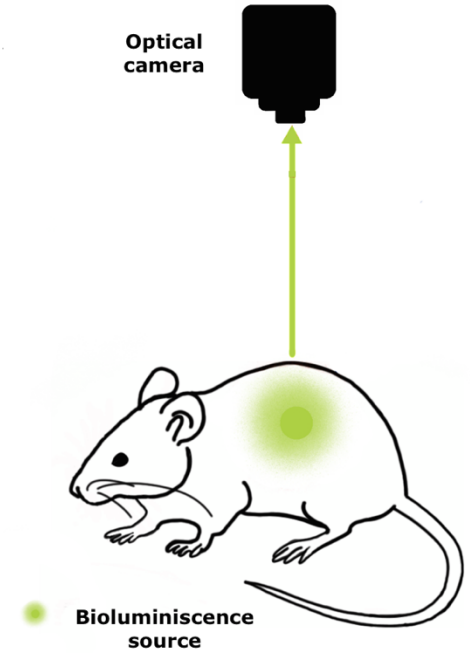

Figure 3 Scheme of 2D BLI. Placement of the optical camera above the mouse. No additional optical devices are required as the light source is provoked by the chemical reaction and occurs after application of the corresponding substrate of the reporter gene.

3.1.4 Features and limitations of BLI

In comparison to other imaging methods BLI allows detection of signals, which are emitted from tissue in a depth within a few centimeters and enable a resolution at organ- level. As a contrast microscopy of GFP has a decreased potential of detecting deep localized signals. [11] Taken in consideration BLI does not depend on external light excitation, such as FLI, and this is also a huge advantage. [6] [9] Furthermore, a high signal-to-noise ratio is given, due to extremely low background signal. Sensitivity and specify is also provided, since non modified tissue without luciferase expression does not undergo light emission when presenting luciferin as a substrate. [5] One of the most important facts is that 2D BLI is a non-invasive method which enables a consistent repetitive preclinical investigation on the same animal at different time points. [13] Performing longitudinal studies using this imaging technique reduce the number of needed animals and is in terms of experimental rights. [13] [14]

Comparing disadvantages of BLI with those of FLI can be a longer acquisition time and the necessity of administration the substrate. [9] This has to be done ten till fifteen minutes before each imaging session and requires also training from the executing investigator. Another point is the lack of tissue penetration of photons which emit light in the visible range [6] [9], therefore the performance of 2D BLI is only suitable with small animals, like rodents. [6] Nevertheless, as a requirement cell engineering has to be done in order to gain a luciferase expression. [9] Thus, there is a difficulty in achieving a standardization of the experiments, due to the fact that BLI is a semiquantitative technique which leads only to relative outcomes. The impact of exogenous and endogenous factors is possible to alter the luciferase-substrate reaction and therefore lead to bias resulting in wrong interpretations. This can be attributed to luciferases, luciferin and cofactors, such as ATP and oxygen, which are very likely to appear in different amounts depending on their localization of different body regions and cells. [14] When using for e.g. firefly luciferase, especially cofactors as ATP and oxygen are a main factor for result disruption. For instance, this might happen when expression of luciferase occurs in diseased tissues, such as tumors, where a higher utilization of the cofactors is needed and ends up with a less supply of oxygen. As a result, the luciferase would have less cofactors to metabolize its substrate which leads to a lower emission of light and would therefore confirm a low-rise signal. [1]

The intensity of the light signal produced by luciferase expressing cells can be affected depending on their location and depth of the cells. [14] Another impact concerning intensity of the light signal is pigmentation of skin and hair since they can extenuate and scatter BLI signal. [14] Signal in albino mice, with less pigmentation is higher than in mice with black fur. [14]

3.2 The IVIS ® SpectrumCT

The IVIS SpectrumCT (Perkin Elmer) imaging platform enables imaging of small animals in preclinical research by using X-ray computed tomography, BLI and FLI. [14]

A light-tight chamber enables the placement of the animals or cells. The platform of the chamber is a moveable and heatable constituent which keeps the animals not only warm but also allows modulation and movement of the platform whilst imaging sessions. According to the movement the distance between the platform and the optical device can be changed which provides an achievement of different field of views. Additionally, a rig with nose cones is as well installed on the platform and allows anesthetic gas delivery, like Isoflurane. The animals are supposed to be placed with their snout into the cones of the rig and therefore get sedated. [11]

Optical devices, such as an ultrasensitive CCD camera implements detecting emitted light, a light source including a wide excitation range allows for FLI two modalities: first surface epi-illumination and secondly transillumination. [5]

Altogether, the system converts 2D optical photography, including FLI and BLI into 3D tomography, such as fluorescence imaging tomography (FLIT) and diffuse luminescence imaging tomography (DLIT). This is done by combination of optical imaging modes with CT imaging. PerkinElmers‘ IVIS SpectrumCT is usually combined with Living Image ® software for image analysis and signal quantification in order to receive an extensive optimal imaging resolution. Investigating a wide range of biological processes is accessed by using IVIS ®SpectrumCT and several imaging agents gaining more importance in preclinical investigations. [5]

3.3 Nucleic acid-based therapeutics in human gene therapy

Nucleic acids and their synthetic oligonucleotide analogs form a big class of promising candidates for therapy a broad range of human diseases. [15]

Lots of marketed drugs belong to small molecules that target proteins such as enzymes and receptors, which represent a considerable poor subset of total cellular proteins. In contrast to them, oligonucleotides are macromolecules targeting pre-mRNA and mRNA. These are the transcribed carriers of genetic information before being translated into proteins. Further, mRNA possess the power to encode all cellular proteins and oligonucleotides. Targeting mRNA could prove to be effective for targets and diseases that are not treatable by current drugs. [16]

Due to our expanding knowledge in genetics, gene expression, regulation and availability of many tools has provided the whole genome and its products recipient for therapeutic intervention with nucleic-acid-based molecules.[17]

3.3.1 Use and interplay of siRNA as an approach for gene silencing therapeutics

Cancer forms a group of diseases that sequences from more than one genetic change and involves abnormal cell division with the capability of invading and spreading to other parts of the body. [18] RNA interference (RNAi)-based therapeutic approaches holding hope in curing cancer, as small interfering-RNA (siRNA) suppresses expression of carcinogenic genes by targeting the mRNA expression at a posttranscriptional level. Therefore, cancer is one of the major targets of RNAi-primarily based therapy. Desired target genes for this kind of therapeutics are oncogenes, mutated tumor suppressor genes and various genes contributing to tumor development. [19]

Aiming any cancer related gene and provoking posttranscriptional gene knock down and gene silencing is achieved by use of siRNA. [19]

3.3.2 Mechanism of RNAi on a molecular level

Early steps in RNAi is processing and cleavage of a longer double stranded RNA (dsRNA) into siRNAs. This is done by an enzyme called DICER and is a RNase like enzyme. siRNA binds to a multiprotein component complex called RNA induced silencing complex

(RISC). Within the RISC complex the siRNA strands are teared apart and the strand with the more stable 5'-end is incorporated to the active RISC complex. Then the antisense siRNA component guides and aligns the RISC complex on the target mRNA. [20] As soon as the siRNA is complementary to its target, the endonuclease argonaute 2 (AGO2), a catalytic constituent of the RISC system, cleaves the mRNA. [16]

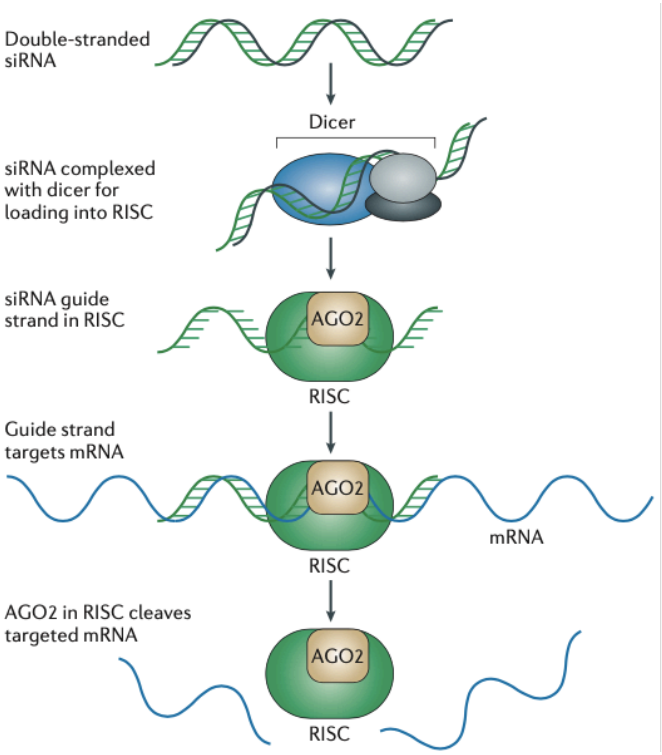

Figure 4 Mechanism of gene silencing by siRNA- Description of RNAi by siRNA in theory. Double stranded RNA (dsRNA) is introduced to the cell and forms a complex with the RNA induced silencing complex (RISC) within there the dsRNA is separated into single stranded siRNA. This guides the strand into the RISC and cleaves the target as soon as it is complementary bound to the target mRNA. Cleavage of this part is provided by Argonaute 2 (AGO2), the catalytic constituent in the RISC. [16]

3.3.3 Chemical features and biodistribution characteristics

In general oligonucleotides direct their biodistribution pattern based on their chemical characteristics such as high molecular weight, hydrophilicity [21] and negative charge. [22]

Excretion via the kidney or distribution to systemic organs can be associated with the clearance, which systemically applied unmodified siRNA undergoes. [23]

Nevertheless, in vivo factors as interaction with plasma proteins and degradation by serum ribonucleases are major barriers to systemic stability. [24] Further, technological approaches are required to obtain efficient delivery to target organs or disease sites. A chemical modification of the molecule itself would prevent degradation by nucleases and/ or formulation into nanoparticulated carriers would promote targeting and cellular uptake. [23] siRNA permits a limited modification as it has to remain RISC-compatible. [16] Therefore, determining aspects of pharmacokinetic profiles of in vivo administered siRNA is a crucial issue for the clinical development of siRNA based medicine. [22] The kidney is an important constituent when talking about pharmacokinetics and biodistribution of oligonucleotides. Molecules with a size of 3-6 nm or less can be ultrafiltrated by the kidney [25] many oligonucleotides are dedicated to this size range and can be rapidly excreted by the renal route. [26] Thus, liver and kidney form the major sites of accumulation for siRNA-based therapeutics. [26]

3.4 Pre-mRNA splicing as a therapeutic target by usage of splice switching oligonucleotides

The process of alternative pre-mRNA splicing is a common method of genetic regulation in higher eukaryotes. [27]. During the expression process of protein-coding genes, pre-mRNA needs splicing, further excision of introns and ligation of the exons [28] Expression of alternatively spliced mRNA variants enables functional diversity of the human genome, especially at specific developmental phases in particular cells and tissues. [29]

Nevertheless, variation in splice site choice can have a broad impact on the encoded protein. Little changes in peptide sequence can impede enzymatic activity, allosteric regulation or even alter ligand binding. [27] Over 90% of multiexon genes offer splicing variants [30] moreover, up to 50% of all genetic mutations affect the mRNA splicing. [31]

Duchenne muscular dystrophy (DMD) is a severe genetic disorder which affects the gene encoding dystrophin. This is a protein which connects intracellular actin filaments

with the aim of maintaining the integrity of the sarcolemma membrane. Patients with DMD translate the amino acid sequence for dystrophin without an internal portion due to deletions which disrupt the translational reading frame causing muscle wasting accompanied by loss of mobility with further outcomes like respiratory failure and cardiac dysfunction. A drug that is able to partially restore the initial function of dystrophin could be a potential treatment for DMD. [16]

Another example is beta-Thalassemia, one of the most common genetic disorders world-wide, affecting the gene encoding beta globin [32] As a result a decrease in beta-globin production is characteristic which leads to insufficient levels of the oxygen carrying hemoglobin. This reduction has also an impact on the alpha-globin subunit, which is in excess and therefore responsible for the red blood cell damage. The main form of treatment is blood transfusion but goes hand in hand with the risk for blood bone infections especially in developing countries as the prevalence there is high. A replacement with an oligonucleotide based therapeutic would ease the patient's life and minimize the risk of blood bone infections.

3.4.1 Mechanism of splice switching oligonucleotides

Splice switching oligonucleotides (SSOs) are antisense oligonucleotides (ASOs) with a length of about 15-30 nucleotides and bind complementary through Watson-Crick base pairing the target pre-mRNA sequence. Their outcome can differ depending on their chemistry and binding location. [28]

One possibility of the mechanism of action consists in blocking the access of splicing machinery to splicing elements with a high specify in the desired pre-mRNA area. [16] This can be achieved when SSO base-pair to the target pre-mRNA and change the recognition of splice sites by the spliceosome. [28] A redirection of the splicing is therefore aimed by avoiding the possibility of an undesired splice variant protein outcome. [16] The causa is an intron mutation, which may create and/or activate aberrant splice sites and therefore results in an inclusion of an unwanted intronic fragment in the spliced mRNA by forming a pseudo exon providing interference with the translational reading frame. [16]

In this thesis a model for in vivo restoration of correct splicing and pre-mRNA repair by SSO will be introduced which will be explained more detailed in the following.

SSO can repair defective RNA and restore the production of crucial proteins. Thus, they can provide novel proteins with desired properties and control the presence of disease-causing splice variant proteins. [16] Therefore, SSO possess the ability to rearrange gene expression through the splicing mechanism by correcting aberrant splicing patterns in genetic disorders. This forms a huge contrast to the lately mentioned siRNA therapeutics, which rely on the mechanism of a protein knockdown.

To achieve a shift in splicing pattern the SSOs must be stable in serum and form duplexes with the targeted RNA, avoiding being processed by RNase H and/ or nucleases. Modification of the sugar with O-methyl, O-methoxyethyl or O-aminopropyl groups or alter the backbone such as in N3`→ P5`phophoroamidate, peptide nucleic acids (PNAs), phosphorodiamidate morpholino (PMO) enable a positive outcome. [29] Additionally, those nucleotides are chemically modified in a way that the RNA-cleaving enzyme RNase H is not recruited to degrade the pre-mRNA-SSO complex. [33] [34]

3.4.2 SSO transfection into cells by polyplex formation

SSOs alone are not very efficient in penetrating through the cell membrane and pass through the nuclear envelope to achieve the target, pre-mRNA, which is localized in the nucleus. [35]
Poor delivery of SSO into cells and cell nuclei is based on their negative charged nature and has to be kept in mind when a successful SSO delivery wants to be obtained. Therefore, co-administration in complex with cationic compounds is a solution for this. [29] Spontaneous formation of such a complex is called polyplex and is contributed to the electrostatic interaction between negatively charged phosphate groups deriving from the nucleic acid and the positively charged polycations. The shaped polyplex is all positive charged and therefore binds to negative charged cell surfaces. Via endocytosis the particles are internalized into the cell and the nucleic acids released from the endosome. The described event is also known as the endosomal escape and occurs

based on the pH change in the endosome. Polycationic structures are able to shift the pH and therefore initiate the activation of endoosmolytic properties in the endosomes. [36]

3.5 Transgenic mice models as a versatile tool in research for human diseases

99% of the mouse genes have a homologue in the human genome. Hence, the mouse is a unique model system for mammalian biology and human disease research. [37]
In 1981, Gordon and Ruddle generated by pronuclear microinjection [38] the first transgenic animals. [39] By then the determination "transgenics" was referring to animals which had exogenous DNA sequence in their genome. [38] [39] Over the years this definition of "transgenics" has evolved as it can be understood as animals with specific genetic modifications. [38] Generating animals with genetic modifications, who are disposed to express a broad range of proteins [38], enable analysis of gene function and therefore investigation on human diseases. [40]

3.5.1 Split transgene based transgenic mouse model

The Split-Luc mouse strain can be utilized for investigation on splice correction after SSO disposition. More precise, the Tg (Luc 705) Split-Luc mouse strain was generated by pronuclear injection of an expression cassette deriving from the plasmid pLuc/705 into a fertilized zygote. [41] Here, the luciferase reporter gene is interrupted by a mutated human beta-globin intron 2 carrying an aberrant splice site located at nucleotide 705. [42] Integration of the gene occurred into the plasmid in combination with a ubiquitous and constitutive gene expression promoter called Rosa26. [41]
The mechanism without correcting the aberrant splice site results in a missing luciferase reporter gene activity. This lack of signal is contributed to the fact that the mutation at nucleotide 705 leads to an activation of the aberrant splice site as the intron is retained in the mRNA. Therefore, the translation of a functional luciferase protein is impeded. [41] As mentioned, SSO possess the power of blocking the aberrant splice side, by base pairing the target sequence, and therefore restore a correct splicing

with the aim of obtaining a functional luciferase protein. Evaluation of splice correction can be performed by in vivo BLI and the achievement of splice correction goes hand in hand with an expected elevation of luciferase gene expression.

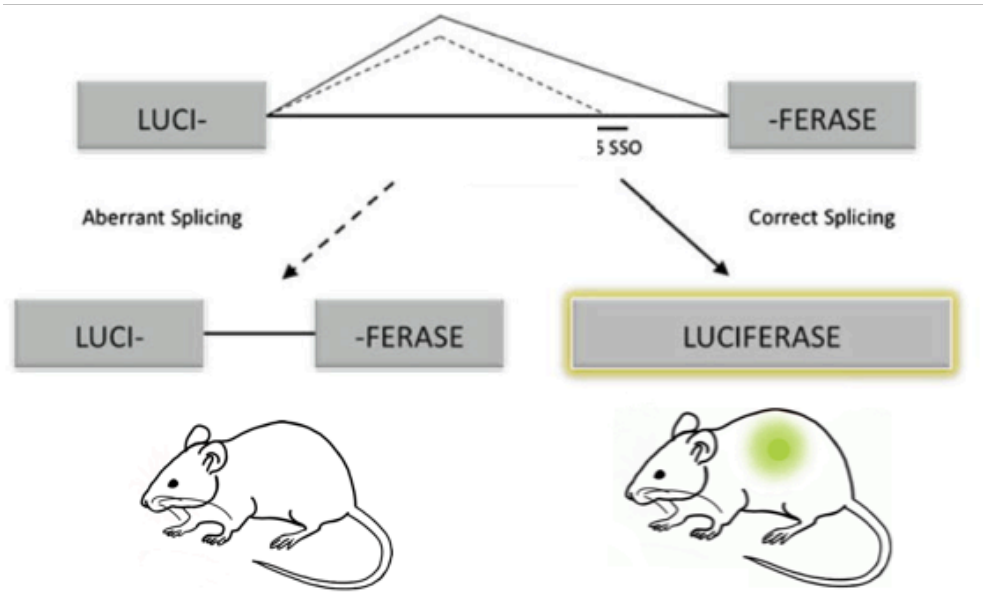

Figure 5 Illustration of the Split-Luc gene which is interrupted and leads to an aberrant splicing resulting in lack of BLI signal in the mouse vs. SSO corrected splicing, which enables expression of the luciferase gene providing a BLI detectable light signal. Source: https://www.ncbi.nlm.nih.gov/pmc/articles/PMC5558459/

3.5.2 Lung specific transgenic mouse model

Investigation on development, alteration, recovery and homeostasis in lung tissue is provided by transgenic mouse lines underlying a lung specific reporter gene expression. [43] Pulmonary surfactant consists out of a protein mixture that enables gas exchange and prevents an collapse of the lung during respiration. [3] The promoter of the surfactant protein C (SFTPC) is one of the frequently used promoters when it comes to generating lung specific transgenic mice. [43] SFTPC, the gene which encodes the hydrophobic surfactant protein C and undergoes a restricted expression located in the lung area and its production solely derives from alveolar type II cells. [3] Therefore, a huge advantage utilizing the SFTPC promoter is its high specificity of expression in the respiratory epithelium and absence in other tissues. [43] Even though, Mo et al. [44] pointed out SpC presence in human skin in higher amounts in fetal skin than in adult ones. [44]

There have already been studies using the SFTPC as a lung-specific promoter in mouse models. [43] Yee et al. [45] studied type II pneumocytes generating a transgenic mouse line expressing the enhanced green fluorescent protein (EGFP) among control of the surfactant protein C (SpC).

In this thesis one side project will examine the localization of reporter gene expression among control of SpC. The used method of signal detection is 2D BLI and is contributed to the fact that the utilized mouse line, Tg SpC-Luc mice, was formed by placing the luciferase expression cassette among control of the SpC promoter. This was achieved by pronuclear injection of the firefly luciferase expression cassette implementing the SFTPC promoter at the Institute for Laboratory Animals Sciences of the University of Veterinary Medicine in Vienna. [41]

3.5.3 Transgenic Thy 1.2-Luc mouse model

Conventional xenograft models enable usage of malignant human cells but are accompanied with the disadvantage of immunodeficiency in the rodent hosts.
As a contrast, syngeneic tumor models can be understood as a mouse tumor growing in mice of the same strain from which the tumor derives. [46] They are nonimmunogenic [46] and can be used in immune compromised mice. [47] Nevertheless, syngeneic tumor models investigate on rodent deriving tumor cells and therefore express mouse homologues of the desired targets and also tumor growth can differ. [46]

B16F10 is a subline of the murine melanoma cell line B16 [48] which is often used as a syngeneic model investigating strategies of cancer therapeutics in mice. [49] As the parental tumor of B16 was heterogeneous, sublines with different metastatic potential evolved. [47]
Intravenously inoculated B16F10 melanoma cells have a high capacity to metastasize into the lung area. [50]

Tumor cells tend to behave in a related way to physiological leukocyte migration and invasion into peripheral tissue. Therefore, they utilize related adhesion molecules for extravasation as the ones used during the process of leukocytes recruitment to site of inflammation. [51]

Initiation of melanoma cell adhesion to activated human endothelial cells (EC) is mediated by the cell adhesion molecule Thy 1. The junction between Thy 1 and melanoma cells is provided by the αVβ3-integrine a constituent situated on the tumors cell surface. This interaction was proved in vitro by Schubert et. al, 2013. However, data for tumor progression and metastatic behavior in vivo is absent/outstanding. [51]

The thymocyte differentiation antigen 1 (Thy 1), also known as cluster of differentiation 90 (CD 90) is a cell surface protein belonging to the immunoglobulin superfamily. Various cells express Thy1 such as thymocytes, T-cells, fibroblasts, neurons, activated EC, hematopoietic, mesenchymal stem cells and mesangial cells. [52] Thus, it is expressed on EC from tumor or at sites of inflammation. As a contrast EC in healthy tissue is not exposed to Thy 1 expression. [51] However, its expression pattern differs among species. [52] In pre-clinical studies Thy 1 mouse model is a prominent used model organism, so more information about the murine Thy 1 is available than for the human Thy 1. (Bradley et al 2009) The murine Thy 1 gene encodes Thy 1.1 and Thy 1.2, both differing in just one amino acid and the fact that Thy 1.2 is expressed with a higher frequency. [53]

The Tg Thy 1.2-Luc strain was generated by the technique of pronuclear injection of an expression cassette which contained promoter elements of Thy 1.2 and firefly Luciferase gene. [54] Therefore, expression of luciferase gene obeys the promoter activity of Thy 1 and generates a detectable 2D BLI signal when applying its substrate. Further, interaction of Thy 1-2 and the αVβ3 -integrins expressed on the surfaces of the B16F10 melanoma cells, can be studied as both bind each other with high affinity. A side project in this thesis devotes attention to the interplay and metastatic behavior pathways of Thy 1-2 after implantation of B16F10 melanoma cells.

4 AIM OF THE THESIS

This diploma thesis aimed to employ in vivo imaging techniques, namely fluorescence and bioluminescence imaging, for studying nucleic acid therapeutics in vivo for biodistribution (AF750-labeled siRNA) and delivery (splice-switching oligonucleotides), in addition to characterizing transgenic mouse models- Tg SpC-Luc and Tg Thy 1.2-Luc. Pharmacokinetic and pharmacodynamic studies in preclinical research are a crucial step in pharmaceutical development of macromolecular therapeutics. A convenient method with good cost effectivity and ease in reproducibility is the usage of fluorophores emitting in near infrared (NIR) for tracking macromolecules. This method was applied to one of the experiments presented in this thesis using siRNA as an agent, which was covalently bound to the fluorophore AF750. The goal was tracking its biodistribution and excretion after intravenous injection into mice. In vivo tracking of the applied was enabled by performing 2D FLI, as well as ex vivo 2D FLI organ imaging.

Another aim of this diploma work was to examine intravenously applied splice switching oligonucleotides (SSO) based polyplexes in transgenic Split-Luc mice (interrupted `splitted´ luciferase reporter gene) via 2D BLI. SSO polyplexes are expected to elevate the reporter gene activity in organs where the SSO is delivered in a functional state after intravenous administration.

Another goal in this diploma thesis was to analyze the localization of reporter gene activity in Tg SpC-Luc mice. The Tg SpC-Luc mice strain is a lung specific transgenic model and includes the luciferase gene under the promoter of surfactant protein C (SFTPC) (which encodes the surfactant protein C SpC), which is exclusively produced by the alveolar type II cells. Former experiments have shown that the reporter gene expression was not only in lungs but also in skin visible. Therefore, we aimed to demonstrate a more precise localization in lungs.

The last goal was to employ BLI to study growth of B16F10 melanoma cells implanted in Tg Thy 1.2-Luc mice strain. Tg Thy 1.2-Luc mice strain expresses luciferase reporter gene under the control of a Thy-1 reporter element. Therefore, trackability for

metastasis and further localization of B16F10 cells was aimed by visualizing the Thy 1.2-Luc reporter gene activity.

5 MATERIALS

5.1 Animals

- B6 albino CR mice

  (Charles river Laboratories, Research Models and Services, Germany GmbH)
- Tg (Luc 705) Split-Luc

  (inhouse breed, G3b wt for siRNA experiment, G3b Tg for SSO project)
- Tg SpC-Luc

  (inhouse breed, G3 wt. G3 Tg, G4 wt, G4 Tg, G5 wt, G5 Tg)
- Tg Thy 1.2

  (inhouse breed, G6a)

5.2 Animal related materials, devices and equipment

- Rodent food

  (SSNiff Spezialdiäten GmbH, Soest, Germany)
- Low fluorescent diet rodent food

  (EF AIN 76A rodent diet, Purified Diet, SSniff Spezialdiäten, GmbH, D-59494, Soest, Germany)
- Induction chamber

  (Rothacher Medical GmbH, Heitenried, Switzerland)
- Combi-vet ® anaesthesia system

  (Rothacher Medical GmbH, Heitenried, Switzerland)
- Warming bench

  (combi-vet ® Surgery table standard with Physitemp temperature controller unit, Rothacher Medical GmbH, Heitenried, Switzerland)
- Aesculap clipper

  (isis Aesculap ® GT420, B. Braun., Bachbach, Germany)
- Eye ointment

  (VitA POS ® Augensalbe, Ursapharm Ges.m.b.H, Saarbrücken, Germany)

- Ventilated cages

  (Blue Line- SEALSAFE ® NEXT IVC System, 1285L, Type 2L, Tecniplast, Hohenpeißenberg, Germany)
- Syringes for intravenous, intraperitoneal and sub-cutaneous injection

  (Omnican ® 100, B.Braun, Melsungen, Germany)
- Scale to weight mice in order to prepare formulation or Luciferin which were calculated based on weight

  (Model CS200, Ohaus Europe GmbH, Greifensee, Switzerland)
- Non-reflecting black tape

  (Insulating Tape, ZD Trading, Zwaagdijk, Netherlands)
- Surgical blade, to cut organs after organ collection

  (BB515, Aesculap AG, Tuttlingen, Germany)
- Eppis

  (Eppendorf Tubes, 1,5 mL; Eppendorf AG, Wesseling-Berzdorf, Germany)

5.3 Chemicals and treatment agents

- D-Luciferin

  (D-Luciferin potassium salt VivoTraceTM, Intrace Medical, Switzerland)

  (D-Luciferin potassium salt, 30mg/kg in Dulbecco's Phosphate Buffered Saline, Intrace Medical SA, Lausanne, Switzerland)
- Glucose 5%

  (B-Braun, Melsungen AG, Germany)
- HEPES Buffered Glucose

  (HBG, 5% glucose w/v, 20mM HEPES pH 7.4)
- Iopamidol

  (Scanlux Iopamidol, Sanochemia, Vienna, 300mg Iodine/ml)
- Isoflurane

  (CP 1ml/ml, CP-Pharma Handelsges.mbH, Ostlandring, Burgdorf, Germany)
- PVP Iodine
- Homemade RNA-lator solution

5.4 In-vivo imaging related devices, analysis and other programs

- IVIS Spectrum CT ® System

  (PerkinElmer Inc., Waltham, MA 02451, USA)

- Living Image Software

  Version 4.5.2, Perkin Elmer, Waltham, Masachusetts)

- PyRAT Animal Facility Software

  (Scionics Computer Innovation GmbH, Dresden, Germany)

- Web-based Electronic Lab Notebook Labguru

  (BioData Ltd., Rosh Ha'ayin, Israel)

- Excel for presenting results and graphs

  (Microsoft Office 365, Microsoft Corporation, Redmond, Washington)

6 METHODS

6.1 Animals

For the presented experiments in this thesis a total amount of four different mice strains were used. In order to examine biodistribution of systemical applied siRNA, B6 Albino CR and Tg (Luc 705) Split-Luc were utilized. Further, the Tg (Luc 705) Split-Luc strain was also used to evaluate splice correction after systemical administration of SSO. Tg SpC-Luc strain was crucial in observation of localization of transgenic expression. Tg Thy 1.2 was used for the B16F10 intravenous administered melanoma cells.

All four used inbred strains were bred in house (MMCT Laboratory at the division of clinical Pharmacy, University of Vienna) three weeks after birthdate weaning and earpunching were performed. In the latter case this was done for further genotyping investigations, with the aim of identification and classification of the intensity of the transgenic gene expression.

Animals were accommodated in individually ventilated cages (Blue Line- SEALSAFE ® NEXT IVC System, 1285L -Type 2 L, Tecniplast Deutschland GmbH, Hohenpeißenberg, Germany) among specific pathogen free conditions. The division of mice in groups from two to five animals per cage was sorted by strain and gender in order to prevent unwanted breeding and also by considering their behavior to avoid fights and injuries. This was enabled by a daily animal check which was done for upholding their wellbeing and refilling essentials as water and food. In individual cases when injuries or fights occurred, a treatment with polyvinyl pyrrolidone (PVP) iodine was applied on the affected area. Autoclaved water and food (SSNiff Spezialdiäten GmbH, Soest, Germany) were provided ad libitum. Animals which were about to be used for FLI investigations were set on low fluorescent diet food (EF AIN 76A rodent diet, Purified Diet, SSniff Spezialdiäten, GmbH, D-59494, Soest, Germany) for at least three weeks before starting the experiment with the aim of lowering background signal by auto

fluorescence of plant based food compounds. For minimizing possible contamination any other material which was in contact with the animals, was autoclaved in advance. To ameliorate housing conditions the animal facility was set for a circadian 12-hour day-night cycle with an adjusted room temperature to 24 +/- 1 °C and a relative humidity of 40-55%. The treatment and housing of the animals were according to the Austrian and European laws for animal protection.

Documentation of crucial information concerning e.g. animal facility, compliance, genotyping, breeding, phenotyping, experiments, special treatments or diets etc., were documented and stored using the PyRAT Animal Facility Software (Scionics Computer Innovation GmbH, Dresden, Germany).

6.2 In vivo administration of AF750 labeled NC-siRNA

This experiment was about studying biodistribution of systemically applied siRNA and elimination. Additionally, aiming of understanding whether renal or hepatical metabolization occurred. The early biodistribution and following excretion is trackable via 2D fluorescence imaging (FLI) and 3D fluorescence imaging tomography (FLIT). Therefore, the applied agent, namely NC-siRNA, is labeled to a fluorophore AF750. Excitation and emission of this fluorophore covers the visible spectrum and extends its emission into near the infrared. In this case AF750 can be excited to a wavelength of 750 nm. The tracking itself is then enabled by 2D FLI and 3D FLIT.

6.2.1 Experimental animals

Two Tg (Luc 705) Split-Luc wild type (wt) and six B6 Albino CR mice were set on low fluorescent diet for at least three weeks before starting the experiment. Three mice were used as control, one was from Tg (Luc 705) Split-Luc wt strain and the other two were B6 Albino CR strain. Experimental mice were compared only in between same strain. Weighting the mice enabled calculation of needed amount of AF750 labeled NC-siRNA, which was administered based on their mass. NC siRNA was prepared in HEPES buffered glucose (HBG, 5% glucose w/v, 20mM HEPES pH 7.4) and injected at a dosage of 2.5 mg/Kg. NC siRNA used for injection was a mix of AF750-labeled NC siRNA (20µg) and unlabeled negative control SSOs, as per the dosage and mouse weight.

Overview of experimental animals for systemic administration of AF750 labeled NC-siRNA:

Mouse	Gender	Strain	Injection date	Weight [g]	Amount NC siRNA (mixture of 20µg AF750-NC-siRNA and unlabeled NC-siRNA) injected at dosage of 2.5mg/Kg.	control
MCT-163	Male	Tg (Luc 705) Split-Luc wt	15.10.2019	43,7	273 µl	MCT-132
MCT-167	Female	Tg (luc 705) Split-Luc wt	16.10.2019	35,7	223 µl	MCT-132
MCT-361	Female	B6 Albino CR	13.11.2019	29,1	182 µl	MCT-364
MCT-362	Female	B6 Albino CR	13.11.2019	22,4	140 µl	MCT-365
MCT-363	female	B6 Albino CR	13.11.2019	23,5	147 µl	MCT-364

Table 2 Systemic administration of AF750 labeled NC-siRNA- experimental animal details.

6.2.2 Workflow overview

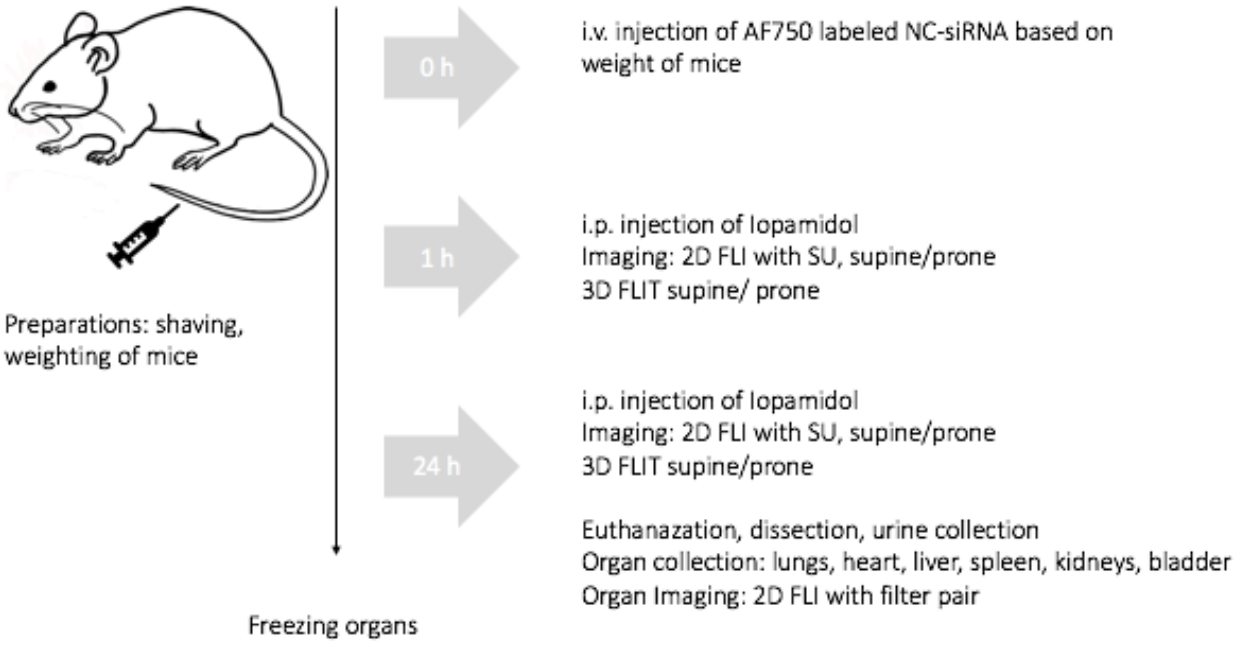

Figure 6 Workflow- systemic administration of AF750 labeled NC-siRNA.

6.2.3 Workflow and Imaging details

Preparation of animals and application of formulation:

Animals to be injected with the formulation, were transferred into a homemade injection tube. This is a modified construct of a 50ml syringe tube where its outlet on the top is cut to a hole and taped, so that there is place for the mouses nose. On the back part the mouse can be fixated with a shortened syringe plunger which is then taped. The formulation, which was to be injected, was calculated based on weight of the mouse and every time recently prepared in the laboratory. Afterwards transported into the animal facility among light excluding conditions and then pulled up into an pre-rinsed syringe (Omnican ® 100, B.Braun, Melsungen, Germany). Pre-rinsing was done with a HEPES Buffered Glucose (HBG, 5% glucose w/v, 20mM HEPES pH 7.4). In order to obtain better intra venous (i.v.) injecting conditions, the tail vein was hold into a tube which contained pre-warmed water up to 43 °C. Right before injecting the formulation, the tail was disinfected with 70% ethanol.

Fluorescence imaging workflow:

For this experiment the following working steps for fluorescence imaging were done one hour and twenty-four hours after intra venous (i.v.) injection of AF750 labeled NC-siRNA. Treated and control mice underwent same imaging conditions and 2D FLI was performed. Only for treated mice 3D FLIT was done. Therefore, all treated mice received also a contrast solution. This consisted of 120µl iopamidol and 180 µl of a 5% glucose solution, which was freshly prepared right before intra peritoneal (i.p.) injection. Application of this contrast agent was done every time before a 3D fluorescence imaging session, in order to ameliorate contrast for the x-ray computer tomography imaging. In this thesis all 3D fluorescence imaging tomography (FLIT) data is excluded. All FLIT analysis of this project was done by Julia Scholda M.Sc. and is mentioned in her master thesis.

Fluorescence imaging was performed using a fluorophore, AF750 which was labeled to the agent. This enabled trackability and further studying the biodistribution of the applied agent.

Mice were individually placed into an induction chamber (Rothacher Medical GmbH, Heitenried, Switzerland) and anesthesia was performed. Using an initial dose of 5% isoflurane (CP 1ml/ml, CP-Pharma Handeslges.mbH, Ostlandring, Burgdorf, Germany) in oxygen which was then reduced to a maintenance dose of 2% isoflurane in oxygen. After total anesthesia the mice were transferred to a warming bench (combi-vet ® Surgery table standard with Physitemp temperature controller unit, Rothacher Medical GmbH, Heitenried, Switzerland) which was also connected to the Combi-vet ® anesthesia system (Rothacher Medical GmbH, Heitenried Switzerland). There the mice were shaved using a hair clipper (Aesculap clipper, isis Aesculap ® GT420, B. Braun, Bachbach, Germany). Shaving them dorsally and ventrally offered an improved imaging signal by avoiding unwanted light scattering. In order to protect the mice eyes, an eye ointment (VitA POS ® Augensalbe, Ursapharm Ges.m.b.H., Saarbrücken, Germany) was applicated. After these steps, mice were transferred into the imaging chamber of the IVIS Spectrum CT® System (PerkinElmer Inc., Waltham, MA 02451, USA) which was already flooded with isoflurane in a maintenance concentration of 2% isoflurane in oxygen.

For each 2D FLI session same placement of mice in the IVIS Spectrum CT ® System imaging chamber was followed, on the left side the control mouse and on the right side the treated mouse were placed. The mice were firstly imaged in supine position and then prone whilst being fixed with non-reflecting tape on their paws (Insulating Tape, ZD Trading, Zwaagdijk, Netherlands).

Imaging was performed with following acquisition parameters which were set up using the Imaging Wizard in the IVIS acquisition control panel of the Living Image Software Version 4.5.2 Perkin Elmer, Waltham, Masachusetts.

Imaging mode	2D Fluorescence
Mode:	Epi-fluorescence with Spectral-unmixing
Filter Scan:	Alexa Fluor 750
Stage of view (FOV):	C
Counts:	600-60.000
Exposure:	Auto
Binning:	8
FStop:	2
Excitation filter [nm]:	640/675
Emission filter [nm]:	680/700/729/740/760/720/740/780/800
Lamp level:	high subject
Subject height:	1,5cm

Table 3 Acquisition parameters for 2D FLI

After the 2D FLI imaging session the control mouse was taken out of the imaging chamber and woken up in hands to avoid a possible cooling out. As soon as the mouse was awake it was returned back to its cage. In meanwhile the treated mouse remained anesthetized at a maintenance concentration of 2% isoflurane in oxygen. Additionally, the 3D FLIT plate was installed in the chamber. Afterwards the mouse was fixated on the new plate with non-reflecting tape and imaging was done in supine and prone position of the mouse. 3D FLIT was performed among following acquisitions.

Imaging mode:	3D fluorescence light imaging tomography
Transillumination points:	12-14
Stage of view (FOV):	B
Computed tomography:	On
CT:	Medium resolution

Table 4 Acquisition parameters for 3D FLIT

Setting of the transillumination points occurred on a photograph, which was taken by the IVIS Spectrum CT ® based on the 2D FLI image. The points were placed on regions where a signal appeared on the 2D image. After finishing the imaging session, the mouse was woken up and further working steps were taken as mentioned above.

Twenty-four hours after injection of the AF750 labeled NC-siRNA and imaging sessions, including 2D FLI and 3D FLIT, the mouse was euthanized. Therefore, the mouse was put back into the induction chamber and deeply anesthetized with a dose of 5% isoflurane in oxygen. Afterwards it was euthanized via cervical dislocation. On a styrofoam plate the mouse was put dorsally and fixed with four needle tips. To avoid fur sticking to the scissor, the corpse was sprayed with 70% ethanol and then dissected. FollowingOrgans were taken out and put on a black non-reflecting plate for the organ imaging:

- lungs
- spleen
-heart
-kidneys
-liver
-bladder

Organ Imaging was done among following acquisition settings:

Method:	2D FLI, Organ imaging
	Filter pair
Stage of view:	1
Lamp level:	High subject
Subject height:	0,5 cm

Table 5 Acquisition for 2D FLI organ imaging.

After the imaging session the organs were put in eppis and if needed cut with a Surgical blade (BB515, Aesculap AG, Tuttlingen, Germany) stored in -80 °C freezer, located in S1 Laboratory at the Department of Clinical Pharmacy at the University of Vienna. Localization of the above-mentioned organs was also entered in the Web-based Electronic Lab Notebook Labguru (BioData Ltd., Rosh Ha'ayin, Israel).

6.3 Systemic administration of SSO based polyplexes

In this experiment systemically applied SSO based polyplexes were expected to result in an increase in luciferase activity in Tg (Luc 705) Split-Luc mice, trackable via 2D bioluminescence imaging (2D BLI) after being exposed to its substrate luciferin.

The transgenic mouse strain Tg (Luc 705) Split-Luc possesses an interrupted luciferase gene. This includes a defective human beta-globin intron which carries an aberrant splice site at nucleotide 705 and initiates an activation of an abnormal site. Further, it leads to a defective splicing and results in obtaining a dysfunctional protein. Blocking of this mutation can be achieved by using SSOs, which bind complementary to the abberrant splice site. Thus, SSO correct splicing and sustain the expression of functional luciferase protein. Increased luciferase activity can then be measured via 2D BLI after sub cutaneous (s.c.) injection of its substrate, luciferin.

6.3.1 Experimental animals

A total amount of six mice were used, all deriving from the same transgenic strain Tg (Luc 705) Split-Luc and genotypically positive for the transgene. Out of these, four mice were injected with Luc-SSO polyplexes and rest two animals were injected with Non coding-SSO polyplexes as control treatments. Both polyplexes were prepared by complexing cross-linked LPEI with the respective SSO (Luc-SSO or non coding-SSO) in HBG buffer and were injected at a SSO dosage of 5mg/Kg as per mouse weight. The luciferase reporter gene activity of two controls and four treated mice were compared to each other.

Overview of experimental animals for systemic administration of SSO:

Mouse	Gender	Strain / Genotyping status/ generation	Injection date	Weight [g]	Formulation	Control
					Luc SSO-Polyplex (Luc ASO+C-LPEI NP9 in HBG)	
MCT-168	female	Tg (Luc 705) Split-Luc Hem - G3b	29.10.2019	25,9	329 µl	MCT-165
MCT-169	female	Tg (Luc 705) Split-Luc Weak hem ++ G3b	02.12.2019	29,7	363 µl	MCT-171
MCT-185	female	Tg (Luc 705) Split-Luc Hem ++ G3b	02.12.2019	39,4	508 µl	MCT-171
MCT-186	female	Tg (Luc 705) Split-Luc Hem +++ G3b	26.11.2019	37,7	479 µl	MCT-171
					Non coding SSO-Polyplex (ASO+CLPEI NP9 in HBG)	
MCT-165	female	Tg (Luc 705) Split-Luc Hem + G3b	29.10.2019	31,1	408 µl	
MCT-171	female	Tg (Luc 705) Split-Luc Hem + G3b	26.11.2019	29,9	374 µl	

Table 6 Systemic administration of SSO- experimental animal details.

6.3.2 Workflow overview

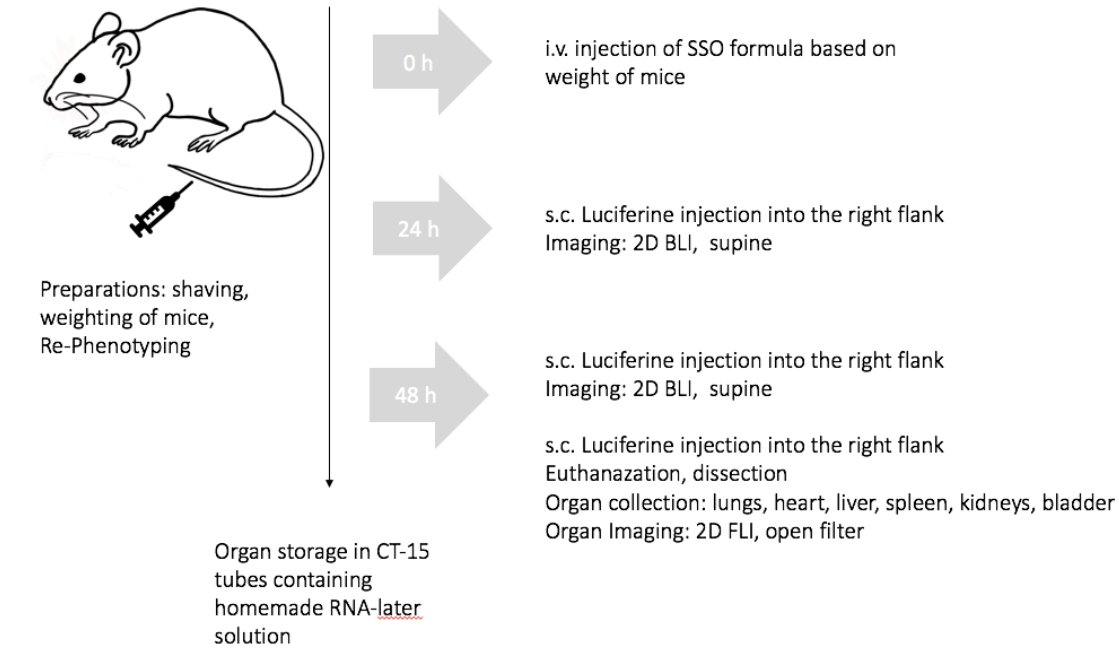

Figure 7 Workflow- systemic administration of SSO.

6.3.3 Workflow and Imaging details

Preparation of animals:

Categorization of control and treated animals was done by evaluating their bare luciferase gene expression activity, which is also known as the process of phenotyping. This could be easily done by injecting luciferin sub cutaneous (s.c.). As luciferin is the substrate for the luciferase, it was altered into oxyluciferin among consumption of oxygen and adenosine triphosphate (ATP) and photons were emitted during this reaction. 2D BLI enables the measurement of these photons, which was performed with the IVIS Spectrum CT ® System, by using a sensitive charged coupled device (CCD) camera. As a result, reporter gene activity could be examined, which was not only essential for phenotyping and categorizing the animals into control and treated ones. In addition to that it was a reference to later performed 2D BLI sessions after systemic administration of SSOs which also proved, whether splice correction occurred or not.

Bioluminescence imaging workflow:

The following content explains the workflow of 2D BLI which was done as well for phenotyping as for further 2D BLI sessions after systemic administration of the formulation. Firstly, all of mice which were used for this experiment were shaved

among anesthesia. This was done in order to prevent unwanted light scattering in later ongoing 2D BLI sessions. (exact procedure concerning shaving and anesthesia was already explained in chapter 6.2.3.) Afterwards mice were weighted in order to calculate the needed amount of D-Luciferin, which was based on their mass. A general 2D BLI workflow consisted in taking the mouse out of its cage and transferring it into an induction chamber. Starting with an initial dose of 5% isoflurane in oxygen anesthesia was induced and then reduced to a maintenance concentration of 2% isoflurane in oxygen. Further, the mouse was placed on the warming bench for applying an eye ointment as protection. Depending on their mass, D-Luciferin was injected sub cutaneously (s.c.) with a syringe. Right after, the mouse was placed into the imaging chamber of the IVIS Spectrum CT® System which was already flooded with isoflurane in a maintenance concentration of 2% isoflurane in oxygen. After 2D BLI session the mouse was taken out of the imaging chamber, woken up in hands to prevent a possible cooling out and afterwards put back into its cage.

All animals were imaged in supine position and subcutaneous (s.c.) luciferin injection was given into the right flank. Phenotyping was performed for all mice with following settings using the Imaging Wizard in the IVIS acquisition control panel of the Living Image Software.

Imaging mode:	2D BLI
Filter:	Open filter
Stage of view (FOV):	B
Segments:	5
Delay:	3 minutes
Max. exposure:	300 sec.
Binning:	8
F-Stop:	1
Subject Height:	1,5 cm

Table 7 Acquisition parameters for 2D BLI phenotyping.

Application of formulation and imaging:

All mice were individually transferred out of their cage into a homemade injection tube. As previously mentioned, it is a modified construct of a syringe where the mouse is placed in order to enable an intravenous injection without anesthetizing the mouse. It is an important fact that blood flow plays a huge role when considering biodistribution and it is reduced among anesthetized conditions. Therefore, injection of the formulation was aimed to be done in a physiological bloodstream state. The formulation to be injected, was calculated based on weight of the mouse and every time recently prepared in the laboratory. Among light excluding conditions the formulation was transferred to the animal facility and pulled up into a pre-rinsed syringe. Pre-rinsing was done with a HEPES Buffered Glucose. The tail vein was hold into a tube which contained pre-warmed water up to 43°C. Right before injection the tail was disinfected with 70% ethanol.

2D BLI was performed twenty-four hours and forty-eight hours after intra venous injection of the SSO. Imaging was performed among above explained workflows and same acquisition settings were adjusted, which are mentioned in table 7.

After finishing the 2D BLI session forty-eight hours post intravenous SSO administration, the mouse was taken out of the imaging chamber and put again into the induction chamber. A second dose of luciferin, which was calculated again based on mass, was given sub cutaneous into the right flank. The induction chamber was flooded with a high dose of isoflurane in a concentration of 5% isoflurane in oxygen. Further, the mouse was euthanized via cervical dislocation, put dorsally on a styrofoam plate and fixated with needle tips. The corpse was sprayed with 70% ethanol to avoid fur sticking on the scissor whilst dissecting.

Following organs were rapidly taken out and placed on a black non-reflecting plate for the organ imaging:

-lungs	- spleen
-heart	-kidneys
-liver	-bladder

Organ Imaging was performed among following acquisition settings:

Imaging mode:	2D BLI
Filter:	Open filter
Stage of view (FOV):	B
Segments:	1
Max. exposure:	300 sec.
Binning:	8
F-Stop:	1
Subject Height:	0,5 cm

Table 8 Acquisition parameters for 2D BLI organ imaging.

After organ imaging session lungs were cut with a surgical blade at the bifurcation and the liver was separated into three pieces. All organs were stored in CT-15 tubes only the liver was stored in a CT-50 tube and all tubes contained a homemade RNA-later solution. Further procedure of the organs enabled detection of splice correction based on a mRNA-level, which will be mentioned in the diploma thesis of Mag. pharm. Ferencz Levente.

6.4 Validation of transgenic gene expression in Tg SpC-Luc mouse strain

The Tg SpC-Luc mouse strain is a common lung specific transgenic model which enables tracking of the luciferase reporter gene activity among 2D BLI performance. This mouse strain includes the luciferase gene after the promoter of surfactant protein C (SFTPC) encoding the surfactant protein C (SpC), which is exclusively produced by the type II pneumocytes. Former studies have shown that SpC-Luc expression pattern is not only strongly kept in in lung area but also emerged in skin area. [44]

6.4.1 Experimental animals

A total amount of sixteen mice deriving from the same strain were taken and divided into two groups. Based on former pheno- and genotypings, which results were documented in the animal facility software PyRAT, group division and categorization were formed into genotypical (TG) positive (+) / negative (-) and phenotypical (PH) positive (+) / negative (-).

Overview of experimental animals for evaluation of transgenic gene expression in Tg SpC-Luc mice:

Group 1 TG(-)/PH(+)	Mouse	Gender	Strain	Generation/ hem	Weight [g]	Luciferin [µl]
	MCT-196	female	Tg SpC-Luc wt	G4 ++	33,1	133
	MCT-238	male	Tg SpC-Luc wt	G3 +++	39,6	159
	MCT-242	female	Tg SpC-Luc wt	G3 +++	36,4	146
TG(+)/PH(+)						
	MCT-194	female	Tg SpC-Luc	G4 +++	35,7	143
	MCT-195	female	Tg SpC-Luc	G4 +++	28,0	112

	MCT-236	male	Tg SpC-Luc	G3 +++	36,5	146
	MCT-239	male	Tg SpC-Luc	G3 +++	42,2	169
Group 2 TG(-)/PH(-)						
	MCT-309	female	Tg SpC-Luc wt	G5 -	21,5	86
	MCT-312	female	Tg SpC-Luc wt	G5 -	24,1	97
	MCT-329	male	Tg SpC-Luc wt	G5 -	29,2	117
TG(+)/PH(+)						
	MCT-193	female	Tg SpC-Luc	G4 +++	27,7	111
	MCT-197	female	Tg SpC-Luc	G4 +++	29,4	118
	MCT-198	female	Tg SpC-Luc	G4 +++	37,7	151
	MCT-307	male	Tg SpC-Luc	G5 +	39,2	157
	MCT-308	female	Tg SpC-Luc	G5 +	25,9	104
	MCT-311	female	Tg SpC-Luc	G5 +	25,4	102

Table 9 Evaluation of transgenic gene expression in Tg SpC-Luc -mice- experimental animal details.

6.4.2 Workflow overview

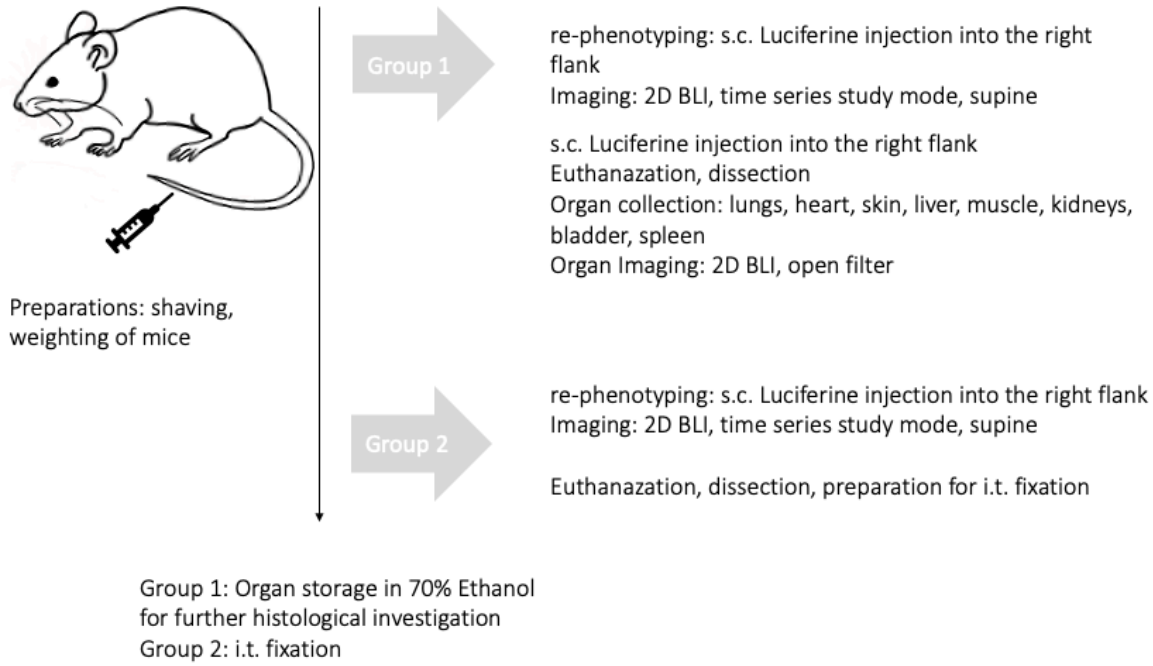

Figure 8 Workflow- evaluation of trangenic gene expression in Tg SpC-Luc mice.

6.4.3 Workflow and Imaging details

Preparation of animals:

Like in previous explained preparations mice were shaved, treated with eye ointment and weighted in order to calculate needed amount of luciferin for ongoing 2D BLI.

Bioluminescence imaging workflow:

All mice were again phenotyped to check if the transgenic genexpression changed in comparison to former results, which were documented in the animal facility software PyRAT. The procedure of 2D BLI based phenotyping is done exactly same as described in Chapter 6.3.3 Systemic administration of SSO, in category workflow and imaging details among rubric bioluminescence imaging workflow.

All animals were imaged in supine position and subcutaneous (s.c.) luciferin injection was given into the right flank. For one 2D BLI session either one mouse was single imaged, or two mice were imaged at the same time. Phenotyping was performed for all mice with following settings using the Imaging Wizard in the IVIS acquisition control panel of the Living Image Software.

Imaging mode:	2D BLI
Filter:	Open filter
Stage of view (FOV):	B- one mouse, C- two mice
Segments:	12
Delay:	3 minutes
Max. exposure:	300 sec.
Binning:	8
F-Stop:	1
Subject Height:	1,5 cm

Table 10 Acquisition parameters for 2D BLI phenotyping.

All mice from group 1 underwent after 2D BLI phenotyping all steps needed for 2D BLI organ imaging. These working steps were explained in former chapter. Following organs were taken out for organ imaging:

-lungs	- heart	-skin
-liver	-muscle	-spleen
-kidneys	-bladder	

Organ imaging was performed among below mentioned acquisition settings:

Imaging mode:	2D BLI
Filter:	Open filter
Stage of view (FOV):	B- one mouse, C- two mice
Segments:	1
Max. exposure:	300 sec.
Binning:	8
F-Stop:	1
Subject Height:	0,5 cm

Table 11 Acquisition parameters for 2D BLI organ imaging.

After imaging, organs were stored in CT-15 tubes filled with 70% ethanol. These organs were then handed in to histology for further working steps.

Mice belonging to group two, were intra tracheal (i.t.) fixated after 2D BLI phenotyping. Broader preparation steps differed from the ones in group one. In the thesis of Mag. pharm. Pan Lina further information is given about the continued experiment pointing out immunohistological aspects.

6.5 B16F10 melanoma cells in Tg Thy 1.2-Luc mouse strain

This experiment is an addendum to previous made investigations of intravenous (i.v.) injected B16F10 melanoma cells in Tg Thy 1.2-Luc strain mice. Systemic administration of B16F10 cells served as a pilot project and should enable an insight on evaluating signal patterns in affected areas. The Tg Thy 1.2-Luc strain includes the luciferase gene after the promoter of Thy-1, encoding a surface protein which has a high affinity in binding αVβ3 integrines. These are in a largely amount expressed on the surface of B16F10 derived melanomas. Thus, formation, development and localization of melanomas can be tracked via 2D BLI.

6.5.1 Experimental animals

Three mice deriving from the same strain, Tg Thy 1.2-Luc were used for this experiment.

Overview of experimental animals for systematic administration of B16F10 melanoma cells:

Mouse	Gender	Strain	Generation/ hem	Injection date	Weight [g]	Luciferin [µl]
MCT-259	female	Tg Thy 1.2-Luc	Ga6 ++	29.07.2019	22,8	92
MCT-261	male	Tg Thy 1.2-Luc	Ga6 ++	29.07.2019	20,1	86
MCT-262	female	Tg Thy 1.2-Luc	Ga6 +	29.07.2019	25,0	96

Table 12 Systemic administration of B16F10 melanoma cells- experimental animal details.

6.5.2 Workflow overview

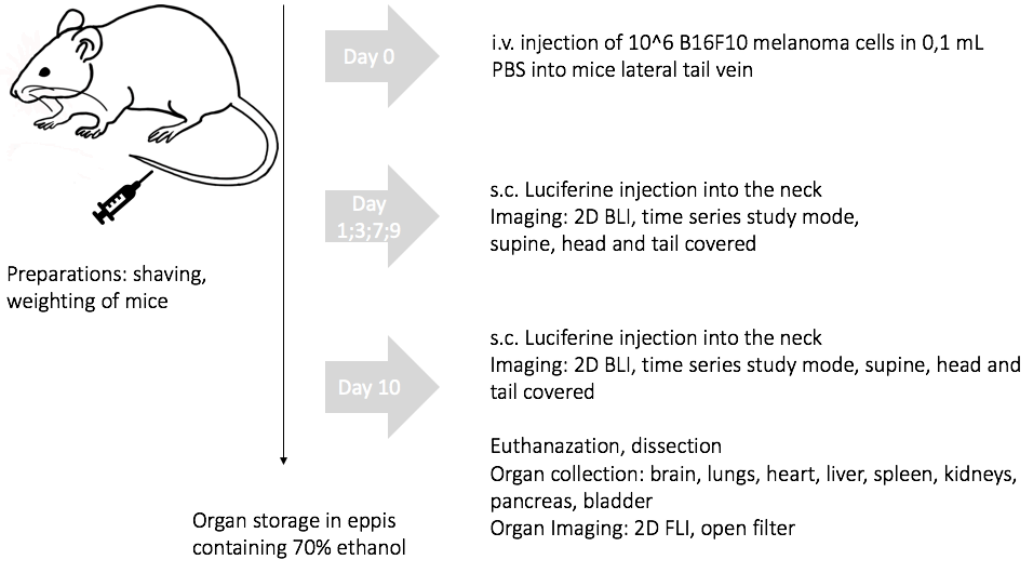

Figure 9 Workflow- systemic administration of B16F10 melanoma cells.

6.5.3 Workflow and Imaging details

Preparation of animals:

Animals were shaved and weighted in order to calculate needed amount of Luciferine for later imaging sessions. Additionally, eye ointment was used before each imaging session in order to prevent possible damages like drying out of mices eyes.

Application of formulation and bioluminescence imaging workflow:

On the injection date 10^6 B16F10 melanoma cells were suspended in 0,1mL PBS and injected into the lateral tail vein. Exact methods for preparation of mice to be injected were mentioned in chapter in vivo administration of siRNA and correspond with the here used working flow. Bioluminescence imaging was here used for in vivo investigation post intravenous application of the melanoma cells. Detailed working steps were already mentioned in previous chapters.

All animals were imaged in supine position, head was covered with a black non-reflecting plate in order to avoid unwanted signals, s.c. Luciferin injection was given into the neck. 2D BLI was performed for all mice with following settings using the Imaging Wizard in the IVIS acquisition control panel of the Living Image Software.

Imaging mode:	2D BLI
Filter:	Open filter
Stage of view (FOV):	B
Segments:	10-12
Delay:	2 minutes
Max. exposure:	300 sec.
Binning:	8
F-Stop:	1
Subject Height:	1,5 cm

Table 13 Acquisition parameters for 2D BLI imaging.

Ten days after injection date the last 2D BLI was done, then all mice were euthanized. Following organs were taken out and placed on a black non-reflecting plate for the organ imaging:

-lungs	- brain	-heart
-kidneys	-spleen	-bladder
-pancreas	-liver	

Organ imaging was performed among following acquisition settings.

Imaging mode:	2D BLI
Filter:	Open filter
Stage of view (FOV):	B
Segments:	1
Max. exposure:	300 sec.
Binning:	8
F-Stop:	1
Subject Height:	0,5 cm

Table 14 Acquisition parameters for 2D BLI organ imaging.

After organ imaging the mentioned organs were stored in eppis filled with 70% ethanol.

7 Analysis with the Living Image® Software

Whilst performing the introduced experiments, several imaging sessions were accomplished from which all images shown in this thesis are related to. Images were analyzed using the Living Image ® software, which is provided by Perkin Elmer. This chapter includes crucial steps on how analysis is done when using fluorescence and bioluminescence imaging.

7.1 Whole body imaging

7.1.1 Fluorescence imaging

7.1.2 2D FLI obtained images in spectral unmixing mode

The mode of spectral unmixing (SU) enables differentiation between autofluorescence and fluorophore signal. Depending on the used fluorophore, SU acquires nine to ten pictures. (Figure 10) These photos are taken with different excitation/emission settings, according to the utilized fluorescent dye. In general, this type of method was used in this thesis to study biodistribution of systemic applied AF750 labeled NC-siRNA, as this method is not dependent on reporter gene activity. During the experiment placement of the used mice was maintained in order to keep up the reproducibility. Treated mouse was placed on the right side and the control on the left. First step consisted in manual highlighting the two different signals (Figure 11), which was enabled by the program. Therefore, background signal in the control mouse could be distinguished from the ´real signal´ deriving from the treated mouse. The following pictures show a representative process of FLI analysis using the same mice:

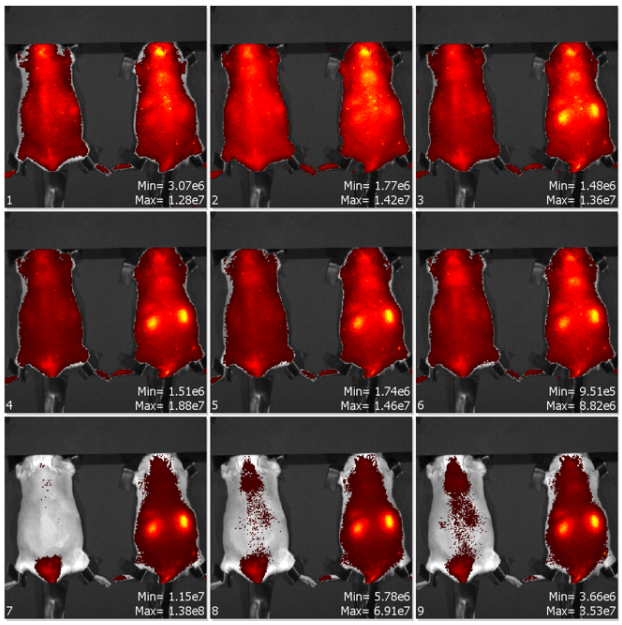

Figure 10 Sample image of pictures taken with different excitation and emission filters, captured in each subpicture 1-9, depending on the used fluorescent dye. The here used fluorophore is AF750. Shown mice: control mouse left, MCT-132 and treated mouse right, MCT-163 1h post AF750 labeled NC-siRNA i.v. injection, both prone positioned.

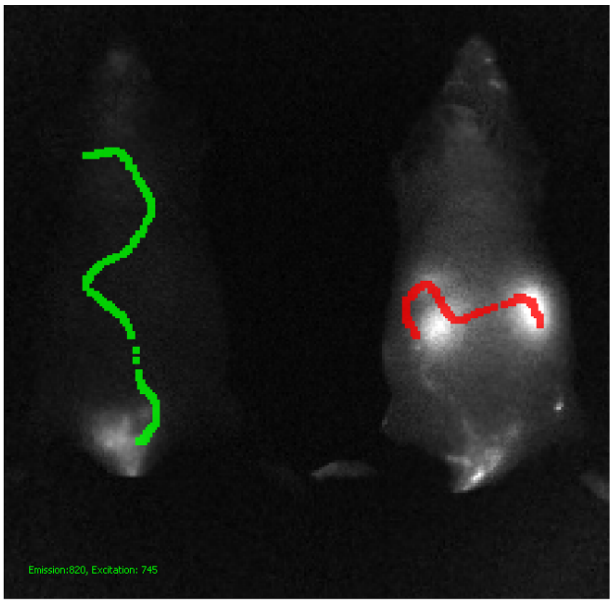

Figure 11 Representative image of manual highlighting the two different signals. On the left side the control mouse is showing in green the background signal and in contrast on the right side the treated mouse which underlines the main signal in red.

After highlighting the wanted body parts, as it is shown in Figure 11, in order to distinguish auto-fluorescence/tissue fluorescence from the main signal an unmixed picture sequence is obtained which is shown in Figure 12.

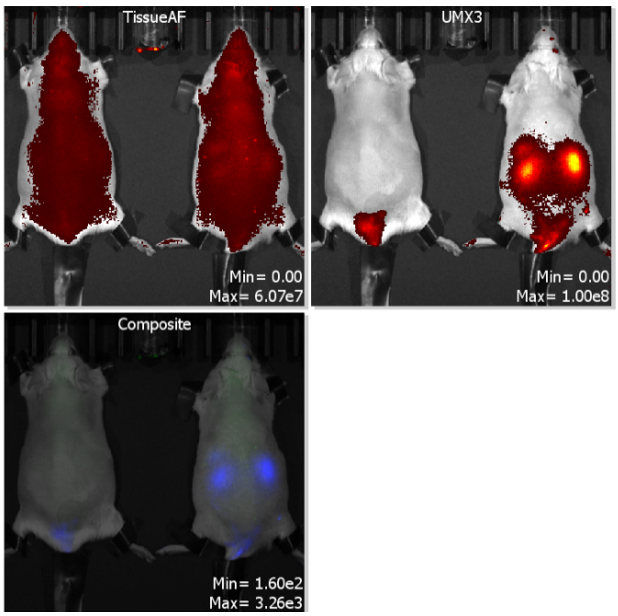

Figure 12 Pictures of the unmixed signals deriving from the previous shown Figure 10. TissueAF= tissue autofluorescence; UMX3= unmixing 3 pictures showing only signal in the right treated mouse.

Modification of smoothing, binning and changing of threshold has to be done individually depending on mice and intensity of signals in order to receive better and clearer signal spots, an example is presented in Figure 13. Evaluation of signal intensity is then done for any kind of imaging method same by manually drawing rectangular regions of interest (ROIs) around the signal spots. These will be shown in the following.

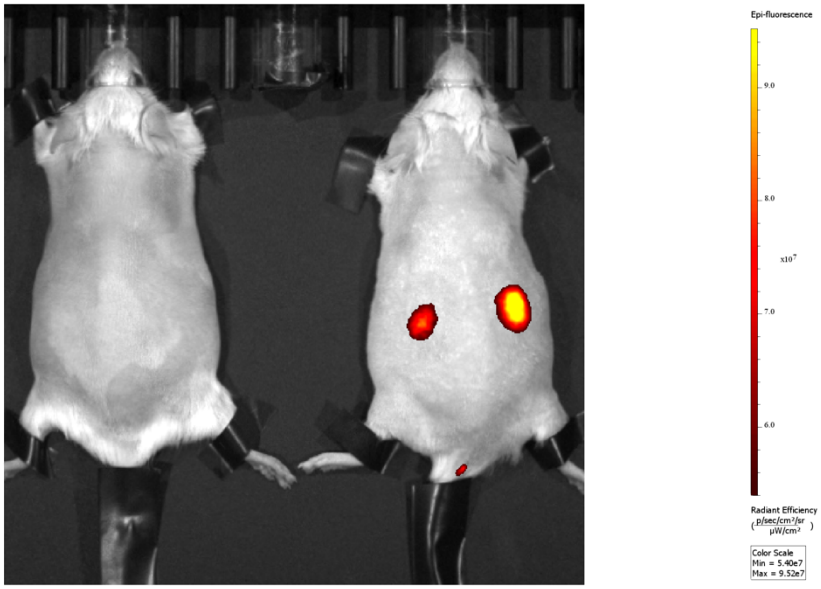

Figure 13 Modified threshold of UMX3 picture, presented above in Figure 12. Changing threshold permits to shift the visible pixels in a way to ameliorate lowering of unwanted background signal but keep up the ´real signal´ here shown in kidney area yellow/red roundly shaped spots.

7.1.3 Bioluminescence imaging

7.1.4 2D BLI obtained images in time series study mode

A well-suited method for studying in vivo reporter gene activity is enabled by performing 2D BLI in time series study mode. In this thesis the reporter gene activity was studied mainly for luciferase in different ways. Increasing reporter gene activity was measured after systemic administration of SSO; examination of luciferase activity was investigated in transgenic SpC mice strain after sub cutaneous Luciferin application; and tracking of reporter gene activity in Thy-1.2.-Luc mice after intravenous injection of B16F10, was also studied. For all above mentioned experiments the time series study mode was chosen which allows to adjust a specific number of segments with a time delay in-between, counted in minutes. The exact picked adjustments for each experiment were already presented in the chapter of ´Material and Methods´. Briefly, this mode permits performance of 2D BLI in a timeframe tracking the kinetics of applied Luciferin. According to the set number of segments, which correspond with receiving a picture for each segment, a time series study of 2D BLI is produced with a conserved time delay in-between each segment shown in Figure 14. Rectangular ROIs, which are drawn around the mice individually, measure in there the surface intensity. Figure 15 gives an example for ROIs drawing. This helps to choose the picture with the highest signal. This image is then taken and also here smoothing, binning and threshold can be modified in order to reduce unwanted background signal and accentuate the ´real signal´.

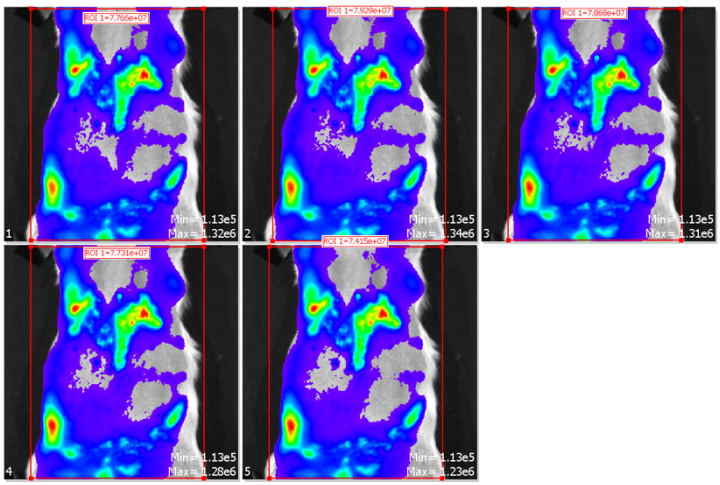

Figure 14 Representative Picture of a 2D BLI session in time series study mode, showing MCT-186 in supine position, 24h post i.v. injection of SSO. Luciferin injection was applied sub cutaneous into the right flank. Acquisition was set for 5 segments with a 3 minutes delay in-between tracking the kinetics of Luciferin. Subpictures 1-5 show pictures taken in series study with a time delay of 3 minutes and each picture represents the segment with the above mentioned set settings.

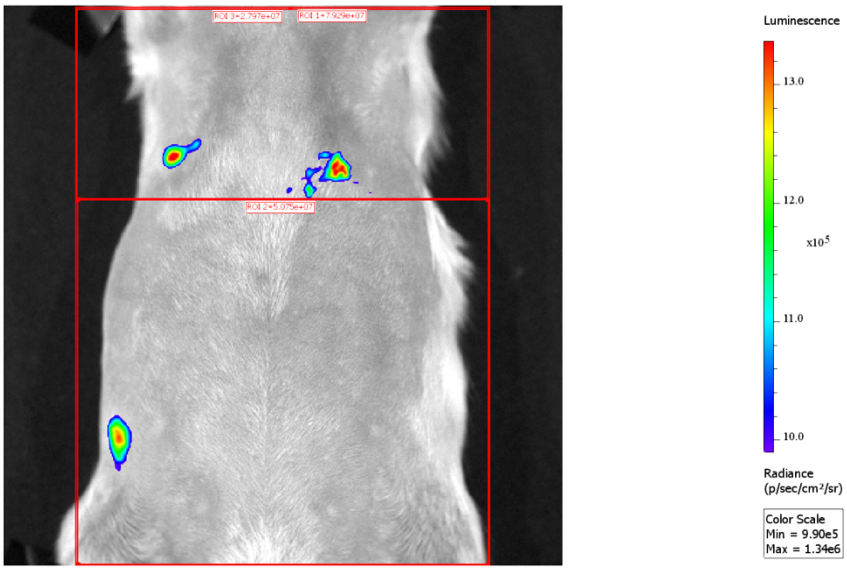

Figure 15 Image 2 with the highest whole-body ROI signal, deriving from the above presented 2D BLI time series. The picture shows an already modified version of changed smoothing, binning and threshold with the aim of minimizing background signal. Thus, it is a representative example for demonstrating how ROIs can be set in order to measure signals. Depending on the experiment different areas were chosen. The picture here implements three ROIs, a whole body ROI, another ROI covering thoracic area and lastly ROI over abdominopelvic area.

7.2 Organ imaging

7.2.1 2D FLI and 2D BLI obtained images in filter pair/ open filter mode

A common method for 2D FLI organ imaging is the filter pair mode, according to the selected fluorophore the best suited excitation and emission filters are selected. Then a single image is acquired detecting the fluorescent signal on the organs surface. For 2D BLI organ imaging the open filter mode is adequate by acquiring a luminescent image at maximal sensitivity. Additionally, concerning BLI, a second Luciferin injection can be done before euthanazation of the mouse for awaiting kinetics and receive a potential enrichment in organs. This results in higher signals, visible on the images. For both imaging methods a single picture is obtained. After receiving the image, provisory ROIs can be manually drawn around each organ with the aim of gaining the ROI values, visualized in Figure 16. This is done with the Living Image® software, which is as mentioned connected to the IVIS Spectrum CT ® System. Further, there is the possibility to continue the 2D organ imaging sessions by excluding the organ with the highest ROI value, this should be done right after organ imaging, to prevent possible dry out of the organs. The organ with the highest signal may cover up other signals, which might have been visible but are in comparison to the highest visible signal too

weak to appear as own signals. Performance of additional 2D organ images among exclusion of such high signaling organs, can result in appearance of signals in other organs. This may be an important hint for further investigations. Pictures can also be modified by changing smoothing binning and threshold to get rid of unwanted backgrund signal.

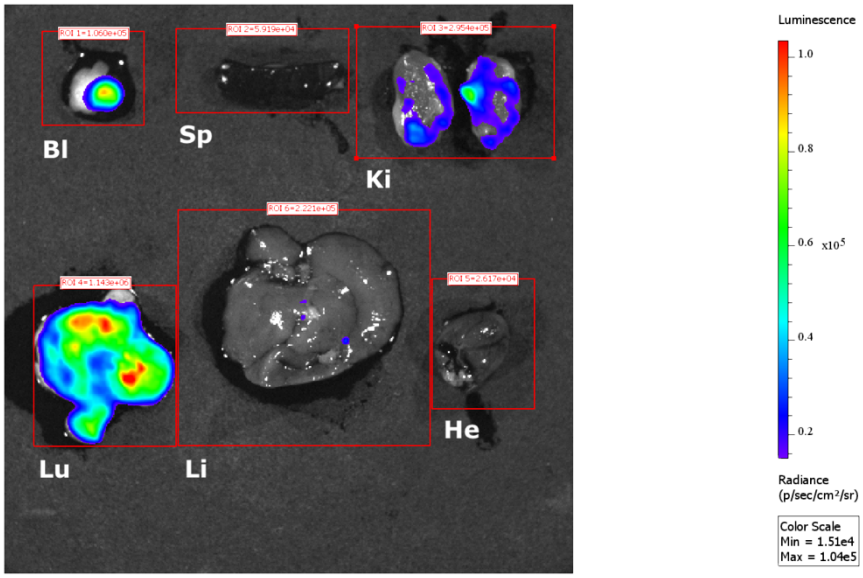

Figure 16 2D BLI organ imaging with adjusted smoothing, binning, threshold and ROIs. Showing bladder, spleen, kidneys, lungs, liver and heart of MCT-186, 48h post i.v. administered SSO. Additional Luciferin injection was applied into the right flank before euthanazation to achieve visible signal enrichment in organs.

In general after drawing ROIs around specific areas e.g. whole body, specific areas, or organs, the measured values in the ROIs can be exported as an excel file and processed with further workflows to representative diagrams. In order to sustain reproducibility of analysis, the ROIs can be saved in the program and same are applied to the other mice for each experiment individually.

Nevertheless, 2D whole-body imaging and 2D organ imaging should be considered in combination, since the obtained information is strongly sticked to the used method and cannot be covered up on the whole by one method itself. So, when it comes to analysis a broader view has to be taken in account on the performed imaging methods and the resultant diagrams which will be shown in the following chapter of `Results and discussion´.

8 RESULTS AND DISCUSSION

8.1 2D FLI based tracking of systemically administered AF750 labeled NC-siRNA

siRNA provokes suppression of any cancer related gene by gene silencing. Modification of siRNA is limited as it has to remain accessible for further processing constituents which lead to a successful outcome. It is known that kidney and liver are the primary tissues of distribution for such molecules.

Investigating the biodistribution pattern of intravenous applied AF750 labeled NC-siRNA via 2D FLI was performed within two experimental rounds. For the first round one control mouse and two treated mice were used. The second round consisted of a total amount of five mice, two served as control and three of them were injected with the formula. Imaging was performed one hour and twenty-four hours after application of the formula, placement of mice regarding imaging conditions was for each time point in prone position as in supine position.
All animals were taken for organ collection after cervical dislocation among deep anesthesia. Organ imaging was done approximately twenty-for hours after systemic administration of the formula into the treated mice. Additionally, all organs were placed for each mouse in the same way whilst imaging, with the aim of increasing reproducibility. As well referring to the analysis, all ROI have for each organ the same size and were placed among every mouse with the same conditions.

<u>Results from AF750 labeled NC-siRNA biodistribution study round 1</u>

Below the imaging data is presented from all mice belonging to round 1. As control mouse MCT-132 was placed alongside both treated mice, MCT-163 and MCT-167.

In vivo 2D FLI based imaging, enables a clear detection of a restricted signal in the kidney area in the treated mice which are distinguishable from the control mouse situated on the left side visible in Figure 17. Furthermore, the signal remains and appears in the same area for both imaging time points in the treated animals. As imaging in prone position shows clear restricted kidney signal spots for both treated

animals, which is visible in Figure 17, a first hint of no change in the biodistribution pattern can be estimated.

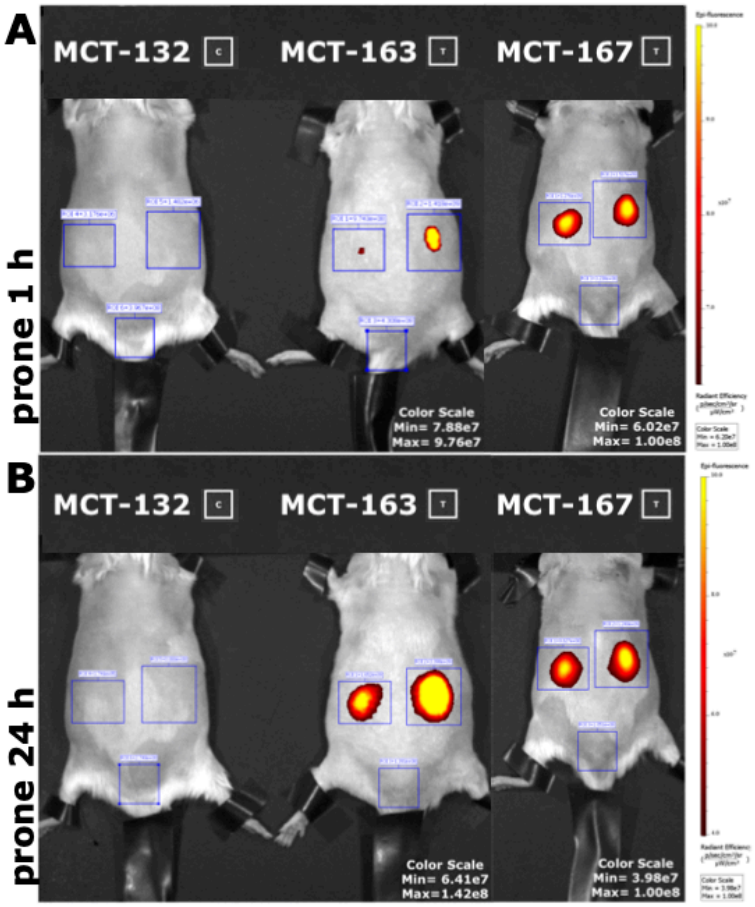

*Figure 17 2D FLI epiillumination mode with spectral unmixing image sequence of mice placed in prone position showing upper sequence **A** one hour and lower sequence **B** twenty-for hours post intravenous injection of AF750 labeled NC-siRNA into MCT-163 and MCt-167 in comparison to the control mouse MCT-132.*

In Figure 18, a diagram is presenting ROI signal values deriving from whole body 2D FLI imaging, presented in Figure 17, comparing control and treated mice. Inbetween one hour and twenty -four hours among the treated group, MCT-163 and MCT-167, do not visualize any big signal difference as the diagram bars are in a height around of log 9. Hence, the signal for both imaging time points from control mouse MCT-132 differ.

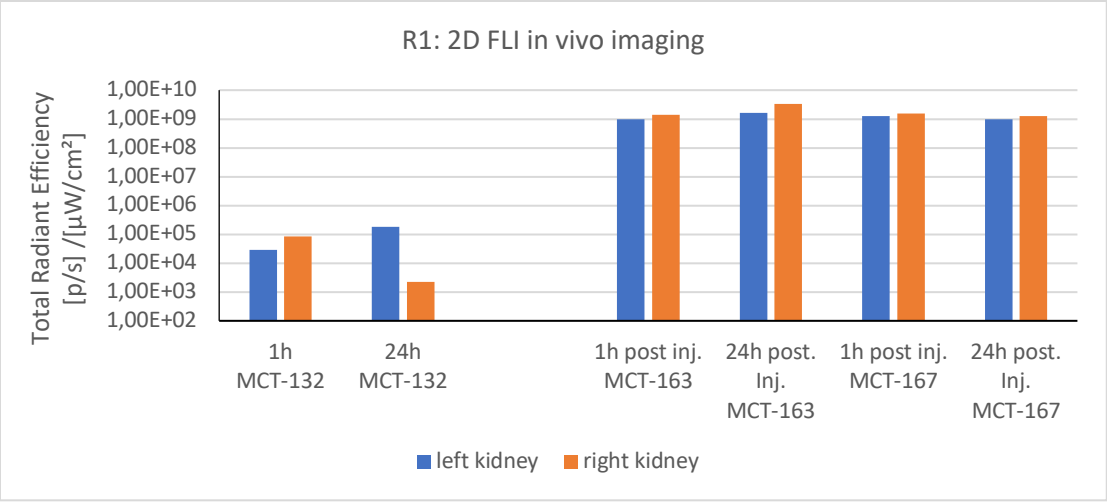

Figure 18 Diagram of exported ROI values from image sequences in prone position, illustrating values from one hour and twenty-four hours post injection of the formula into MCT-163 and MCT-167 in relation to the control mouse, MCT-132.

Figure 19 presents the obtained results from 2D FLI whole body imaging in supine position for both imaging time points, one hour and twenty-four hours after injection of the formula into the treated mice.

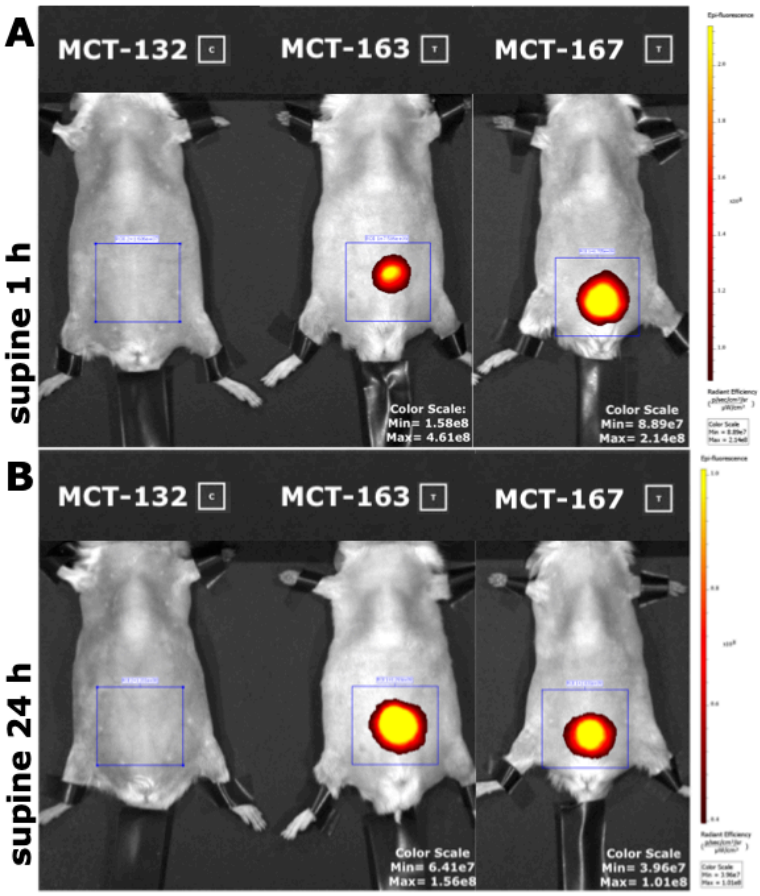

*Figure 19 2D FLI epiillumination mode with spectral unmixing image sequence of mice placed in supine position showing upper sequence **A** one hour and lower sequence **B** twenty-for hours post intravenous injection of AF750 labeled NC-siRNA into MCT-163 and MCT-167 in comparison to the control mouse MCT-132.*

Changing the imaging position into supine, demonstrates clear signals in bladder area. The signals are limited to this zone for both imaging time points and appear as well just in the treated mice, MCT-163 and MCT-167 shown in Figure 19.

In Figure 20 the signals from bladder area, deriving from Figure 19, are visualized in a diagram. The left side shows MCT-132 as a control mouse, which did not receive any treatment and therefore has a weak signal. In comparison to the control mouse, both treated mice, MCT-163 and MCT-167 show comparable high bladder signals for both imaging time points.

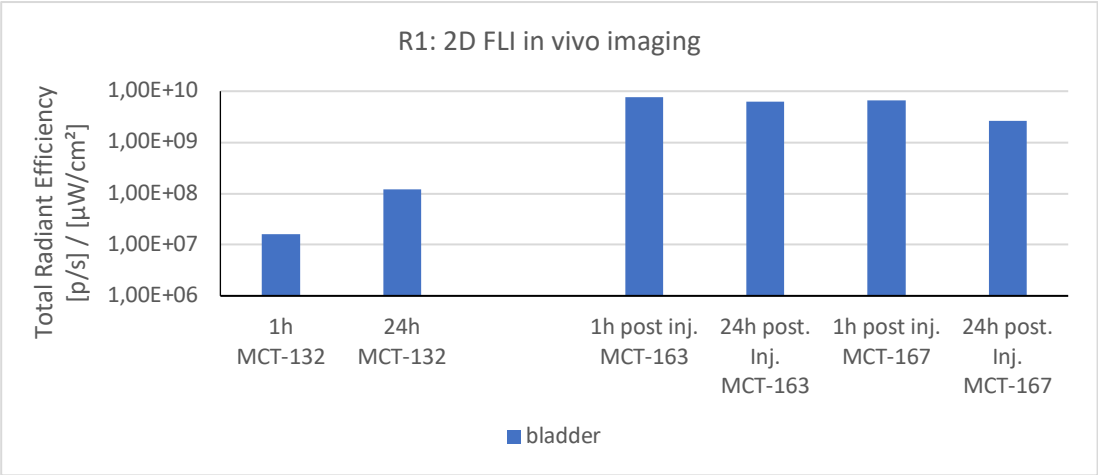

Figure 20 Diagram of exported ROI values from image sequences in supine position, illustrating values from one hour and twenty-four hours post injection of the formula into MCT-163 and MCT-167 in relation to the control mouse, MCT-132.

The results obtained from ex vivo 2D FLI organ imaging lead to a clear detection of signal in the kidneys regarding the treated mice, MCT-163 and MCT-167 visible in Figure 21. The corresponding exported ROI signal values were exported and converted into a diagram presenting the data in Figure 22 Moreover, the outcome sustains the results obtained by in vivo 2D BLI whole body imaging, which present signals in kidney area when imaging in supine position.

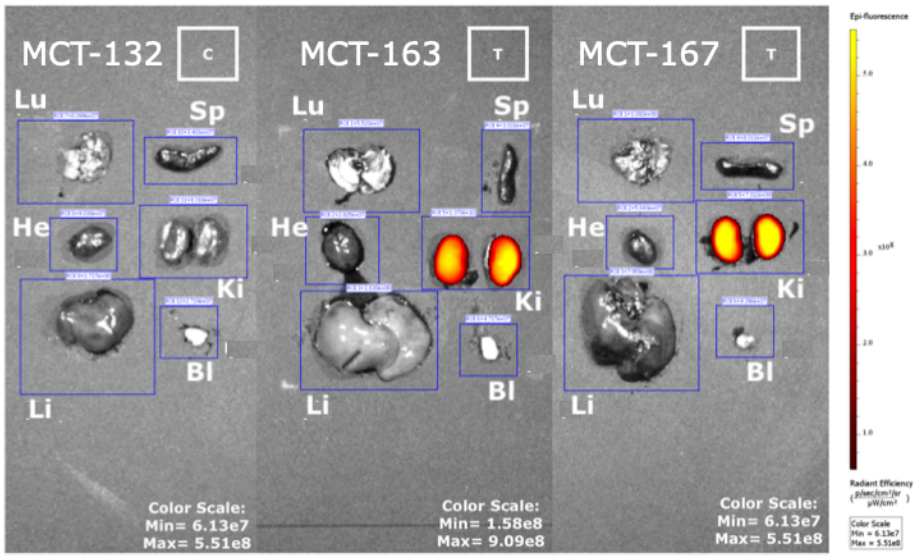

Figure 21 2D FLI epiillumination mode with filter pair ex vivo organ imaging after cervical dislocation and organ collection of Lu= lungs, He= heart, Li= liver, Sp=spleen, Ki= kidneys, Bl= bladder at a timepoint of approximately twenty-four hours after systemic administration of NC-siRNA into treated mice, MCT-163 and MCT-167 in contrast to the non-treated control mouse, MCT-132.

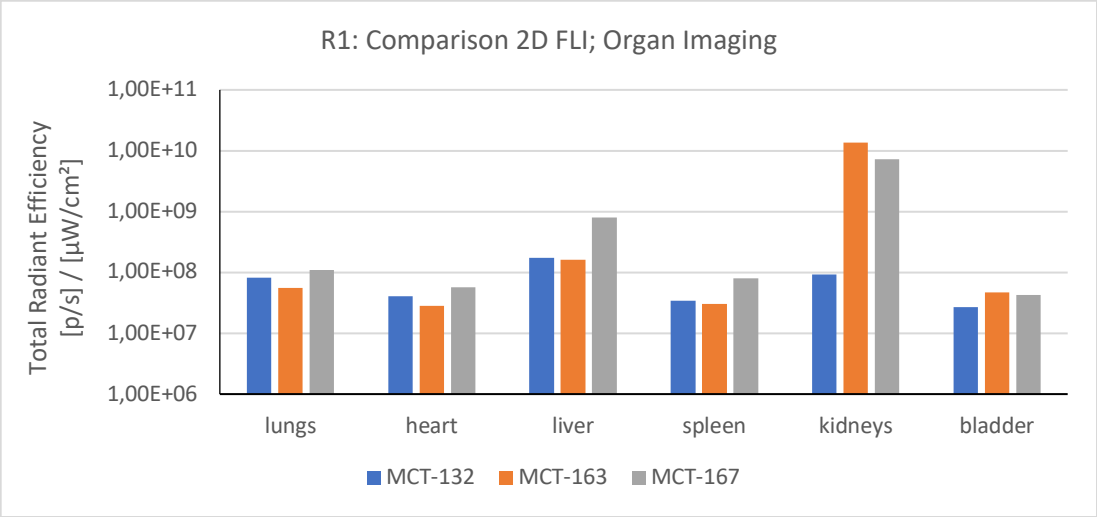

Figure 22 Diagram presenting signal values obtained from ex vivo 2D FLI organ imaging of MCT-163 and MCT-167, twenty four-hours post i.v. injection of the formula and comparison to the non-treated control mouse, MCT-132.

A crucial factor has to be kept in mind when organ imaging is performed. It may occur that organs, which show up signals have such a high value that it may cover up a possible signal from another weaker signaling organ. Therefore, it has to be taken in account that a re-imaging of the organs has to be done by excluding the organ with the highest signal intensity. Hence, a re-organ imaging was done, without the kidneys, as they reveal a strong signal. Following picture in Figure 23 demonstrates the outcome of the re-organ imaging, resulting in a background signal of liver for the treated mice.

As the results are comparable to those of the re-organ imaging performed in round two, these results are not presented in this thesis as the background signal does not fortify the aiming of biodistribution survey.

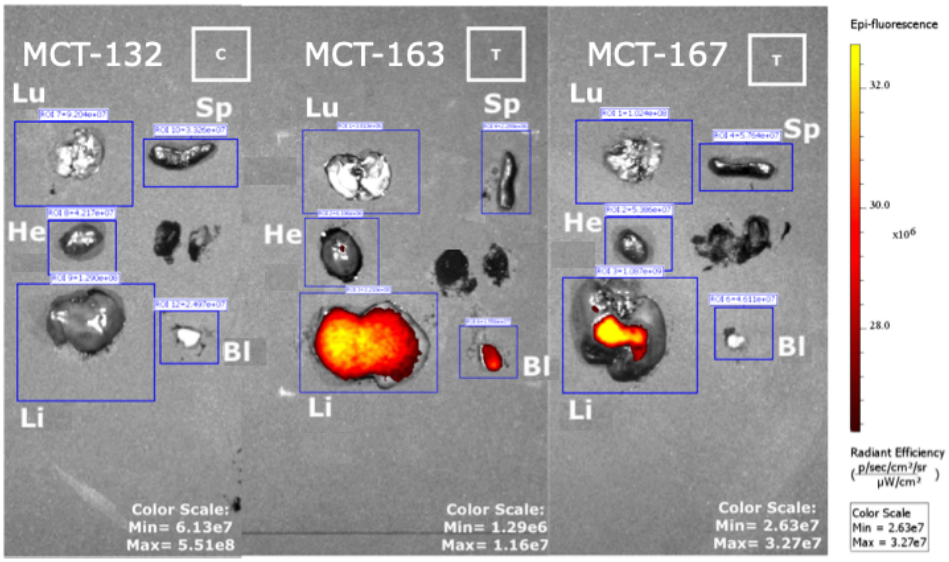

Figure 23 2D FLI epiillumination mode with filter pair ex vivo organ imaging after cervical dislocation and organ collection of Lu= lungs, He= heart, Li= liver, Sp=spleen, Bl= bladder at a timepoint of approximately twenty-four hours after systemic administration of NC-siRNA into treated mice, MCT-163 and MCT-167 in contrast to the non-treated control mouse , MCT-132.

The diagram presented in Figure 24 shows the exported ROI signal values received from ex vivo 2D FLI re-organ imaging among exclusion of kidneys. For each mouse, control MCT-132 and treated MCT-163 and MCT-167 the liver signal appears as the highest signal among the rest of the organs.

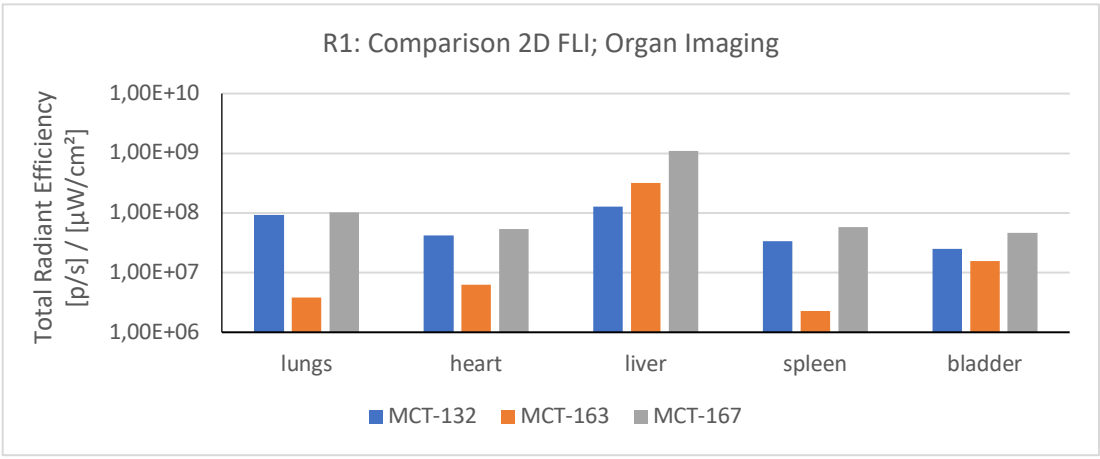

Figure 24 Diagram presenting signal values obtained from ex vivo 2D FLI re-organ imaging, excluding kidneys, with highest signal shown in Figure 23, of MCT-163 and MCT-167, twenty-four hours post i.v. injection of the formula and comparison to the non-treated control mouse, MCT-132.

Results from AF750 labeled NC-siRNA biodistribution study round 2:

Among same experimental conditions as mentioned before the results of AF750 labeled NC-siRNA biodistribution study round 2 are presented below. A comparable restricted kidney signal pattern regarding the prone imaging position can be witnessed in Figure 25 for the treated animals. The signal in kidney area remains restricted over the experimental time frame and is comparable to the obtained results from in vivo imaging in prone position from round 1. This strengthens the fact of a persistent renal biodistribution route after systemic application of the formula.

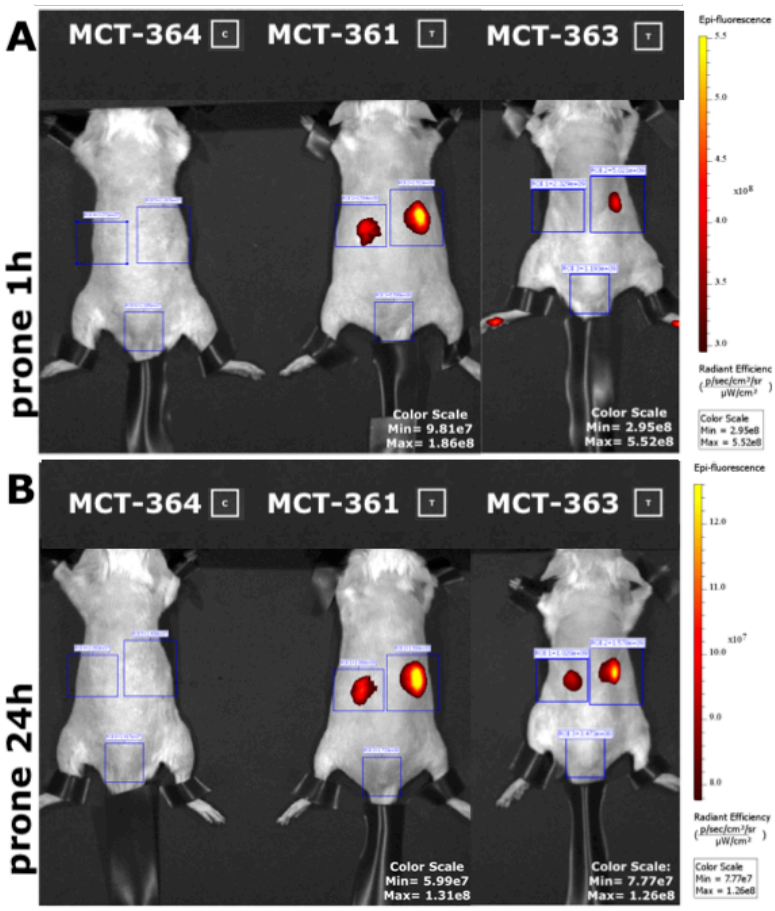

*Figure 25 2D FLI epiillumination mode with spectral unmixing image sequence of mice placed in prone position showing upper sequence **A** one hour and lower sequence **B** twenty-for hours post intravenous injection of AF750 labeled NC-siRNA into MCT-361 and MCT-363 in comparison to the control mouse MCT-364.*

In Figure 26 the ROI signal values deriving from 2D FLI body imaging in Figure 25 can be seen. MCT-364 which served as control mouse has lower signal, almost two log segments, and differs from the treated mice. Therefore, existence and renal exrection of AF750 labeled NC-siRNA can be underpinned.

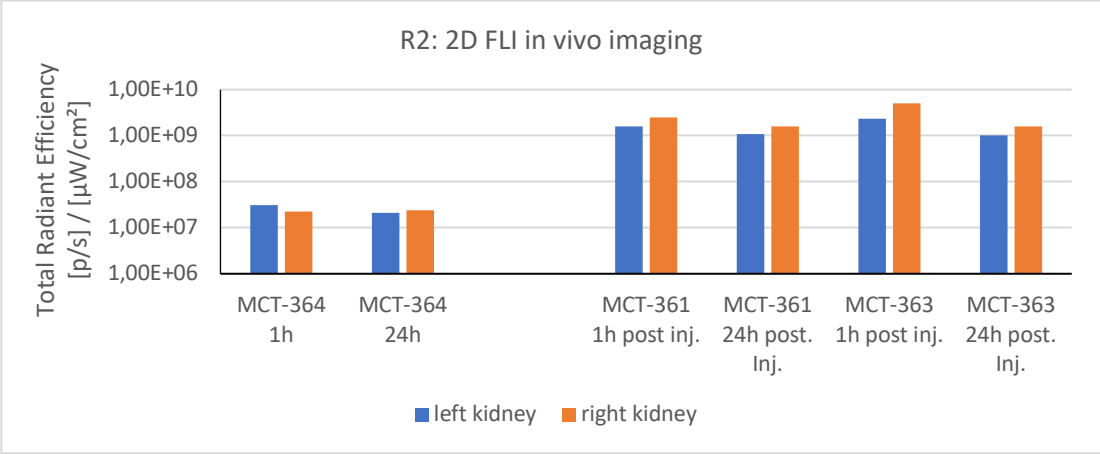

Figure 26 Diagram of exported ROI values from image sequences in prone position, illustrating values from one hour and twenty-four hours post injection of the formula into MCT-361 and MCT-363 in relation to the control mouse, MCT-364.

In Figure 27 the results from in vivo imaging in supine position are illustrated, a clear bladder signal is visible in the treated mice which appears in the bladder area among both imaging time points.

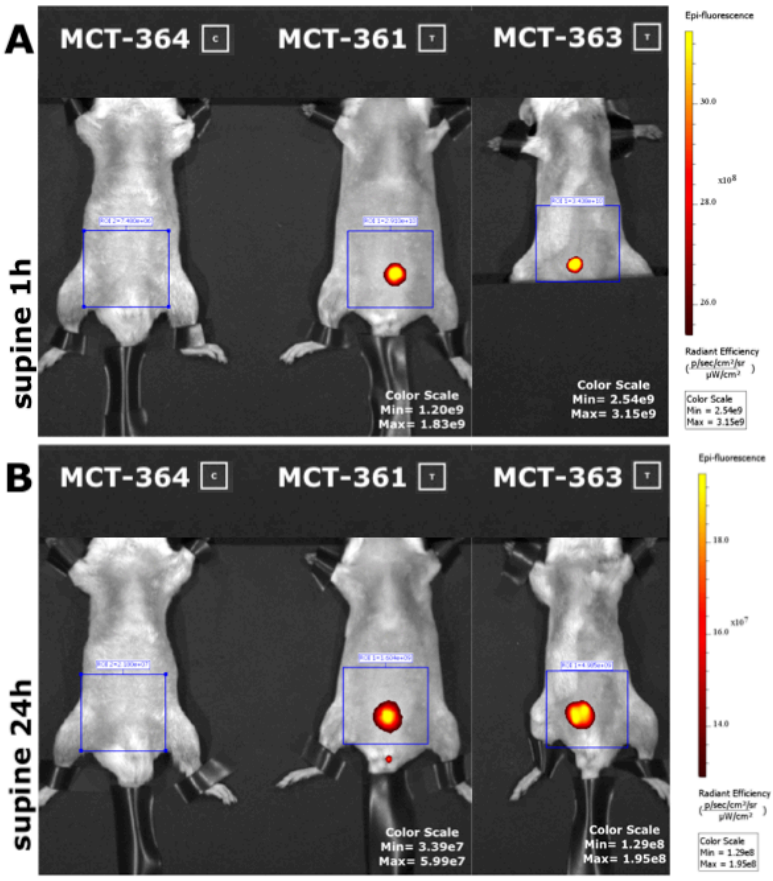

*Figure 27 2D FLI epiillumination mode with spectral unmixing image sequence of mice placed in supine position showing upper sequence **A** one hour and lower sequence **B** twenty-for hours post intravenous injection of AF750 labeled NC-siRNA into MCT-361 and MCT-363 in comparison to the control mouse MCT-364.*

All ROI signal values deriving from former figure, Figure 27, are presented in the diagram in Figure 28. In the treated mice, MCT-361 and MCT-363 the signals decrease in a maximum till one log segment as over the time frame a small amount of the formula is excreted via the urinary tract.

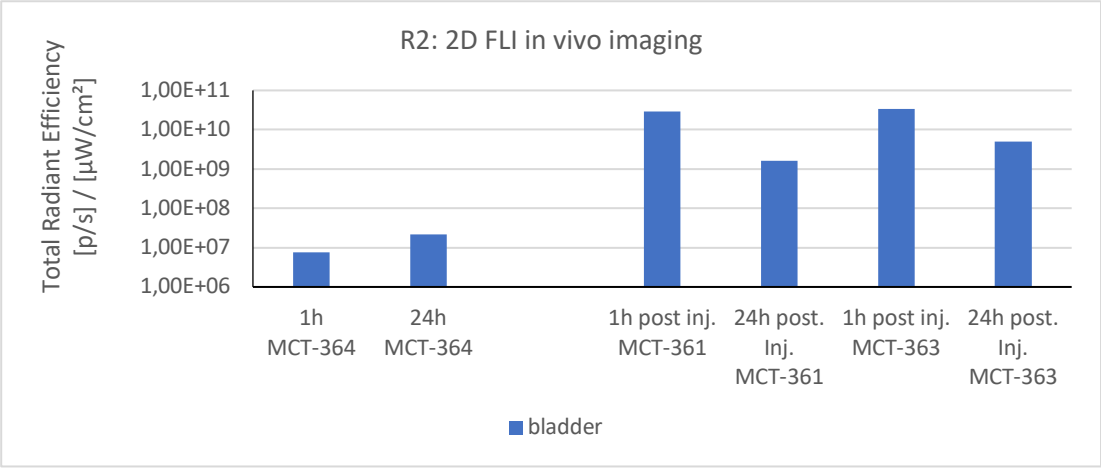

Figure 28 Diagram of exported ROI values from image sequences in supine position, illustrating values from one hour and twenty-four hours post injection of the formula into MCT-361 and MCT-363 in relation to the control mouse, MCT-364.

Both imaging positions, supine and prone, show reproducibility regarding signal availability. A restricted signal in kidney area appears in prone position, which stays during the imaging time points. Bladder signal is visible when imaging supine position, which is also applicable to the other mice from round 1. Therefore, a direction of assumption can be concluded when talking about biodistribution. Due to the localization of signals, which stay restricted for each timepoint in the mentioned positions, for prone kidney area and for supine position bladder area, a hint of renal excretion and no change in biodistribution pattern can be pointed out.

Figure 29 shows the obtained results from ex vivo 2D FLI organ imaging. The treated mouse, MCT-361 shows comparable signal pattern with the first round. Again, kidney area is marked with a high signal in relation to the non-treated control mouse, MCT-364. As mentioned above the re-organ imaging among exclusion of kidneys in round two, obeys to the signal pattern presented in round one and shows just background

signal located in liver area. As background signal is not essential for the investigation of the biodistribution, the data from re-organ imaging from round two is excluded. The corresponding exported ROI signal values are illustrated in a group diagram, shown in Figure 35.

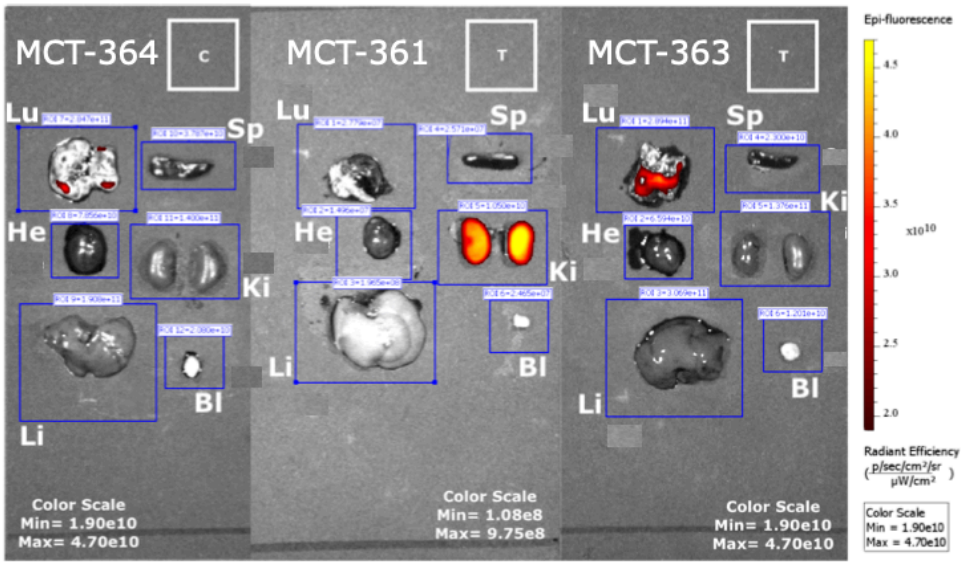

Figure 29 2D FLI epiillumination mode with filter pair ex vivo organ imaging after cervical dislocation and organ collection of Lu= lungs, He= heart, Li= liver, Sp=spleen, Ki= kidneys, Bl= bladder at a timepoint of approximately twenty-four hours after systemic administration of NC-siRNA into treated mice, MCT-361 and MCT-363 in contrast to the non- treated control mouse, MCT-364.

As a contrast, the treated mouse MCT-362 does not show reproducible character when it comes to signal appearance in supine position, Figure 32, in comparison to the other mice. Nevertheless, as shown in Figure 30 and Figure 31, kidney signals in the treated mouse MCT-362 are comparable with the other treated mice mentioned above for in vivo 2D FLI imaging in prone position. Hence, signal localization stays similar as it does not appear in an additional area, than kidney and bladder area. For MCT-362 an additional region of interest is needed in supine position for the kidneys, as the signal is not only restricted to bladder area, visible in Figure 32. Supplemental signal in kidney area of treated MCT-362 in supine position however still does not make any huge difference regarding biodistribution pattern. The referring results are presented below.

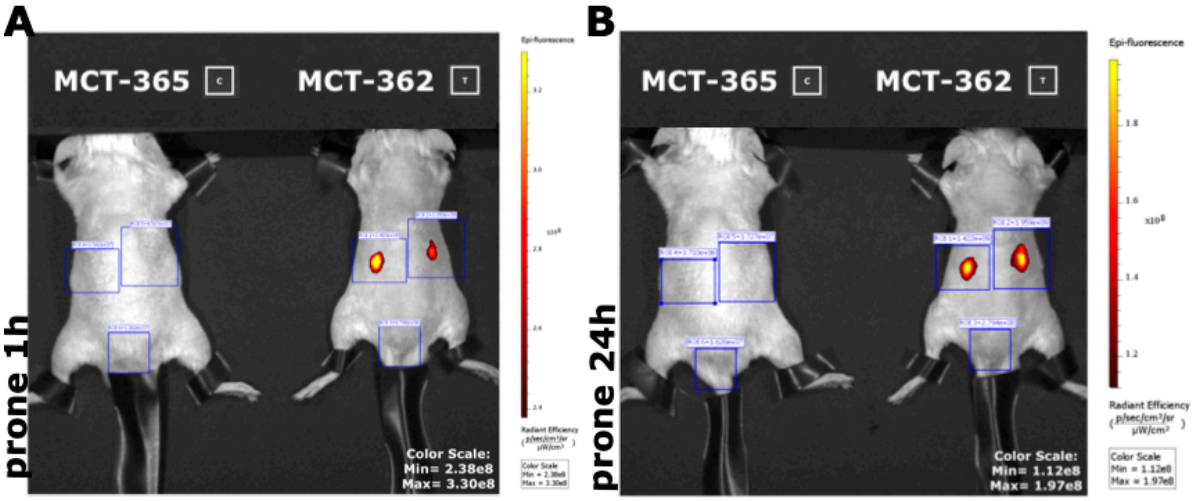

*Figure 30 2D FLI epiillumination mode with spectral unmixing of mice placed in prone position showing left image **A** one hour and right image **B** presenting twenty-for hours post intravenous injection of AF750 labeled NC-siRNA into MCT-362 in comparison to the control mouse MCT-365.*

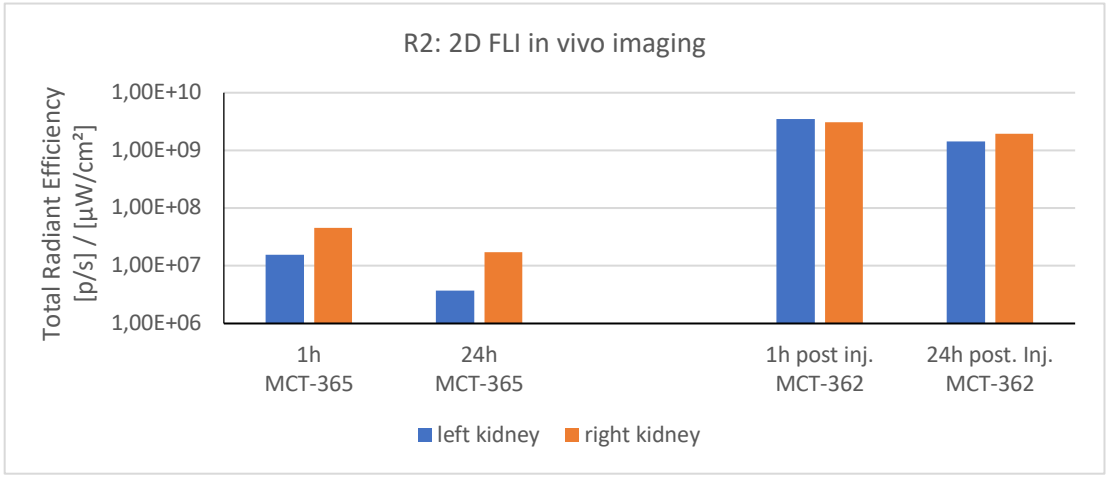

Figure 31 Diagram of exported ROI values from image sequence in prone position, illustrating values from one hour and twenty-four hours post injection of the formula into MCT-362 in relation to the control mouse, MCT-365.

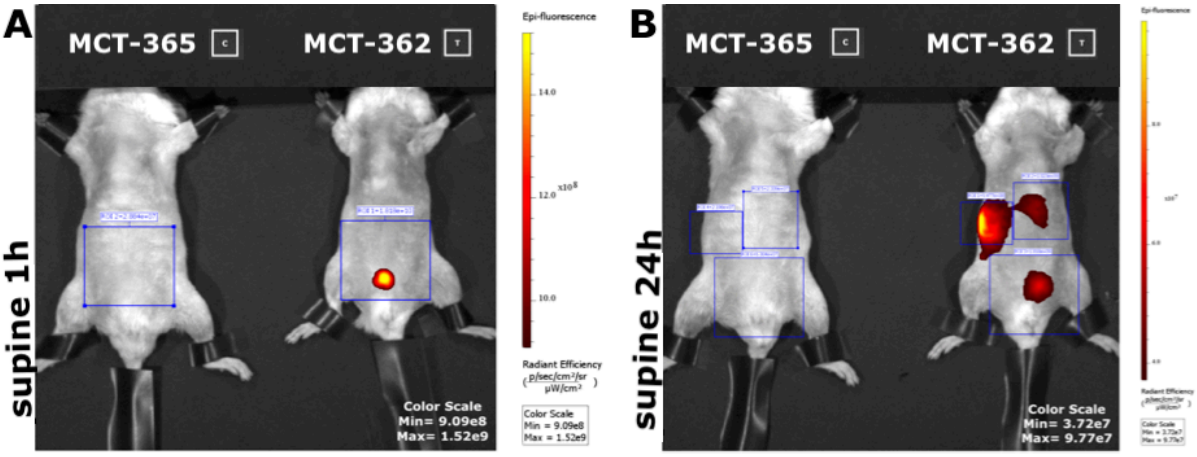

*Figure 32 2D FLI epiillumination mode with spectral unmixing image of mice placed in supine position showing left image **A** one hour and right image **B** presenting twenty-for hours post intravenous injection of AF750 labeled NC-siRNA into MCT-362 in comparison to the control mouse MCT-365. As the signal appearance additionally shows up in kidney area, a supplementary ROI around the kidneys fort MCT-362 is required.*

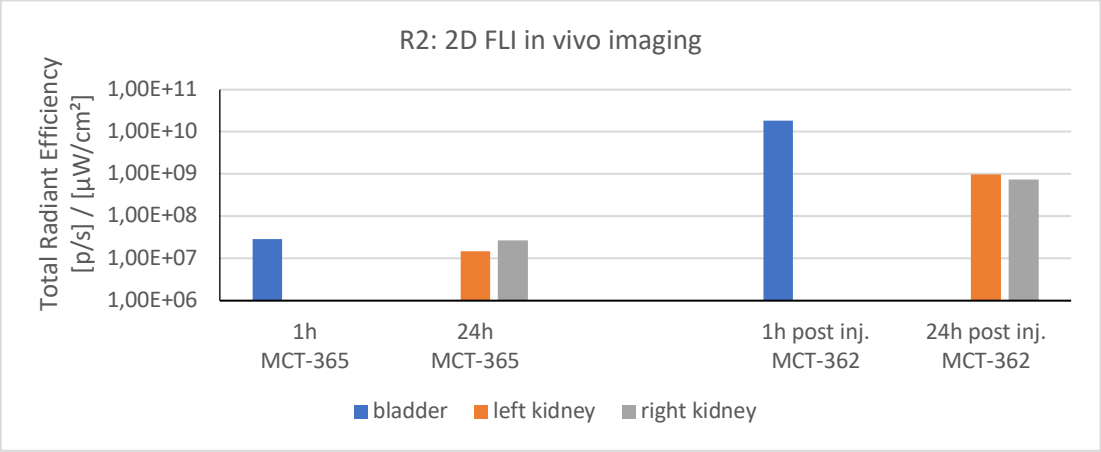

Figure 33 Diagram of exported ROI values from image sequence in supine position, illustrating values from one hour and twenty-four hours post injection of the formula into MCT-362 in relation to the control mouse, MCT-365.

In Figure 34 the obtained picture from ex vivo 2D FLI organ imaging is shown and demonstrates again good visible kidney signals in the treated mouse MCT-362.

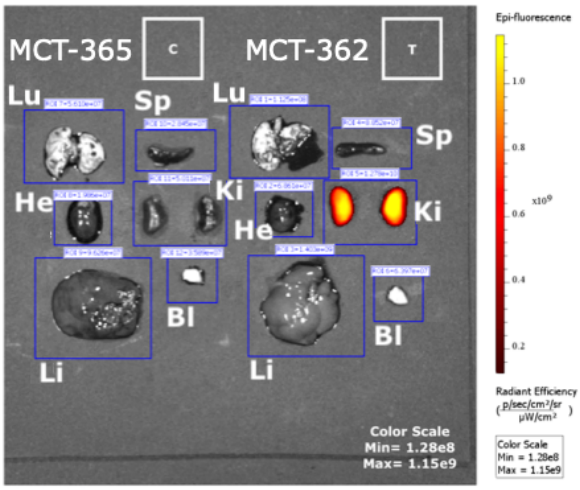

Figure 34 2D FLI epiillumination mode with filter pair ex vivo organ imaging after cervical dislocation and organ collection of Lu= lungs, He= heart, Li= liver, Sp=spleen, Ki= kidneys, Bl= bladder at a timepoint of approximately twenty-four hours after systemic administration of NC-siRNA into treated mice, MCT-362 in contrast to the non-treated control mouse, MCT-365.

Referring to Figure 35 which is a signal value overview from the organ imaging of round 2, MCT-363 is not comparable to the other treated mice, when talking about signal appearance It shows a high background signal in lung area. Moreover, the organ imaging was directly performed next to the control mouse, MCT-364, which also has a background signal in lung area. Having a look at Figure 35, which includes the exported

signal values from both mice, control (MCT-364) and treated (MCT-363), a very high signal is visible in comparison to the other mice. This strongly leads to the presumption of a possible error while imaging or in the data, due to the fact of having comparable high signal in treated mouse MCT-363 as in non-treated control mouse MCT-364.

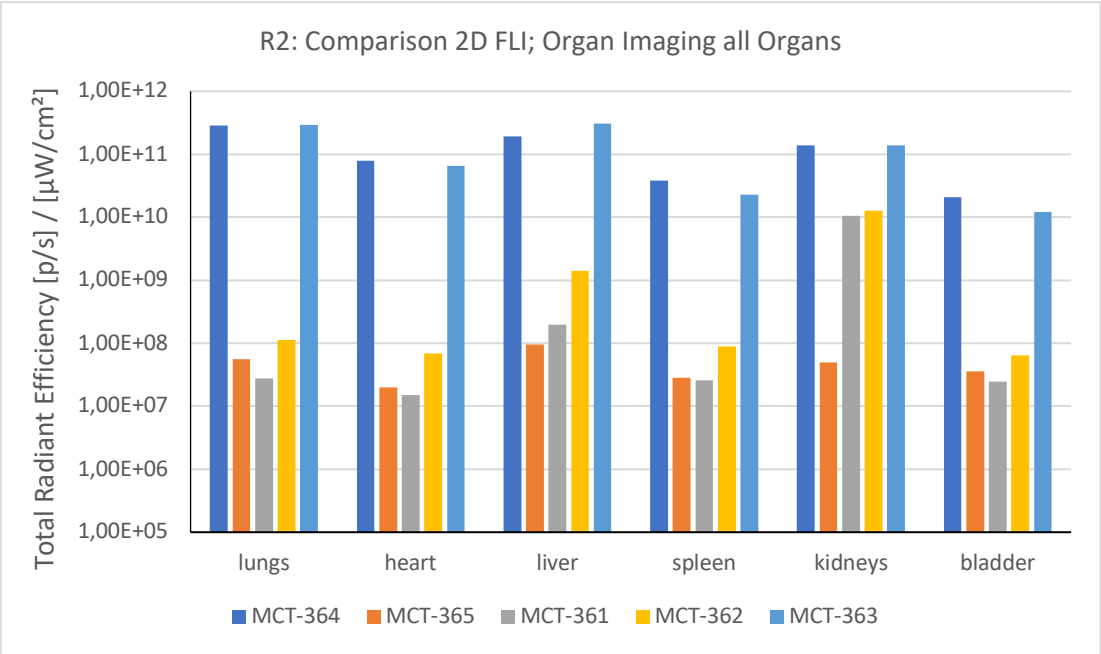

Figure 35 Diagram presenting signal values obtained from ex vivo 2D FLI organ imaging of MCT-361, MCT-362 and MCT-363, twenty four-hours post i.v. injection of the formula and comparison to the non-treated control mice, MCT-364 and MCT-365.

The investigation on behavior of biodistribution-pattern after systemic administration of AF750 labeled NC-siRNA was aimed to be pointed out, whether reproducibility could be shown and if similarities were to be found regarding biodistribution, by using the technique of 2D FLI imaging in vivo (position supine and prone) as well as ex vivo, by organ imaging.

Two different timepoints; one hour and twenty-four hours post injection of the formulation into the treated mice, should lead to a clarification of biodistribution pattern, further excretion potential. The results presented on the former pages, definitely lead to a clear signal evaluation in vivo as well sustained by the results obtained from ex vivo imaging. An obvious difference is visible in-between treated and non-treaded control mice, as latter do not show any signals. Concerning in vivo 2D FLI

imaging, a reproducible signal among the treated mice is available localized in the kidneys, when imaging prone position and a signal in the bladder, when imaging in supine position. Furthermore, these signals remain visible among both experimental time frames and no additional signals light up. This is an evidence of no change in the biodistribution pattern. Moreover, the signals obtained from ex vivo 2D FLI organ imaging show highest signals in kidneys and also in bladder, which sustain and correlate with the signal appearance obtained from in vivo imaging. This strengthens the fact of a renal excretion [26] of A750 labeled NC-siRNA, with no change of biodistribution pattern regarding the treated animals.

8.2 2D BLI based evaluation of splice correction after systemic application of SSO polyplexes

2D BLI based in vivo whole-body imaging and ex vivo organ imaging can be used for studying the potential of splice correction in Tg (Luc 705) Split-Luc mice after systemic injection of SSO cLPEI based polyplexes. The used mouse strain featured a firefly luciferase reporter gene, which is interrupted by a mutated human beta globin intron 2 which includes an aberrant splice site at nucleotide 705. This results in a non-functional reporter gene. SSO should restore the aberrant splice site and lead to a functional reporter gene outcome, capturable via 2D BLI which was aimed to be demonstrated in this experiment. Furthermore, localization of SSO delivery was aimed to be investigated. Therefore, a total amount of four mice were intravenously injected with Luc SSO cLPEI based polyplexes and categorized as the treated group. As a treatment control, two mice served as negative controls and non-coding cLPEI based SSO polyplexes were systemically administered. In general, in vivo 2D BLI whole-body imaging was performed in supine position including following timeframes; pre-SSO treatment, twenty-four- and forty-eight-hours post injection of the formula for both groups. Afterwards mice underwent a cervical dislocation under deep anesthesia and their organs were collected and ex vivo 2D BLI organ imaging was done.

8.2.1 Animals injected with Luc-SSO cLPEI Polyplex

MCT-168

The results obtained from whole body 2D BLI imaging, visualized in Figure 36 and Figure 37, show signal in abdominopelvic area and its intensity increased at the last imaging time point. The localization of the signal area remains same over the experimental time frame. Thus, the exported ROI signal values shown in the diagram of Figure 37 do not point out any huge signal intensity elevation comparing first experimental time-frame as pre-treatment and last experimental time-point as forty-eight-hour post i.v. injection.

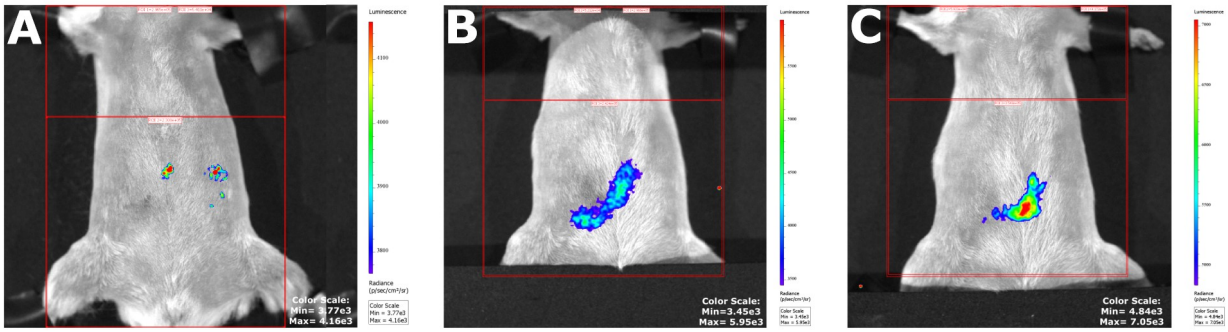

*Figure 36 2D BLI in vivo imaging of MCT-168 in supine position after i.v. injection of 329µl Luc-SSO cLPEI NP9 in HBG. Pictures taken in 2D BLI time series study mode showing highest signal of the mouse from **A** pre-treatment, **B** twenty-four hours and **C** forty-eight hours post injection of the formulation. The picture here implements three ROIs, a whole body ROI, another ROI covering thoracic area and lastly ROI over abdominopelvic area.*

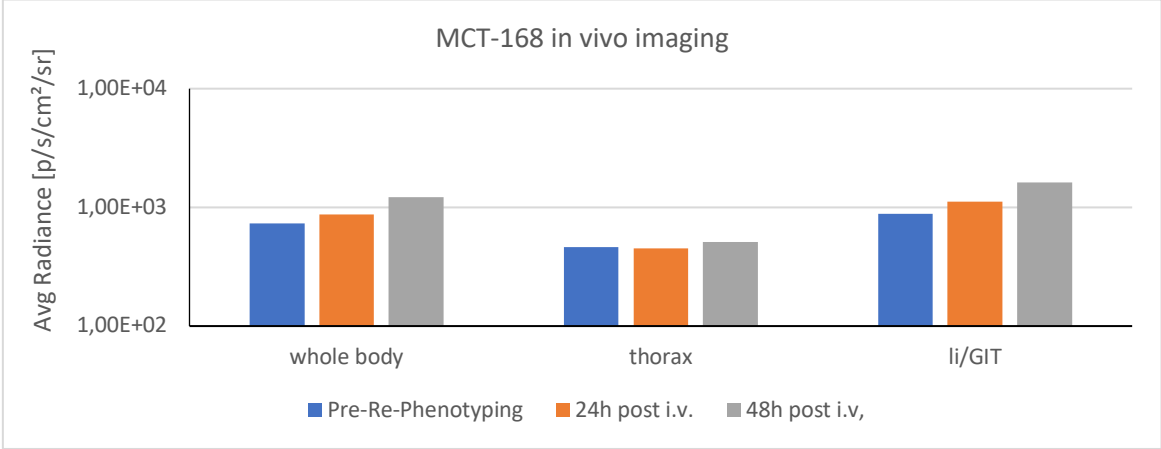

Figure 37 Diagram comparing in vivo 2D BLI whole body imaging of MCT-168 at different time points: pre-treatment, twenty-four hours and forty-eight hours post i.v. injection of the formulation.

In contrast to the in vivo 2D BLI whole body imaging, in which clear signal spots could be visualized in the abdominopelvic area over the whole experimental time frame, the ex vivo 2D BLI organ imaging, presented in Figure 38, did not show any BLI signals and appears to be within the background as shown in the plotted graph.

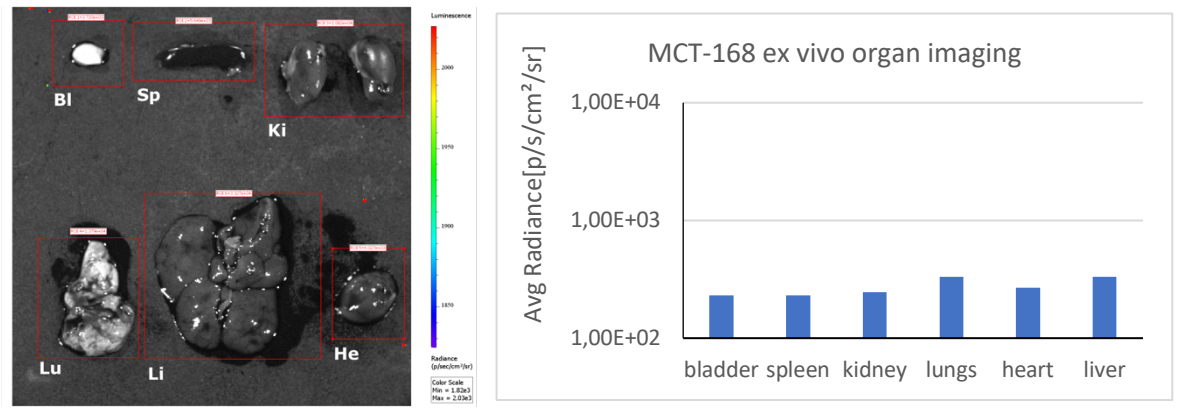

Figure 38 Ex vivo 2D BLI organ imaging and diagram of exported ROI values of MCT-168, Left sided: ex vivo 2D BLI organ imaging picture of forty-eight hours post i.v. injection of the formulation and after cervical dislocation followed by organ collection showing below imaged organs: bl= bladder, sp= spleen, Ki= kidneys, Lu= Lungs, Li= liver, He= heart. Right sided: diagram presenting signals deviated from ex vivo 2D BLI organ imaging of MCT-168, forty-eight hours post i.v. injection of the formula.

MCT-169

MCT-169 demonstrates by in vivo 2D BLI whole body imaging an increasing signal within the imaging time points. This is visible in Figure 39 and Figure 40. Evaluation of signal in the same areas and its intensity elevates in comparison to the pre-treatment imaging time point. The signal appears to be in the thoracic and abdominopelvic area.

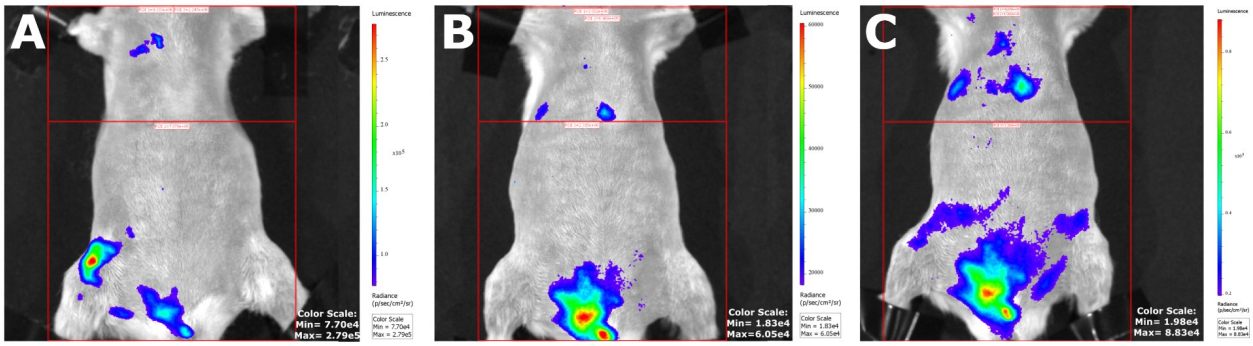

*Figure 39 2D BLI in vivo imaging of MCT-169 in supine position after i.v. injection of 363µl Luc-SSO cLPEI NP9 in HBG. Pictures taken in 2D BLI time series study mode showing highest signal of the mouse from **A** pre-treatment, **B** twenty-four hours and **C** forty-eight hours post injection of the formulation. The picture here implements three ROIs, a whole body ROI, another ROI covering thoracic area and lastly ROI over abdominopelvic area.*

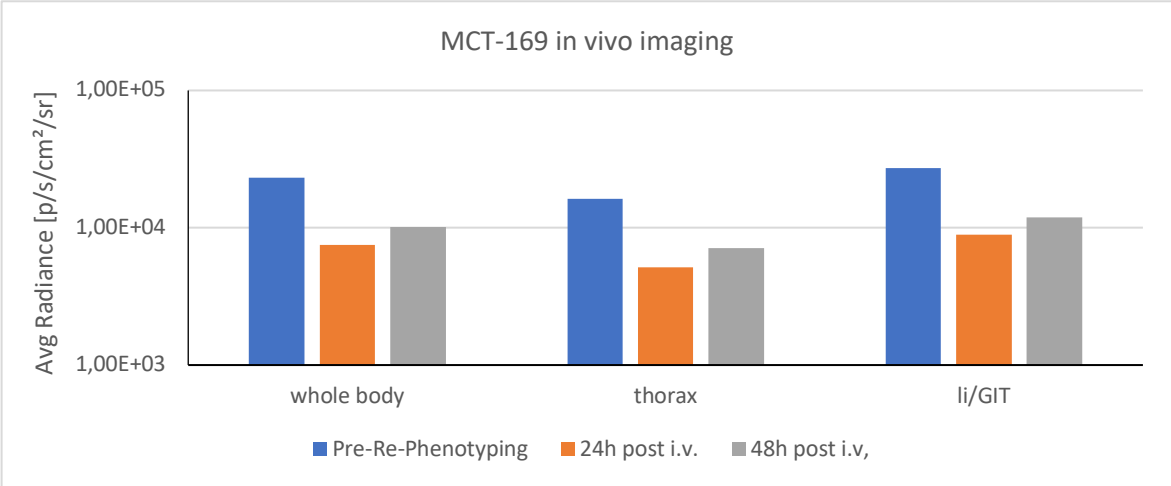

Figure 40 Diagram comparing in vivo 2D BLI whole body imaging of MCT-169 at different time points: pre-treatment,, twenty-four hours and forty-eight hours post i.v. injection of the formulation.

Additionally, results from the ex vivo 2D BLI organ imaging, which are visualized in Figure 41, highlight the outcome obtained in whole body in vivo imaging. Clear signals in bladder and lungs are visible which may give a hint about localization of splice correction. As signal intensity increases in in vivo imaging in thoracic and

abdominopelvic area and is sustained by high signals in ex vivo imaging showed in lungs and bladder.

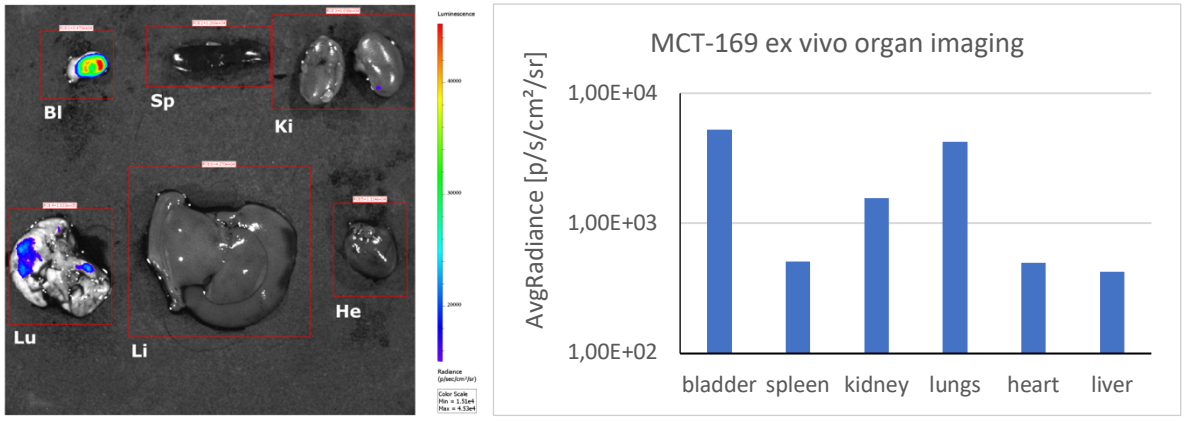

Figure 41 Ex vivo 2D BLI organ imaging and diagram of exported ROI values of MCT-169, Left sided: ex vivo 2D BLI organ imaging picture forty-eight hours post i.v. injection of the formulation and after cervical dislocation followed by organ collection showing below imaged organs: bl= bladder, sp= spleen, Ki= kidneys, Lu= Lungs, Li= liver, He= heart. Right sided: diagram presenting signals deviated from ex vivo 2D BLI organ imaging of MCT-169, forty-eight hours post i.v. injection of the formula.

MCT-185

Monitoring the signal pattern MCT-185 shows just a small signal spot before treatment situated on the right lower thoracic area and abdominopelvic area, visible in Figure 42, A. The signal increases in intensity at the end of the experimental time frame shown in Figure 42, C. Moreover, signal formation in abdominopelvic area can be observed which matches with the above presented signal pattern in the former presented results from in vivo imaging of MCT-169, Figure 39.

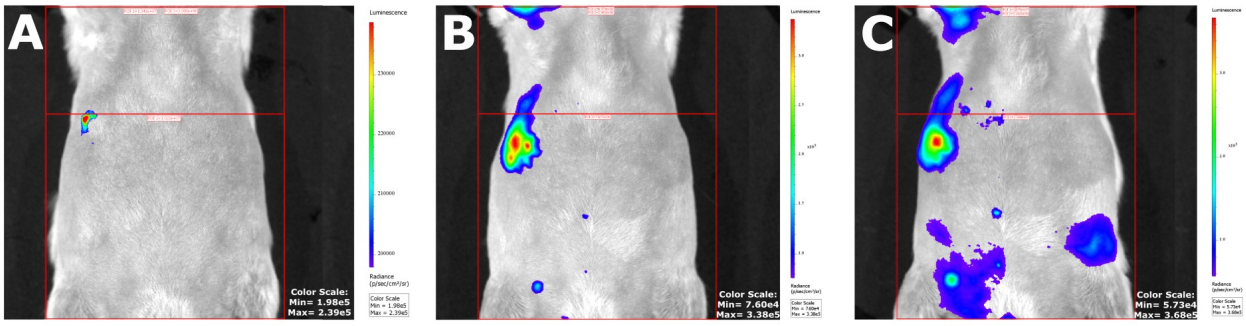

*Figure 42 2D BLI in vivo imaging of MCT-185 in supine position after i.v. injection of 508 µl Luc-SSO cLPEI NP9 in HBG. Pictures taken in 2D BLI time series study mode showing highest signal of the mouse from **A** pre-treatment, **B** twenty-four hours and **C** forty-eight hours post injection of the formulation. The picture here implements three ROIs, a whole body ROI, another ROI covering thoracic area and lastly ROI over abdominopelvic area.*

The exported ROI signals from Figure 42, which are illustrated in the diagram from Figure 43, do not indicate a splice correction linked to an expected signal elevation as

the diagram bars show similar height at the beginning and end of the experiment. However, organ imaging does indicate clear presence of luciferase activity in lungs and bladder, as observed in Figure 44 and thus validates observation from whole body imaging.

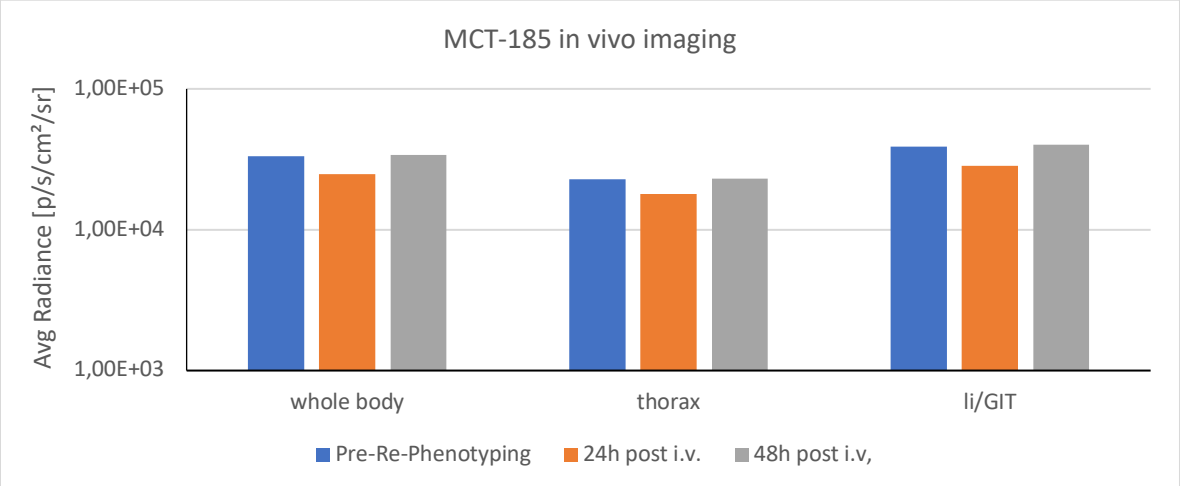

Figure 43 Diagram comparing in vivo 2D BLI whole body imaging of MCT-185 at different time points: pre-treatment, twenty-four hours and forty-eight hours post i.v. injection of the formulation.

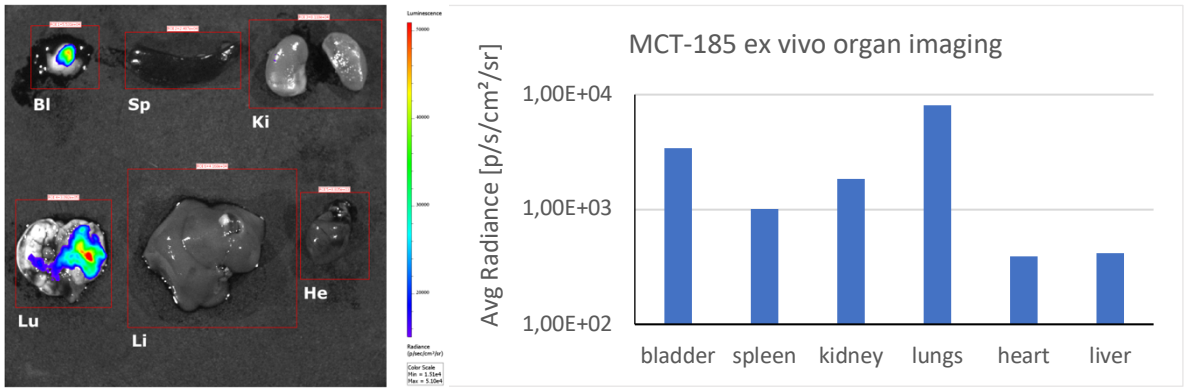

Figure 44 Ex vivo 2D BLI organ imaging and diagram of exported ROI values of MCT-185. Left sided: ex vivo 2D BLI organ imaging picture forty-eight hours post i.v. injection of the formulation and after cervical dislocation followed by organ collection showing below imaged organs: bl= bladder, sp= spleen, Ki= kidneys, Lu= Lungs, Li= liver, He= heart. Right sided: diagram presenting signals deviated from ex vivo 2D BLI organ imaging of MCT-185, forty-eight hours post i.v. injection of the formula.

MCT-186

In vivo 2D BLI whole body imaging from MCT-186, illustrated in Figure 45, does not show a comparable signal pattern to the above presented mice, considering a signal evaluation, as the signals here are pretty equal over the whole experimental time frame. Additionally, the corresponding exported ROI values from MCT-186, shown in Figure 46, do not indicate a significant signal elevation.

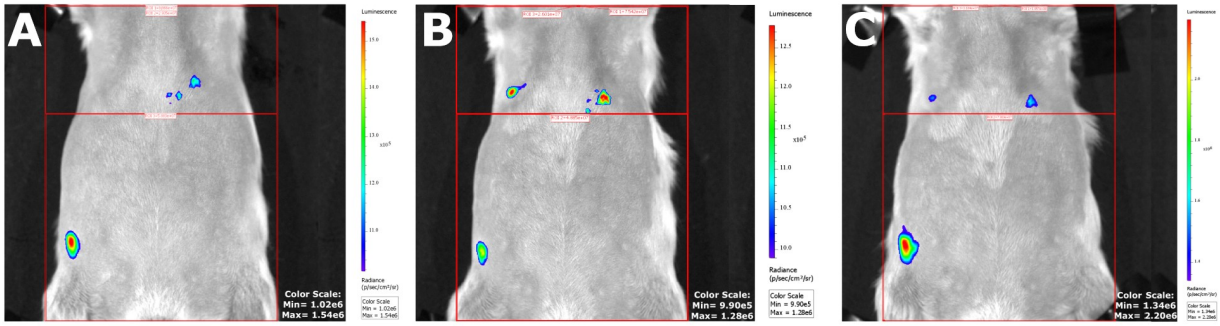

*Figure 45 2D BLI in vivo imaging of MCT-186 in supine position after i.v. injection of 479 µl Luc-SSO cLPEI NP9 in HBG. Pictures taken in 2D BLI time series study mode showing highest signal from **A** pre-treatment, **B** twenty-four hours and **C** forty-eight hours post injection of the formulation of the mouse. The picture here implements three ROIs, a whole body ROI, another ROI covering thoracic area and lastly ROI over abdominopelvic area.*

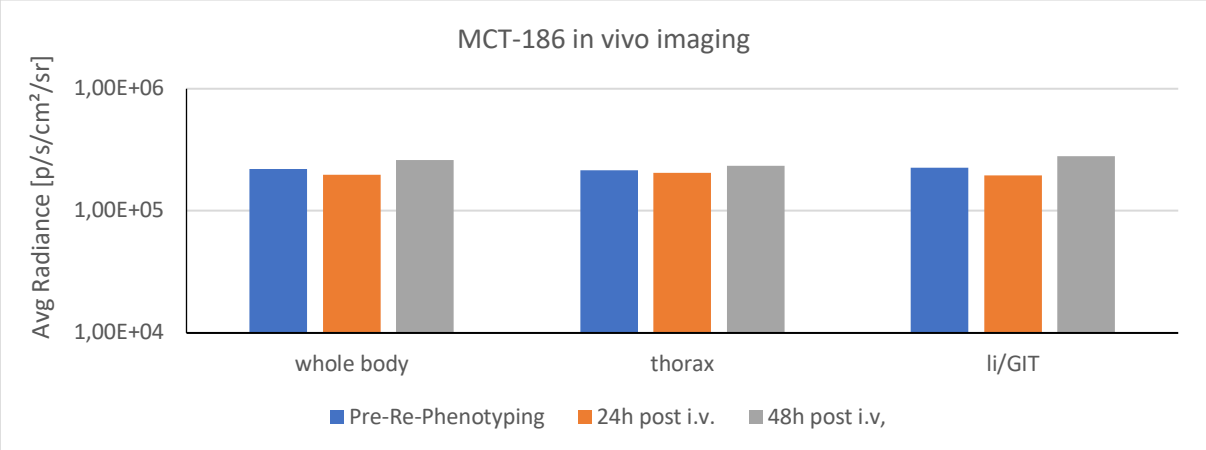

Figure 46 Diagram comparing in vivo 2D BLI whole body imaging of MCT-186 at different time points: pre-treatment, twenty-four hours and forty-eight hours post i.v. injection of the formulation.

In contrast to the in vivo 2D BLI whole body imaging, Figure 45, which does not provide any kind of visible signal elevation over the different imaging time points, the ex vivo 2D BLI organ imaging visible in Figure 47, enables visualization of clear signal existence in lungs and bladder.

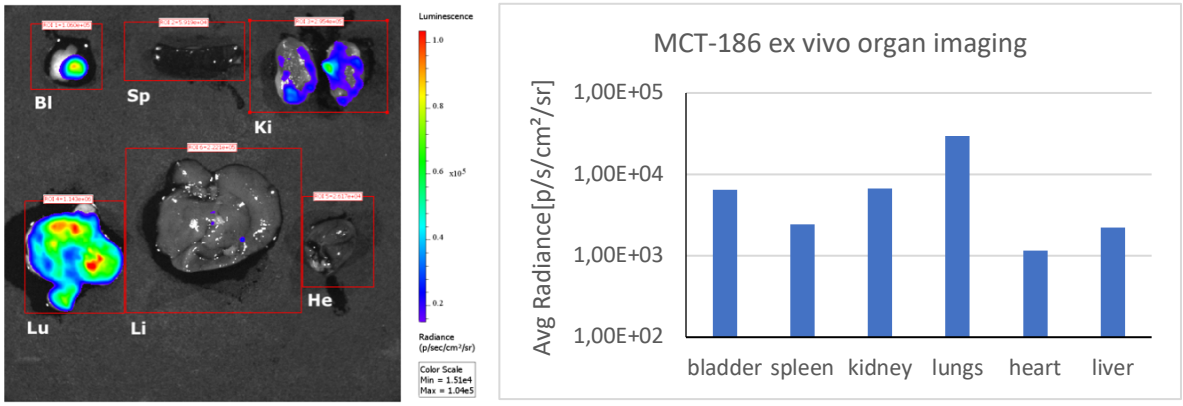

Figure 47 Ex vivo 2D BLI organ imaging and diagram of exported ROI values of MCT-186. Left sided: ex vivo 2D BLI organ imaging picture forty-eight hours post i.v. injection of the formulation and after cervical dislocation followed by organ collection showing below imaged organs: bl= bladder, sp= spleen, Ki= kidneys, Lu= Lungs, Li= liver, He= heart. Right sided: diagram presenting signals deviated from ex vivo 2D BLI organ imaging of MCT-186, forty-eight hours post i.v. injection of the formula.

As conclusion, in vivo 2D BLI whole body imaging does not provide a clear direction for interpretation but organ imaging does. It is clearly visible that ex vivo 2D BLI organ imaging enables investigating localization of SSO delivery, as the process of splice correction results in an increased signal capturable via 2D BLI. All treated animals, which got intravenously injected with Luc-SSO cLPEI formula show high signals in bladder and lung area forty-eight hours post i.v. injection and after cervical dislocation, followed by organ collection and ex vivo 2D BLI organ imaging. Figure 48 compares luciferase signals across animals and shows high signal intensity in lungs and bladder area among the treated animal group.

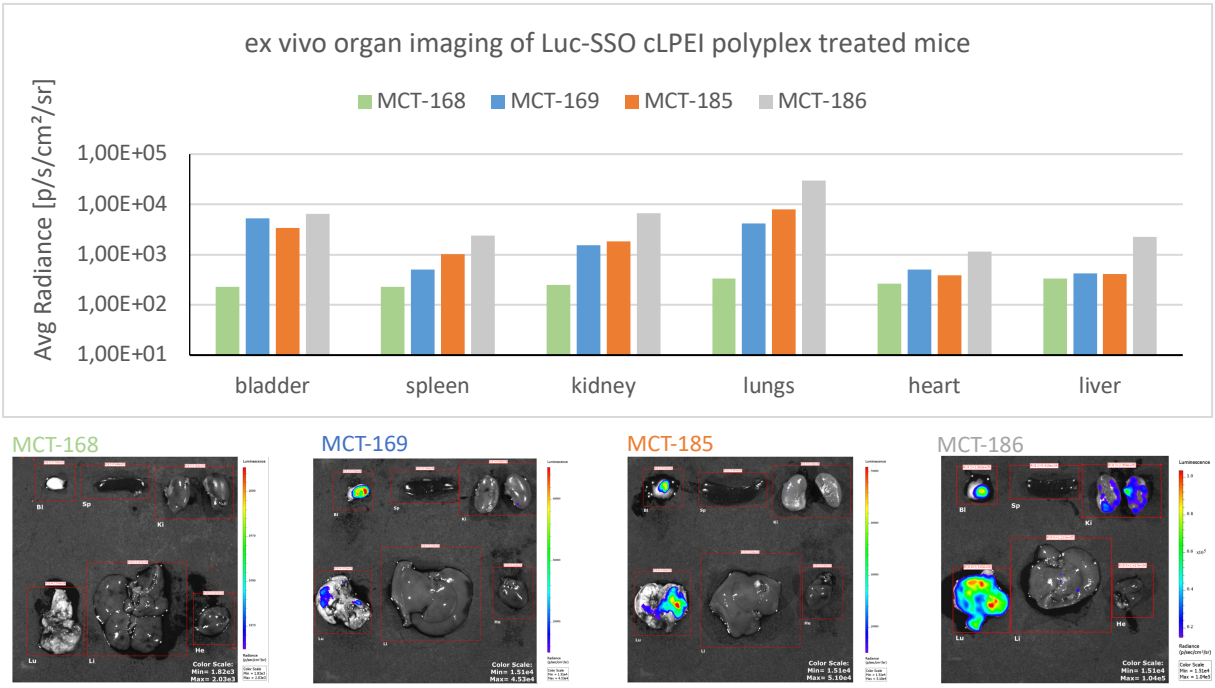

Figure 48 Comparison of ex vivo 2D BLI organ imaging of all mice, forty-eight hours post intravenous injection of Luc-SSO cLPEI polyplex. Presentation of data in diagram and below for each mouse its picture deriving from organ imaging.

8.2.2 Animals injected with Non coding-SSO cLPEI Polyplex

MCT-165

Neither in vivo 2D BLI whole body imaging shown in Figure 49 and Figure 50, nor ex vivo 2D BLI organ imaging presented in Figure 51, enable a visualization of signal among the experimental time frame. Especially the organ imaging, which does not show any differences in signal intensities among the organs, brings up the hint that no splice correction occurred. This result was aimed as this group served as a control group and no splice correction was expected.

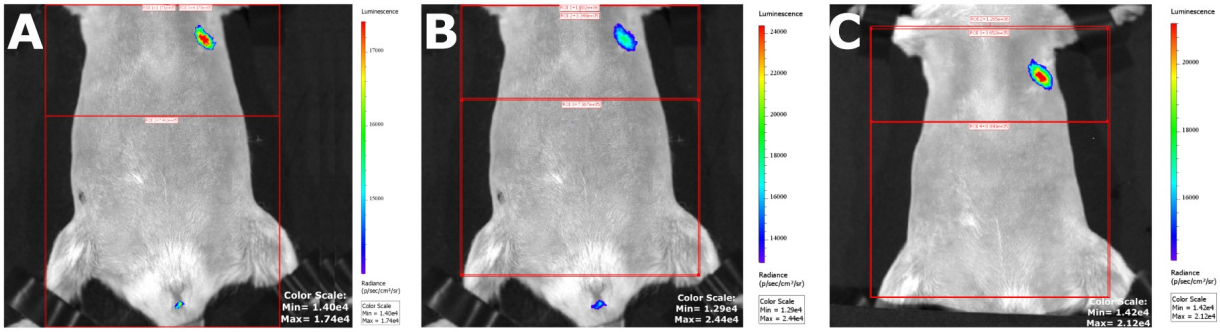

*Figure 49 2D BLI in vivo imaging of MCT-165 in supine position after i.v. injection of 408 µl Non coding-SSO cLPEI NP9 in HBG. Pictures taken in 2D BLI time series study mode showing highest signal of the mouse from **A** pre-treatment, **B** twenty-four hours and **C** forty-eight hours post injection of the formulation. The picture here implements three ROIs, a whole body ROI, another ROI covering thoracic area and lastly ROI over abdominopelvic area.*

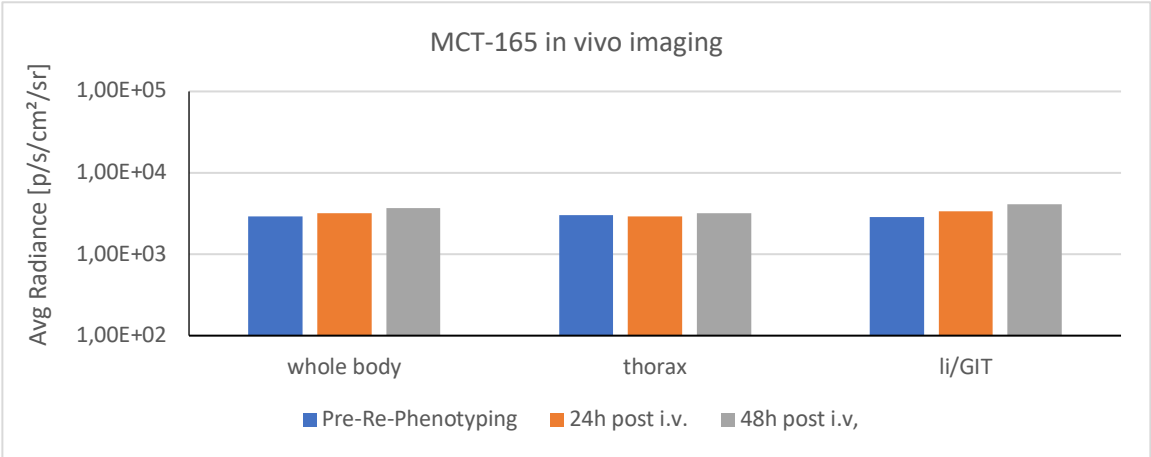

Figure 50 Diagram comparing in vivo 2D BLI whole body imaging of MCT-165 at different time points: pre-treatment, twenty-four hours and forty-eight hours post i.v. injection of the formulation.

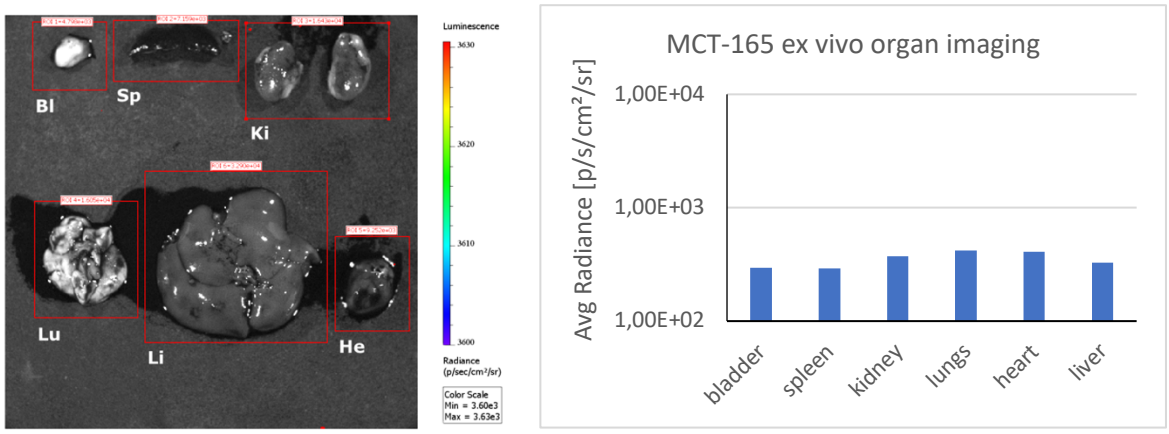

Figure 51 *Ex vivo 2D BLI organ imaging and diagram of exported ROI values of MCT-165. Left sided: ex vivo 2D BLI organ imaging picture forty-eight hours post i.v. injection of the formulation and after cervical dislocation followed by organ collection showing below imaged organs: bl= bladder, sp= spleen, Ki= kidneys, Lu= Lungs, Li= liver, He= heart. Right sided: diagram presenting signals deviated from ex vivo 2D BLI organ imaging of MCT-165, forty-eight hours post i.v. injection of the formula.*

MCT-171

MCT-171 shows similar signal of in vivo 2D BLI whole body imaging among the experimental time frame, which is visible in Figure 52 and Figure 53. It is not comparable to the former presented mouse from the same group, MCT-165 shown in Figure 49. Moreover, the signal pattern of MCT-171 can be dedicated to the Luc-SSO cLPEI polyplex group based on signal behavior, although it was intravenously injected with non-coding SSO cLPEI polyplex aiming for no splice correction.

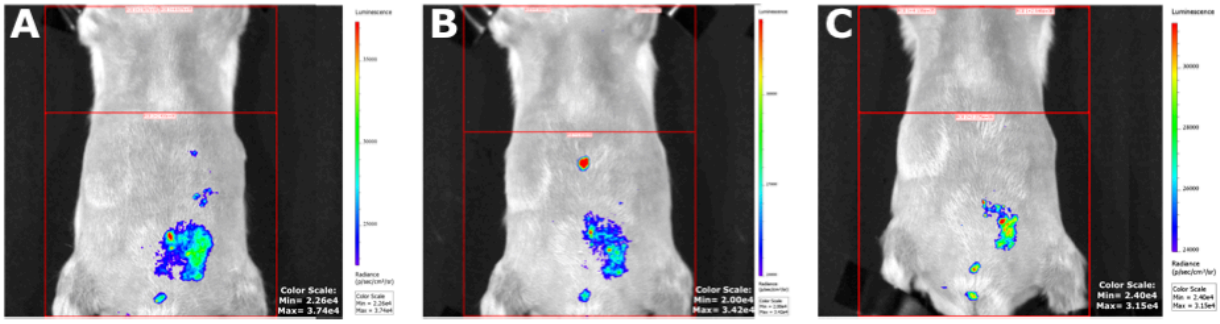

*Figure 52 2D BLI in vivo imaging of MCT-171 in supine position after i.v. injection of 374 µl Non coding-SSO cLPEI NP9 in HBG. Pictures taken in 2D BLI time series study mode showing highest signal of the mouse from **A** pre-treatment, **B** twenty-four hours and**C** forty- eight hours post injection of the formulation.*

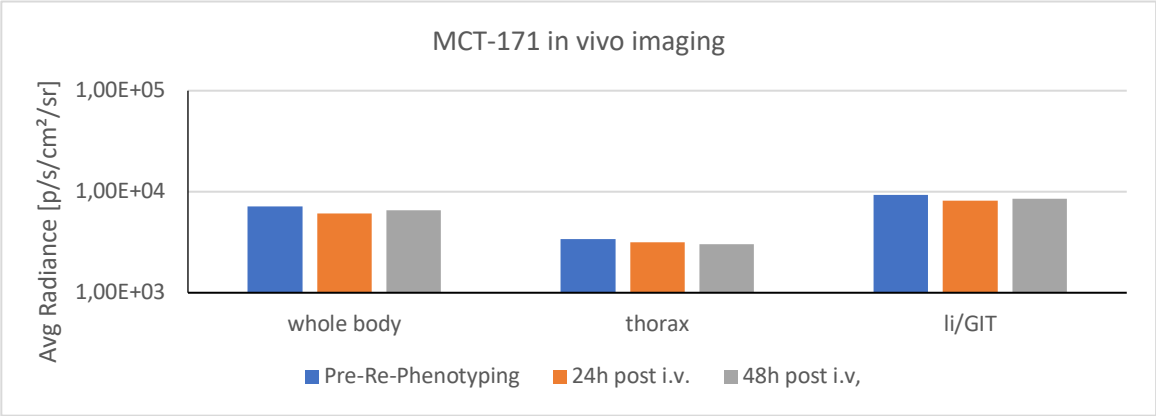

Figure 53 Diagram comparing in vivo 2D BLI whole body imaging of MCT-171 at different time points: pre-treatment, twenty-four hours and forty-eight hours post i.v. injection of the formulation.

In ex vivo 2D BLI organ imaging, there seems to be a slight signal in lungs, liver and bladder, as they result in the same intensity range of log three. Results from MCT-171 ex vivo 2D BLI imaging are presented in Figure 54. In Figure 54, the ex vivo 2D BLI outcomes are captured pointing out a visible red spot located in the lung an also a red spot located in the liver for MCT-171. Moreover, signal appearance is not underpinned by the exported ROI values, as liver demonstrates a weaker signal thank bladder which does not visualize any visible spot in Figure 54 from organ imaging.

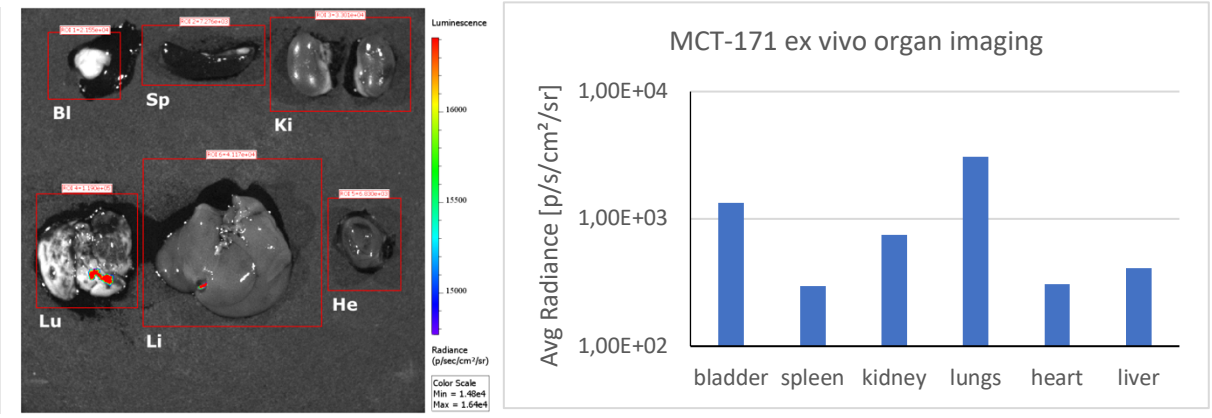

Figure 54 Ex vivo 2D BLI organ imaging and diagram of exported ROI values of MCT-171. Left sided: ex vivo 2D BLI organ imaging picture forty-eight hours post i.v. injection of the formulation and after cervical dislocation followed by organ collection showing below imaged organs: bl= bladder, sp= spleen, Ki= kidneys, Lu= Lungs, Li= liver, He= heart. Right sided: diagram presenting signals deviated from ex vivo 2D BLI organ imaging of MCT-171, forty-eight hours post i.v. injection of the formula.

All in all regarding the group which received Luc SSO cLPEI based polyplexes, a characteristic signal pattern was witnessed. A slight decrease of the whole-body signal which was then followed by an increase in comparison to the initial ground state was visible. Moreover, these signals differed in intensity among the mice and were not that

high. The signal emitting areas were mainly thoracic and abdominopelvic area indicative and did not lead to a concrete direction of conclusion, where SSO delivery and splice correction possibly occurred concerning the obtained results from in vivo 2D BLI whole body imaging.

Referring to the results obtained from ex vivo 2D BLI organ imaging a more precise direction of interpretation could be given. Clear reproducible signals seem to be received, as lung and bladder light up with the highest intensity among the organs.
Therefore, not only a comparable splice correction could be pointed out, by aiming a signal elevation via in vivo 2D BLI whole body imaging, but also a localization of SSO delivery situated in lungs and bladder area could be demonstrated via ex vivo 2D BLI organ imaging. Linked to it, there was also a signal enhancement expected by theory. Wherever Luc-SSO were delivered, an increased signal was estimated. This strengthens the fact of a successful splice correction, as the findings are comparable to Resina et al. . [29]
Signal appearance in lungs and bladder is representable among the group which got intravenous injected with Luc-SSO cLPEI polyplex and was applicable to three out of the four mice, as one mouse did not show up any signal in the organ imaging. Regarding this mouse it is assumable that the signal was in in general too weak to be taken as significant, as the in vivo imaging results seem to be also just GIT background signals.

As a conclusion the Luc SSO cLPEI based polyplex treated mice show a slight increase regarding in vivo imaging which is not that revealing but in combination with the ex vivo imaging, a meaningful fact on splice correction and SSO delivery into lungs and bladder could be pointed out. However, which value can be marked as significant for assessing the splice correction is unenlightened as the number of mice is too less to permit the performance of a statistical test. Concerning the results from the non-coding cLPEI based SSO group, which served as a negative control and therefore no signal was estimated. When comparing the two mice treated with non-coding SSO cLPEI polyplex, MCT-171 appears to have slight different outcome in terms of signals in lungs and bladder. This could be the variation of signal intensities across mice and also across different intensities of transgene expression (uncorrected).

Following graph, shown in Figure 55, confirms the differences among both animal groups and sustains the proof of signal enrichment in lungs and bladder among Luc-SSO cLPEI polyplex treated group in comparison to the non-coding SSO cLPEI polyplex group.

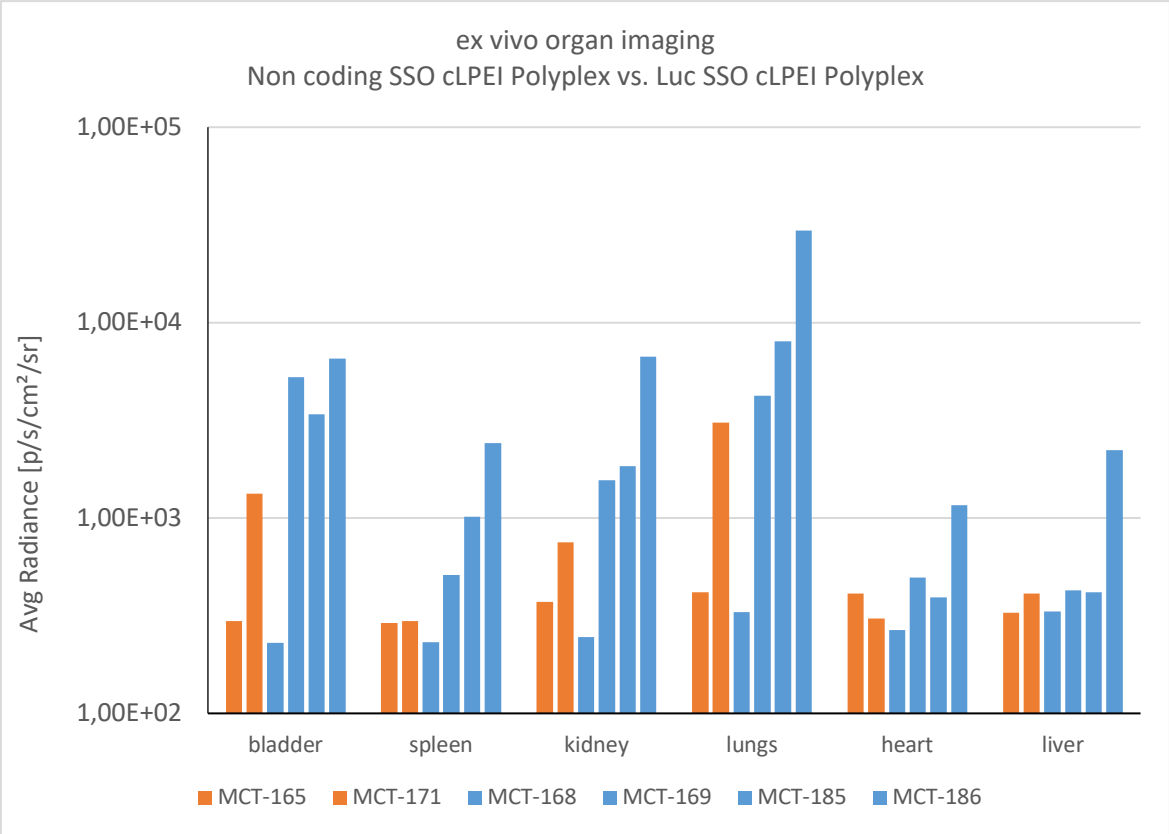

Figure 55 Diagram comparing ROI data from ex vivo 2D BLI organ imaging from non-coding SSO cLPEI polyplex treated group (MCT-165 and MCT-171) and Luc-SSO cLPEI polyplex treated group (MCT-168, MCT-169, MCT-185, MCT-186)

8.3 Investigation of transgenic gene expression in Tg SpC-Luc mouse strain by 2D BLI

The Tg SpC mouse strain has the luciferase reporter gene expression cassette under control of the SFTPC promoter, with an estimated restricted expression in the respiratory epithelium. [43] Due to the fact that evidence of findings of the SpC not only in lungs but also in skin [44], the evaluation of localization of transgenic gene expression was pointed out in this experiment.

A total amount of six-teen mice of the Tg SpC strain were used and divided into two groups. For group one the process was in vivo 2D BLI whole body imaging, and then mice were dissected and an ex vivo 2D BLI organ imaging was performed to validate the presence of absence of luciferase expression. The second group was imaged in vivo 2D BLI whole body and afterwards taken for intra tracheal fixation and thus no ex vivo validation was possible. Results in this section are obtained from in vivo 2D BLI whole body imaging (for group one and two) and afterwards ex vivo 2D BLI organ imaging (for group one) after sub cutaneous injection of the luciferase reporter genes substrate, luciferin. The injection was given sub cutaneous into the right flank to maintain reproducibility and avoid a signal overlapping in lungs which might have led to a higher signal if substrate injection was given in neck.

8.3.1 Group 1: Normal organ collection

TG (-) PH (+)

Following mentioned mice were categorized as transgenic negative (TG (-)) and phenotype positive (PH (+)). Figure 56 and Figure 57 refer to the results obtained from mouse MCT-196. Signal values for whole body and lungs obtained from in vivo imaging are equally high and additionally ex vivo organ imaging does not show any significant signal evaluation as the intensity is in a range of log two to three. Therefore, it is assumable that the mice has no luciferase expression as it is also genotypically negative. As a contrast Figure 58, Figure 59 and Figure 60 present the outcome for mouse MCT-242. Findings for mouse MCT-238 are visualized in Figure 61, Figure 62 and Figure 63. Referring to MCT-242 and MCT-238 the deriving signals are above log six. Moreover, ex vivo organ imaging results, Figure 60 for MCT-242 and Figure 63 for

MCT-238, highlight a higher luciferase expression not only in lungs detectable but also in skin. Thus, surprisingly, mice MCT-242 and MCT-238 show presence of luciferase signal in ex vivo organ imaging despite their genotypically negative status.

MCT-196

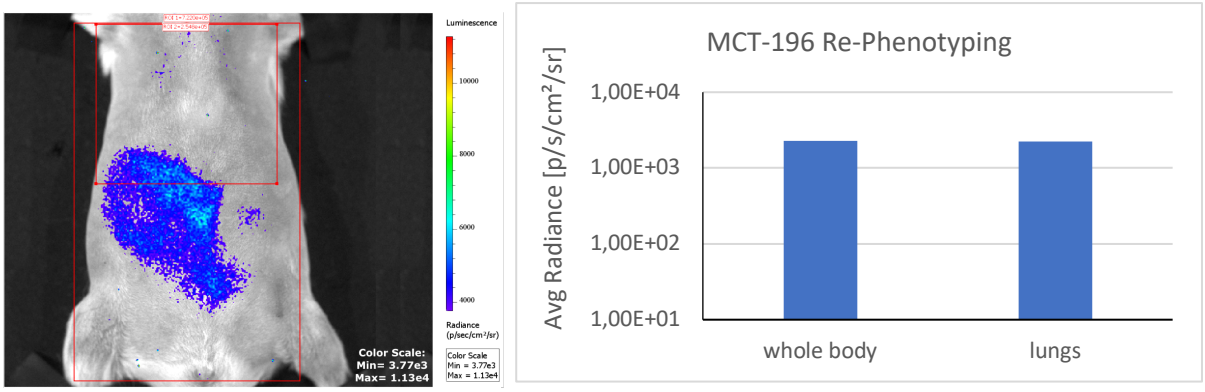

Figure 56 On the left side in vivo 2D BLI imaging picture performed in time series study mode of MCT-196 in supine position after s.c. injection of Luciferine into the right flank. Export of the image with highest whole-body signal deriving from the time series study sequence. Placed on the right side, the corresponding diagram, containing ROI values exported from mentioned image.

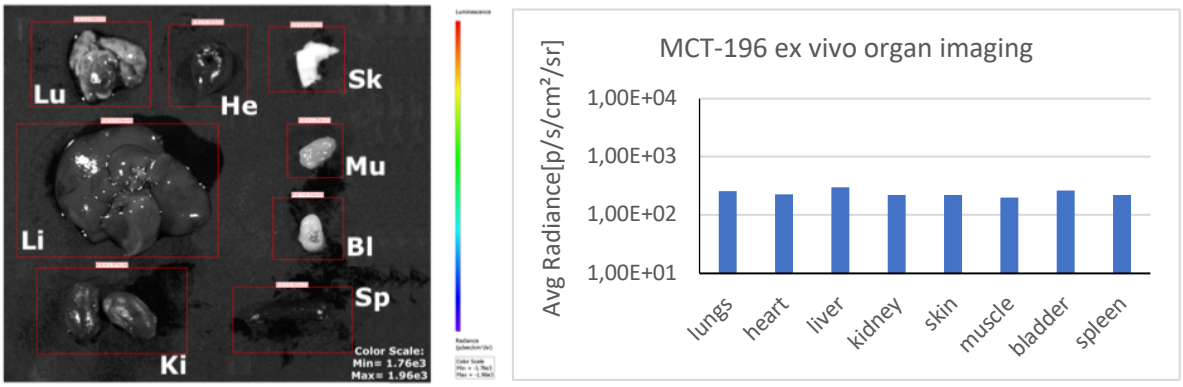

Figure 57 Left sided the ex vivo 2D BLI organ imaging of Lu=lungs, He= heart, Sk=skin, Li= liver, Mu= muscle, Bl= bladder, Ki= kidneys and spleen of MCT-196. Organ collection procedure after second s.c. injection of Luciferine into the right flank awaiting for kinetics, approximately ten minutes, and cervical dislocation among deep anesthesia. Right situated the referring diagram with the exported ROI values deriving from mentioned organ imaging.

MCT-242

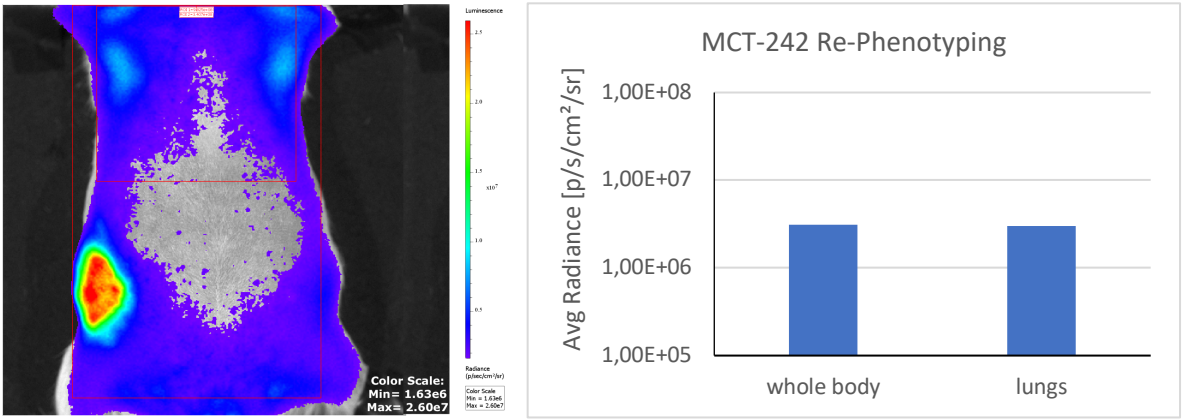

Figure 58 On the left side in vivo 2D BLI imaging picture performed in time series study mode of MCT-242 in supine position after s.c. injection of Luciferine into the right flank. Export of the image with highest whole-body signal deriving from the time series study sequence. Placed on the right side, the corresponding diagram, containing ROI values exported from mentioned image.

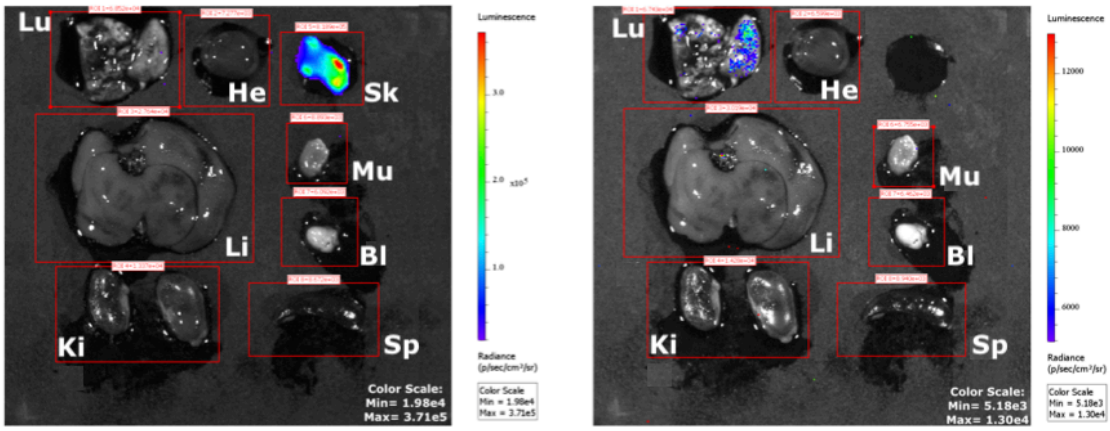

Figure 59 Left sided the ex vivo 2D BLI organ imaging of Lu=lungs, He= heart, Sk=skin, Li= liver, Mu= muscle, Bl= bladder, Ki= kidneys and spleen of MCT-242. Organ collection procedure right after second s.c. injection of Luciferine into the right flank awaiting for kinetics, approximately ten minutes, and cervical dislocation among deep anesthesia. Right situated, re-organ imaging of mentioned organs among exclusion of skin, as it showed highest signal. Moreover, a possible signal overlay and therefore an apparent signal leak in other organs aimed to be avoided.

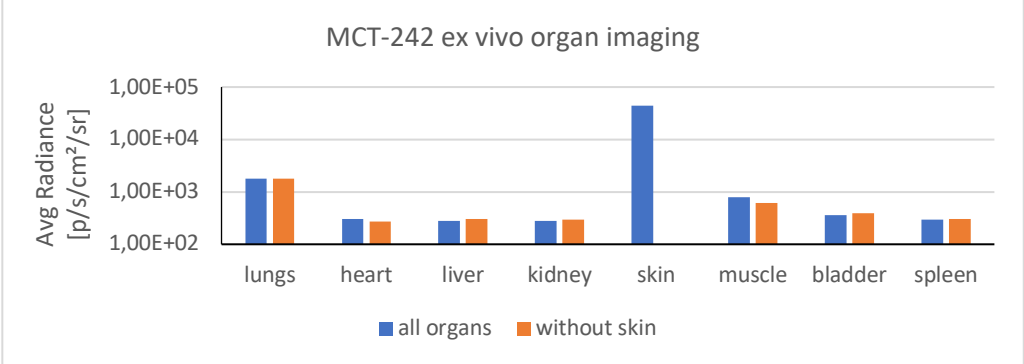

Figure 60 Diagram containing data from exported ROI values deriving from Figure 59 comparing ex vivo 2D BLI organ imaging of all organs vs. exclusion of skin.

MCT-238

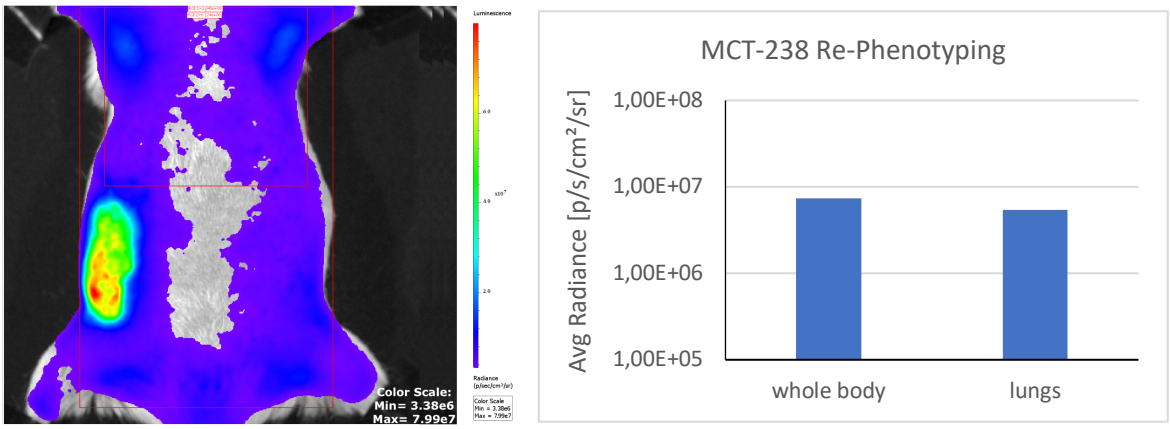

Figure 61 On the left side in vivo 2D BLI imaging picture performed in time series study mode of MCT-238 in supine position after s.c. injection of Luciferine into the right flank. Export of the image with highest whole-body signal deriving from the time series study sequence. Placed on the right side, the corresponding diagram, containing ROI values exported from mentioned image.

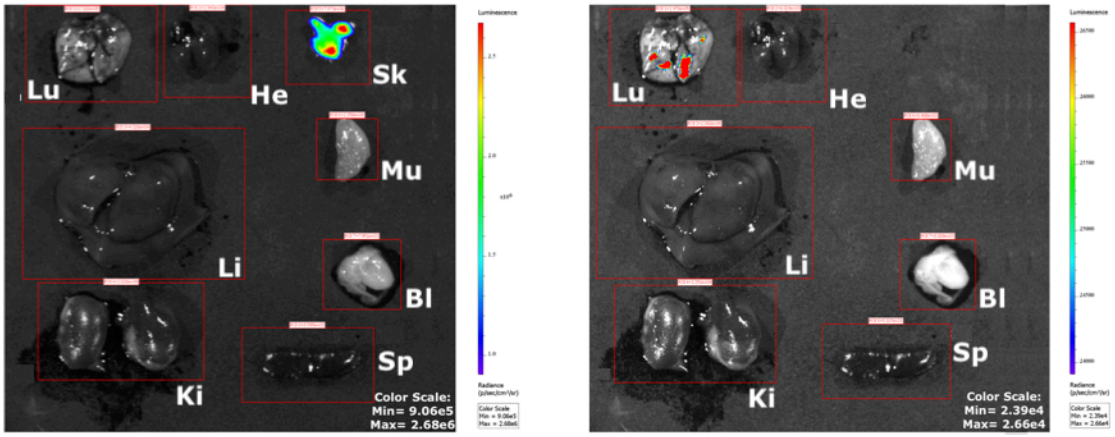

Figure 62 Left sided the ex vivo 2D BLI organ imaging of Lu=lungs, He= heart, Sk=skin, Li= liver, Mu= muscle, Bl= bladder, Ki= kidneys and spleen of MCT-238. Organ collection procedure right after second s.c. injection of Luciferine into the right flank awaiting for kinetics, approximately ten minutes, and cervical dislocation among deep anesthesia. Right situated, re-organ imaging of mentioned organs among exclusion of skin.

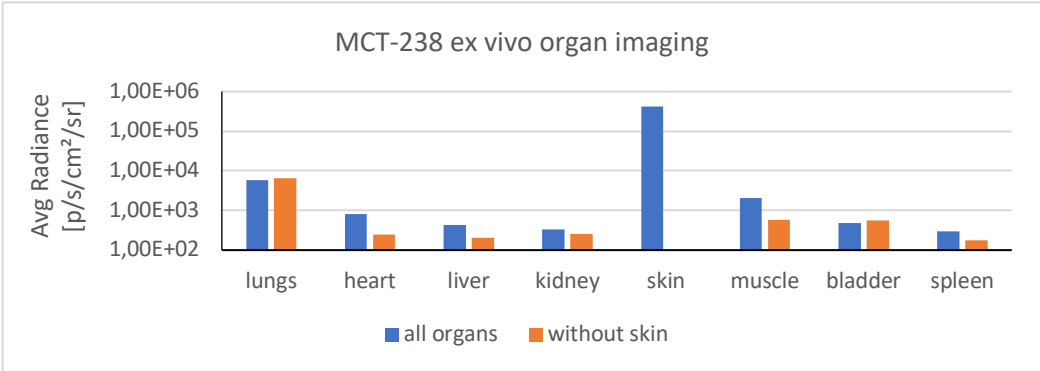

Figure 63 Diagram containing data from exported ROI values deriving from Figure 62 comparing ex vivo 2D BLI organ imaging of all organs vs. exclusion of skin.

TG (+) PH(+)

The ongoing presented results are obtained from mice which were categorized as transgenic positive (TG (+)) and phenotype positive (PH (+)). All findings are comparable and as expected as per the genotypic status, as ex vivo 2D BLI organ imaging result in high skin and lung signals. Signal intensity for lungs reach in a range from log three to six. For MCT-236 and MCT-239 the highest signal is witnessed in skin, MCT-194 and MCT-195 have the highest signal in lungs. After re-organ imaging among exclusion of skin, for all mice the next higher signaling organ is lung. The results refer to following figures: MCT-194: Figure 64 and Figure 65, MCT-195: Figure 66 and Figure 67, MCT-236: Figure 68 and Figure 69, MCT-239: Figure 70 and Figure 71.

MCT-194

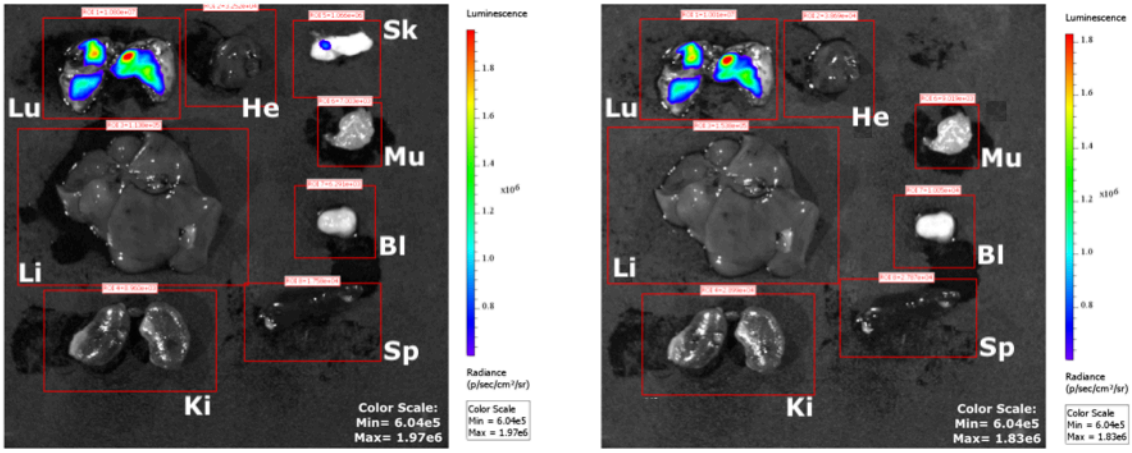

Figure 64 Left sided the ex vivo 2D BLI organ imaging of Lu=lungs, He= heart, Sk=skin, Li= liver, Mu= muscle, Bl= bladder, Ki= kidneys and spleen of MCT-194. Organ collection procedure right after second s.c. injection of Luciferine into the right flank awaiting for kinetics, approximately ten minutes, and cervical dislocation among deep anesthesia. Right situated, re-organ imaging of mentioned organs among exclusion of skin.

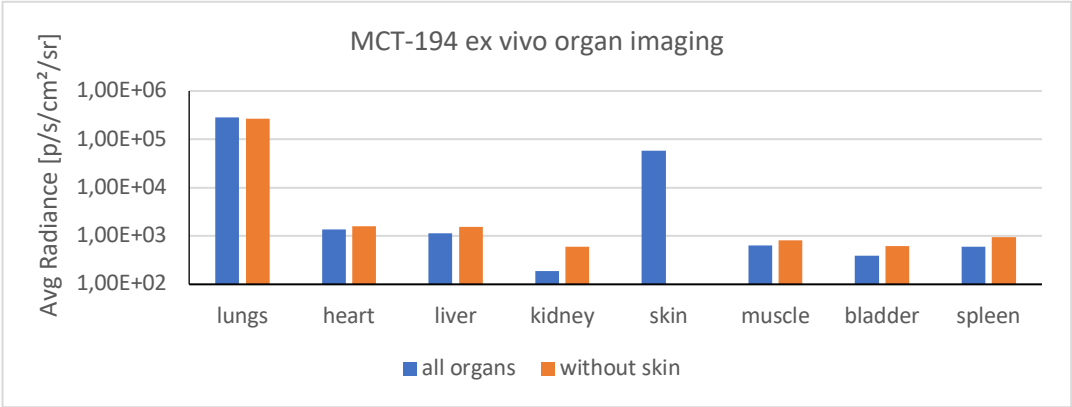

Figure 65 Diagram containing data from exported ROI values deriving from Figure 64 comparing ex vivo 2D BLI organ imaging of all organs vs. exclusion of skin.

MCT-195

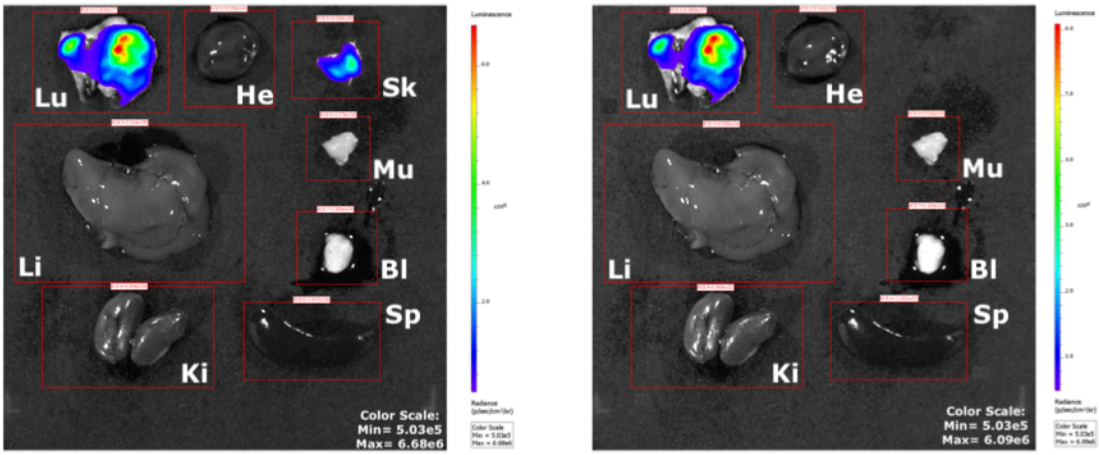

Figure 66 Left sided the ex vivo 2D BLI organ imaging of Lu=lungs, He= heart, Sk=skin, Li= liver, Mu= muscle, Bl= bladder, Ki= kidneys and spleen of MCT-195. Organ collection procedure right after second s.c. injection of Luciferine into the right flank awaiting for kinetics, approximately ten minutes, and cervical dislocation among deep anesthesia. Right situated, re-organ imaging of mentioned organs among exclusion of skin.

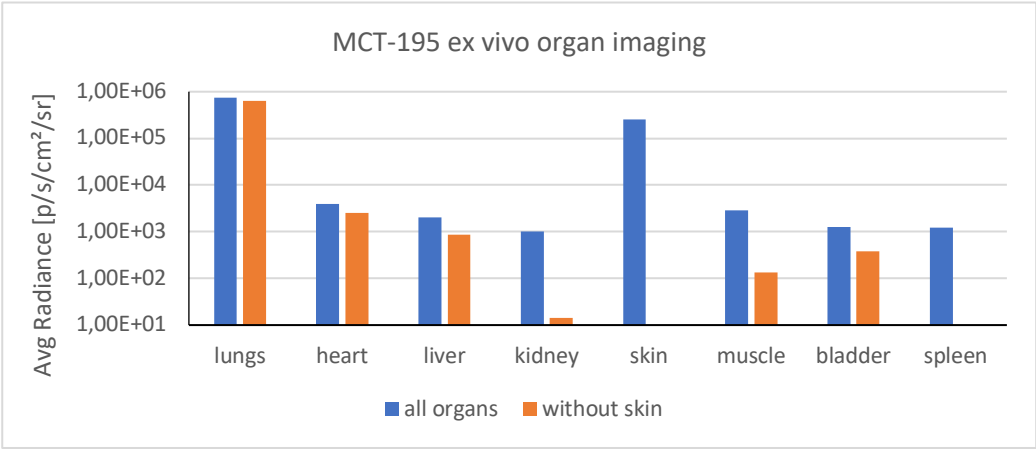

Figure 67 Diagram containing data from exported ROI values deriving from Figure 66 comparing ex vivo 2D BLI organ imaging of all organs vs. exclusion of skin.

MCT-236

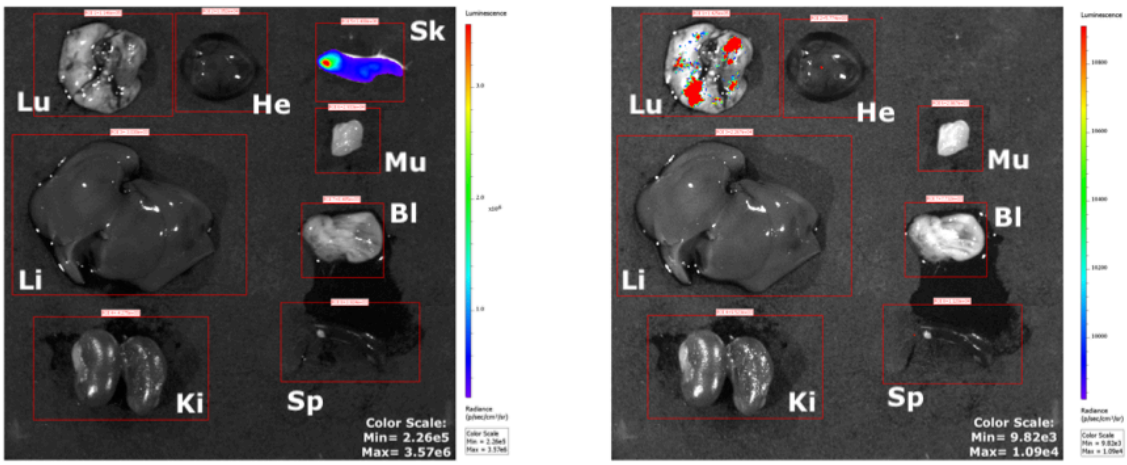

Figure 68 Left sided the ex vivo 2D BLI organ imaging of Lu=lungs, He= heart, Sk=skin, Li= liver, Mu= muscle, Bl= bladder, Ki= kidneys and spleen of MCT-236. Organ collection procedure right after second s.c. injection of Luciferine into the right flank awaiting for kinetics, approximately ten minutes, and cervical dislocation among deep anesthesia. Right situated, re-organ imaging of mentioned organs among exclusion of skin.

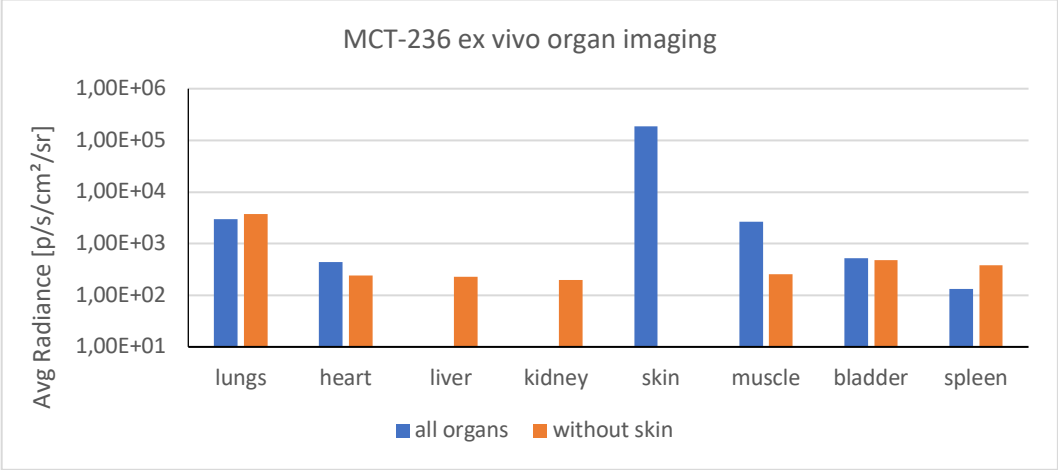

Figure 69 Diagram containing data from exported ROI values deriving from Figure 68 comparing ex vivo 2D BLI organ imaging of all organs vs. exclusion of skin.

MCT-239

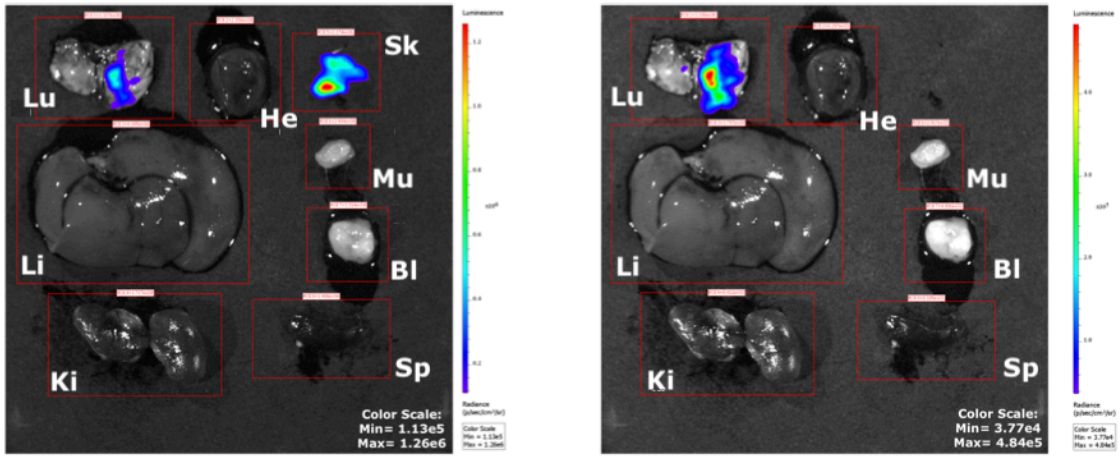

Figure 70 Left sided the ex vivo 2D BLI organ imaging of Lu=lungs, He= heart, Sk=skin, Li= liver, Mu= muscle, Bl= bladder, Ki= kidneys and spleen of MCT-239. Organ collection procedure right after second s.c. injection of Luciferine into the right flank awaiting for kinetics, approximately ten minutes, and cervical dislocation among deep anesthesia. Right situated, re-organ imaging of mentioned organs among exclusion of skin.

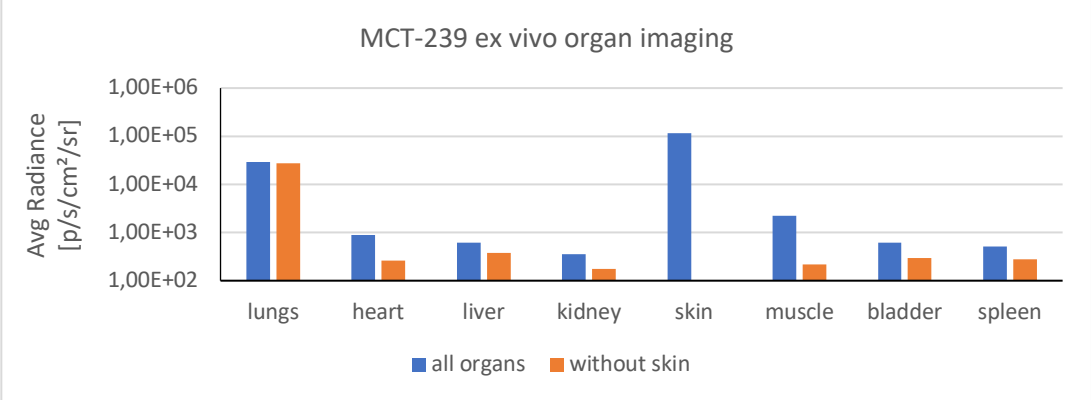

Figure 71 Diagram containing data from exported ROI values deriving from Figure 70 comparing ex vivo 2D BLI organ imaging of all organs vs. exclusion of skin.

Figure 72 compares obtained ex vivo 2D BLI organ imaging results of all organs from all mentioned mice of this category. Lung signals differ among the mice, but skin signals are comparable equal for all.

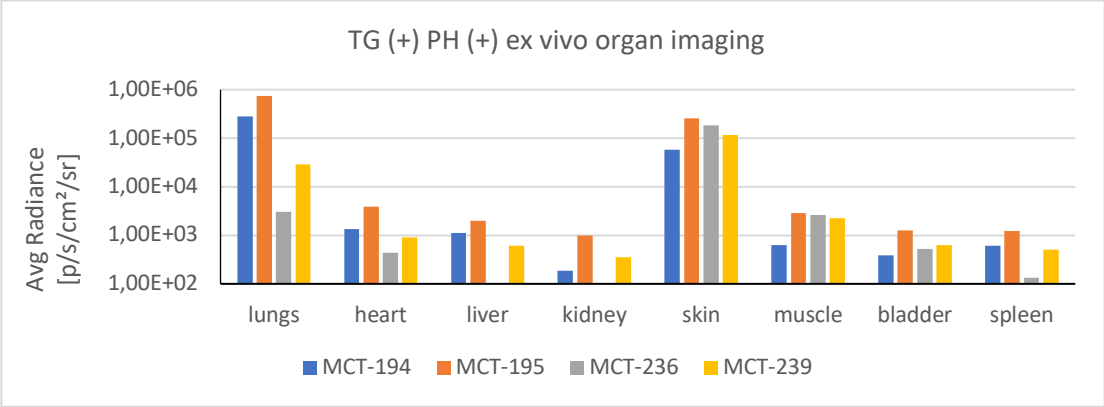

Figure 72 Comparison of exported ROI signal values from ex vivo 2D BLI organ imaging of all mice belonging to the TG (+) PH (+) group, MCT-194, MCT-195, MCT-236 and MCT-239.

8.3.2 Group 2: Re-Phenotyping for i.t. fixation

TG(-)PH(+)

MCT-309; MCT-312; MCT-329

Figure 73 presents the results of the re-Phenotyping for following mice, MCT-309, MCT-312, MCT-329, after sub-cutaneous injection of the luciferase reporter genes substrate, luciferin. The mentioned mice were categorized as transgenic negative (TG (-)) and positive phenotype (PH (+)). The outcome shown in the diagram below, Figure 73, leads to a comparable signal intensity above log two among each mouse for whole body and lung signal. As the whole body ROI is bigger than the lung ROI, but both exported ROI value signals are considerable equal, it is assumable that SpC expression is higher in lungs but also present in other parts of the skin beyond lung area.

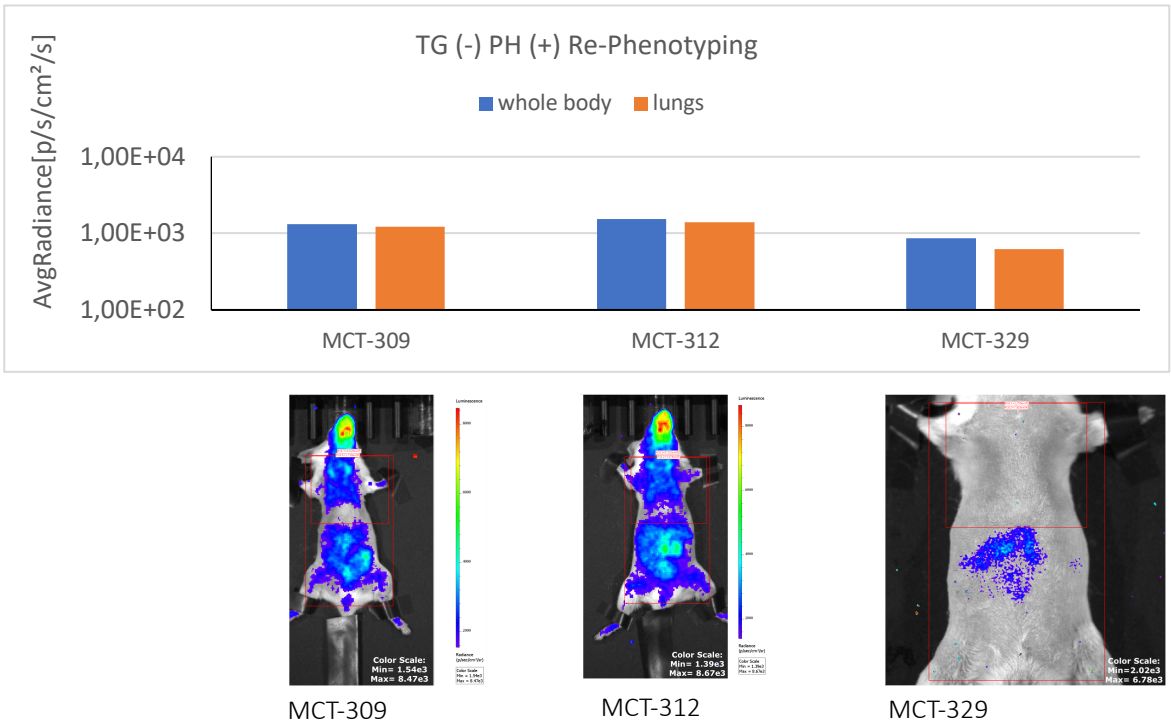

Figure 73 Upper part presenting the diagram with exported ROI values deriving from in vivo 2D BLI whole body imaging in time series study mode which are presented below from MCT-309, MCT-312 and MCT-329 in supine position. Imaging was performed after s.c. injection of Luciferine into the right flank, for each mouse.

TG(+) PH (+)

MCT-193; MCT-197; MCT-198; MCT-307; MCT-308; MCT-311

Figure 74 shows the outcome of the re-Phenotyping for following mice, MCT-193, MCT-197, MCT-198, MCT-307, MCT-308, MCT-311, after sub-cutaneous injection of the luciferase reporter genes substrate, luciferin. All mice were categorized in the group of transgenic positive (TG (+)) and positive phenotype (PH (+)) which strengthens the in vivo 2D BLI whole body imaging results, as all of them reveal high whole body and lung signals in the intensity range above log five. Concerning for each mouse individually, the signal relation for whole body and lungs ROI are comparable high.

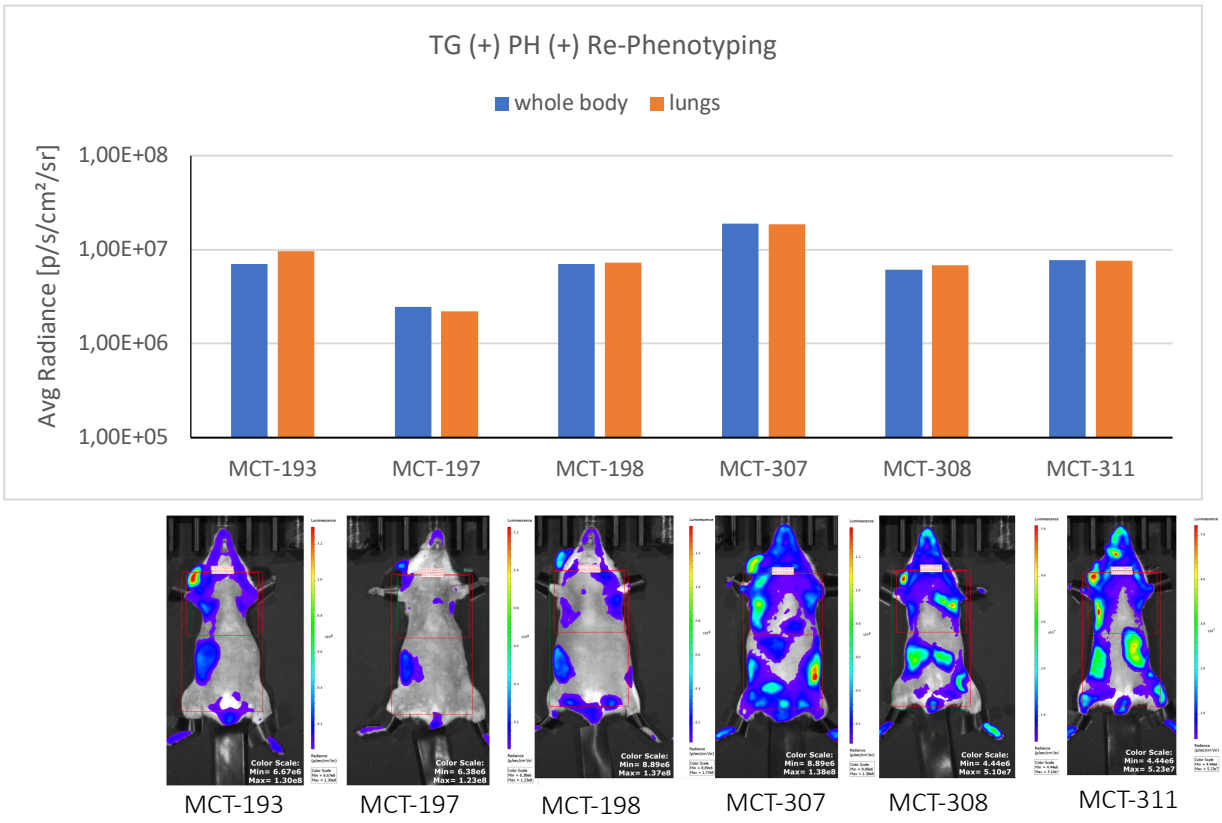

Figure 74 Upper part presenting the diagram with exported ROI values deriving from in vivo 2D BLI whole body imaging in time series study mode which are presented below from MCT-193, MCT-197, MCT-198, MCT-307, MCT-308 and MCT-311 in supine position. Imaging was performed after s.c. injection of Luciferine into the right flank, for each mouse.

To sum up the previous outcomes, the results received from group one consisting out of in vivo 2D BLI whole body imaging and ex vivo 2D BLI organ imaging were following: The transgenic negative, but phenotypical positive mice show that two out of three mice had a whole body signal in vivo, which got underpinned by ex vivo organ imaging as skin signal. For both mice the results of re-organ imaging among exclusion of skin, had a high signal in lungs. Therefore, these two animals could be identified as phenotypical positive although transgenic negativity. The outcome of the ex vivo 2D BLI organ imaging from the transgenic positive and phenotype positive group was constructively revealing for all four mice. High signals in skin could be detected but as well in lungs. The second group which was taken for i.t. fixation proved that all three phenotypical negative mice had low log scale ROI values in a field of log three. As a contrast, in all six phenotypical positive mice the ROI signal values showed much higher log scale values in the field of log six. All in all, based on the obtained results phenotypical positive mice show higher signals in whole body imaging than the transgenic and or phenotypical negative mice. Further, phenotypical positive mice

reveal clear signals in skin and lungs when looking at ex vivo organ imaging results. This strengthens the outcomes from Mo et al. regarding a non-restricted localization of SpC expression in lungs and additional presence in skin. [44]

8.4 2D BLI based evaluation of growth of B16F10 melanoma cells in Tg Thy 1.2-Luc mice

In this experiment the used strain was Tg Thy 1.2-Luc which is highlighted by the fact that the luciferase reporter gene expression cassette is under control of the Thy 1 promoter.
B16F10 melanoma cells are a model for investigating metastasis and tumor formation. These cells reveal a high surface expression of integrins, αVβ3, to which Thy-1 binds with a high affinity. The desired trackability for metastatic formation and localization of systemic applied B16F10 melanoma cells can be demonstrated by the visualization of the Thy 1.2-Luc reporter gene activity sustained by 2D BLI.

Studying the role of Thy-1.2. in implanted B16F10 melanoma cells and metastatic potential was performed with 2D BLI in vivo and ex vivo imaging. A total amount of three mice were injected with the cells into the lateral tail vein and imaged in supine position on day one, three, seven, nine and ten post injection of the melanoma cells. Afterwards ex vivo 2D BLI imaging was performed.

MCT-259

In Figure 75 and Figure 76 the findings of MCT-259 are visualized after implantation of B16F10 melanoma cells. Signal location in GIT-area over the experimental days could be pointed out. These seem to be background signal as during the experiment a wrong former phenotypization was detected. MCT-259 was wrongly phenotyped as Thy 1.2-Luc positive, but was actually phenotypical negative. The conclusion is based on the obtained in vivo 2D BLI whole body imaging results and is also underpinned by the ex vivo 2D BLI organ imaging which are shown in Figure 77.

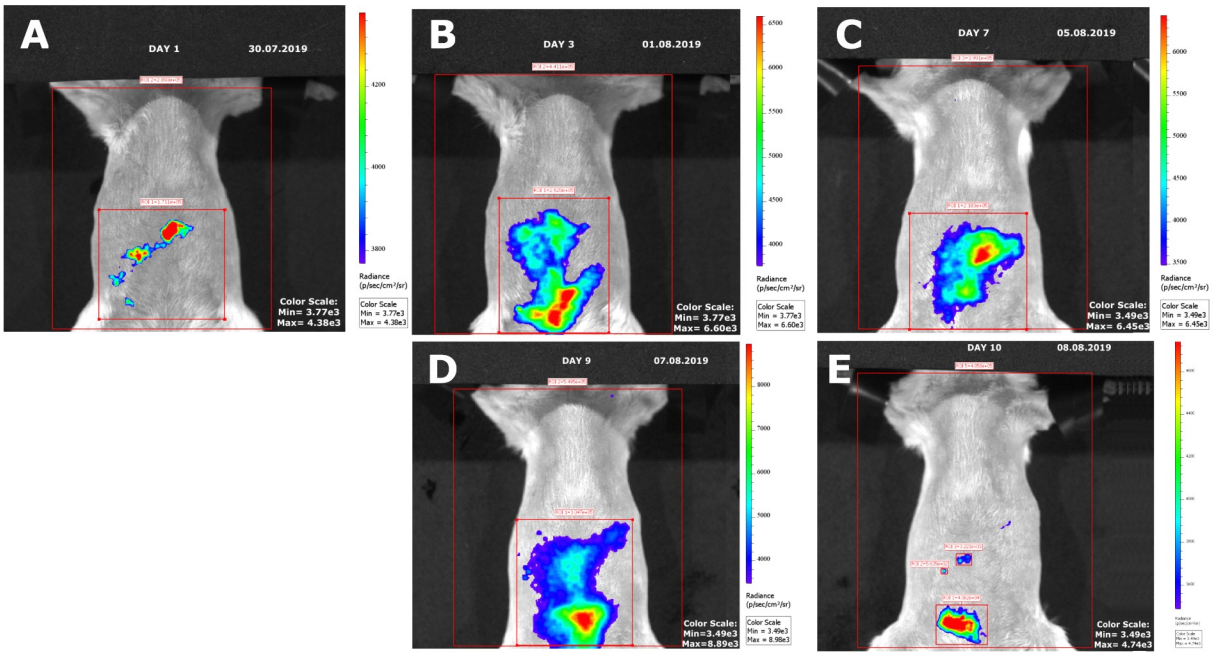

*Figure 75 In vivo 2D BLI whole body imaging in time series study mode of MCT-259 in supine position after s.c. Luciferine injection into the neck before every imaging session. Representation of images with the highest whole-body ROI, taken from each time series study imaging on **A** day 1, **B** day 3, **C** day 7, **D** day 9 and **E** day 10 after systemic injection of the B16F10 melanoma cells. Signal location in GIT-area over the experimental days, as the mouse was wrongly phenotyped as Thy-1.2-Luc positive, but was actually phenotypical negative, conclusion based on the results and also referring to the following presented ex vivo 2D BLI organ imaging.*

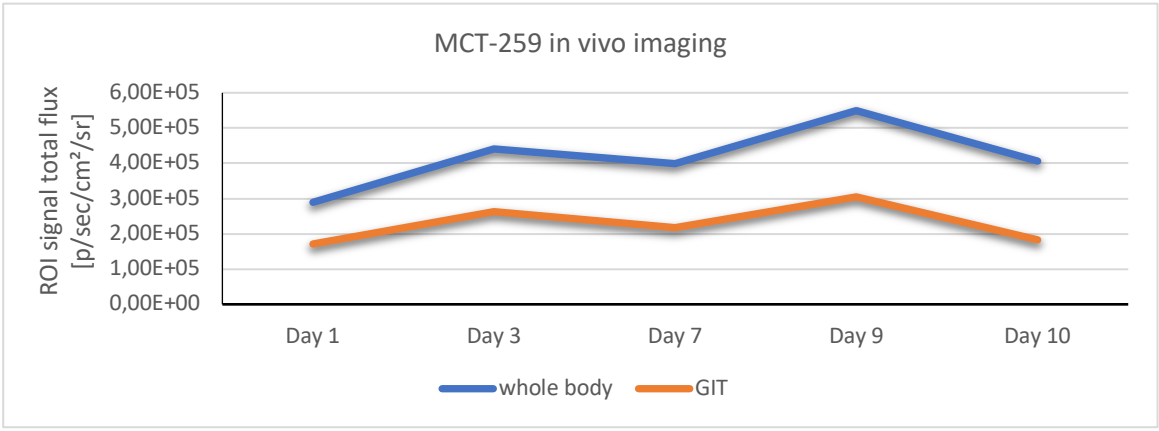

Figure 76 Diagram of exported ROI values deriving from images presented in Figure 75.

Referring to Figure 77, as no signal in brain is detectable a proof of negative phenotype is given. Tg Thy 1.2-Luc have a high Thy 1.2 expression in the brain. [53] As this transgenic line has the luciferase gene coupled to the Thy 1.2 promoter and no signal in brain for MCT-259 is shown the conclusion of a wrong phenotypization is given.

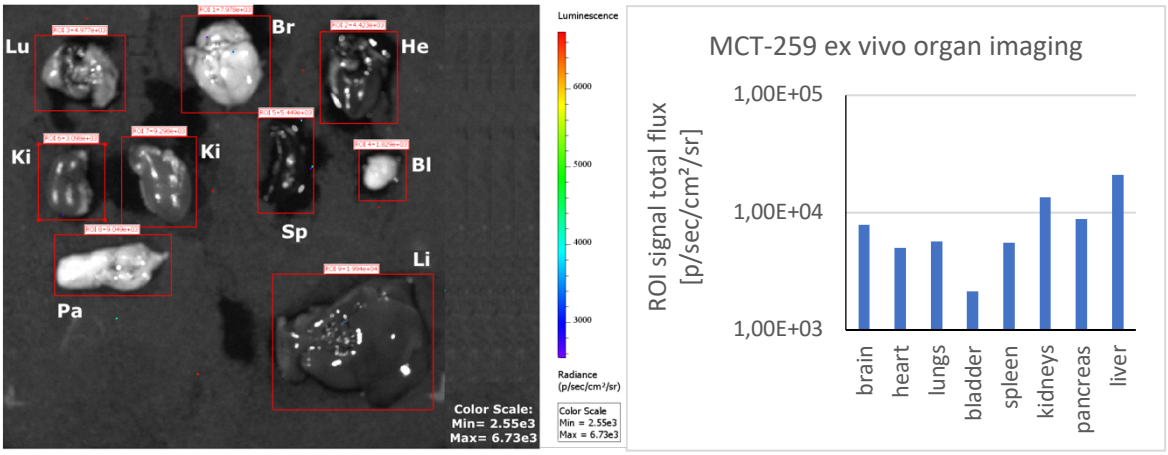

Figure 77 Left sided: Ex vivo 2D BLI organ imaging from MCT-259 of Lu= lungs, Br= brain, He= heart, Ki= kidneys, Sp= spleen, Bl= bladder, Pa= pancreas and Li= liver. Imaging was performed ten days after systemic administration of B16F10 cells, s.c. luciferine injection into the neck afterwards cervical dislocation among deep anesthesia and organ collection was done. Right sided: The corresponding graph, containing exported ROI values from organ imaging. Notification: As no signal in brain is visible, although it should be there due to Thy-1.2-Luc expression, an additional evidence of a phenotypical negative mouse which was wrongly phenotyped as positive, can be concluded.

MCT-261

Figure 78 and Figure 79 reveal the outcome for MCT-261 after implantation of the B16F10 melanoma cells. Starting from day one, Figure 78 **A**, a double round shaped signal spot located in the right lung area is visible which moves within day three, Figure 78 **B**, a bit down in direction of the liver. On the seventh day after injection, Figure 78 **C**, the signal spot is visible clear captured and roundly shaped in the middle part between lower lung area and liver. The ongoing signal enrichment correlating with spot growth reaches its peak on the nineth experimental day, Figure 78 **D**, but flattens at the end of the experiment. Thus, referring to Figure 79, the signal intensity change can be visualized, and the peak of the signal is clear on day seven.

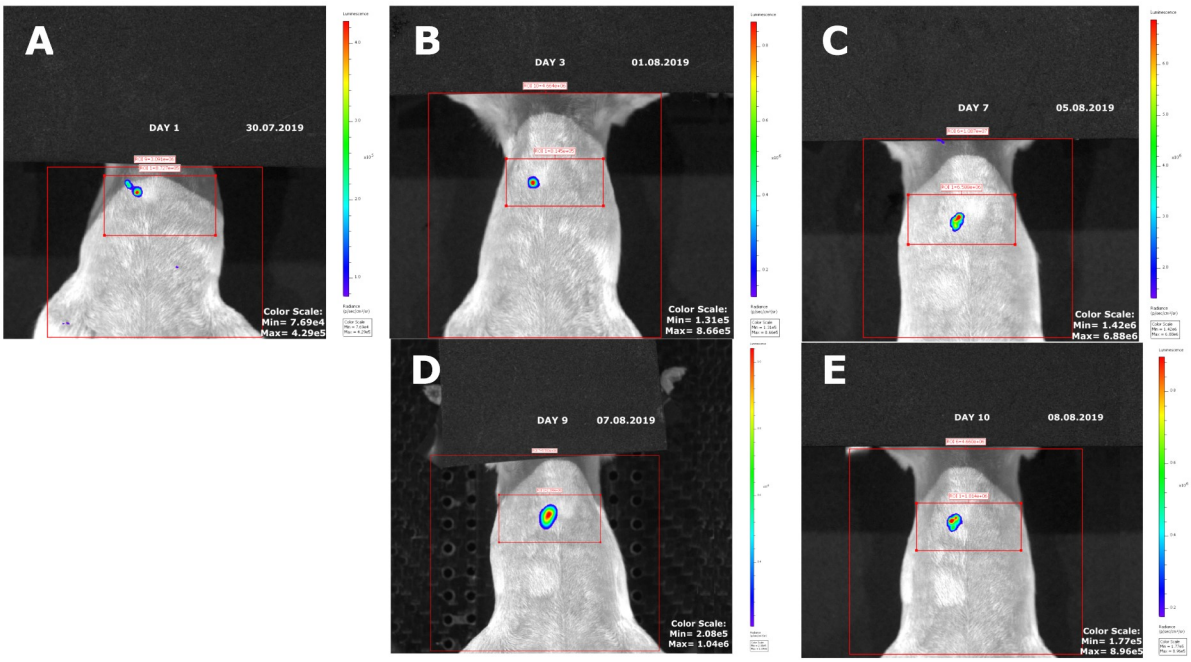

*Figure 78 In vivo 2D BLI whole body imaging in time series study mode, of MCT-261 in supine position after s.c. Luciferine injection into the neck before every imaging session. Representation of images with the highest whole-body ROI, taken from each time series study imaging on **A** day 1, **B** day 3, **C** day 7, **D** day 9 and **E** day 10 after systemic injection of the B16F10 melanoma cells. Signal location in lung area over the experimental days, small movement of the signal a bit lower located in lung area, mainly visible on the midderly right sided lung lobe.*

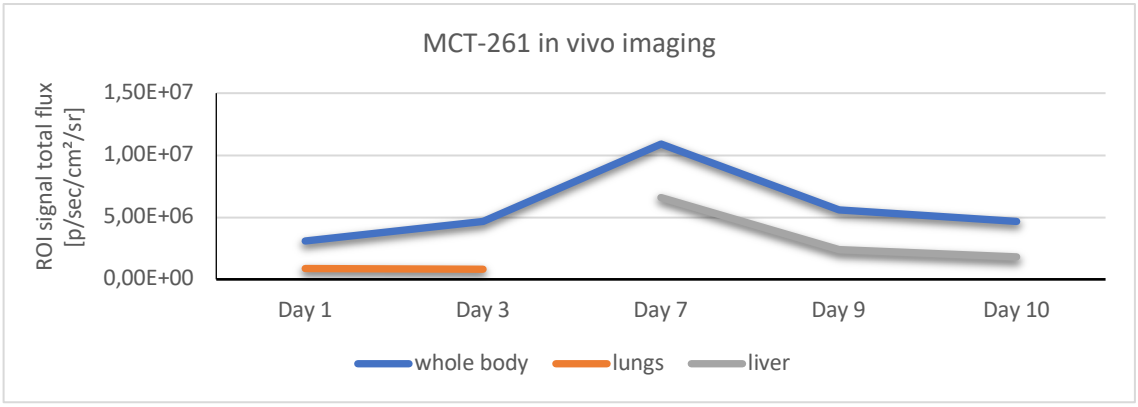

Figure 79 Diagram of exported ROI values deriving from images presented in Figure 78.

The results obtained from ex vivo 2D BLI organ imaging demonstrate a clear brain signal, which is typical for Tg Thy 1.2-Luc mice, Figure 80 and Figure 81. After exclusion of the brain and a re-imaging of the other organs a small signal spot in the heart seems visible also a signal on one kidney. Comparing those signals, the heart signal is a little higher than that deriving from the kidneys, Figure 81.

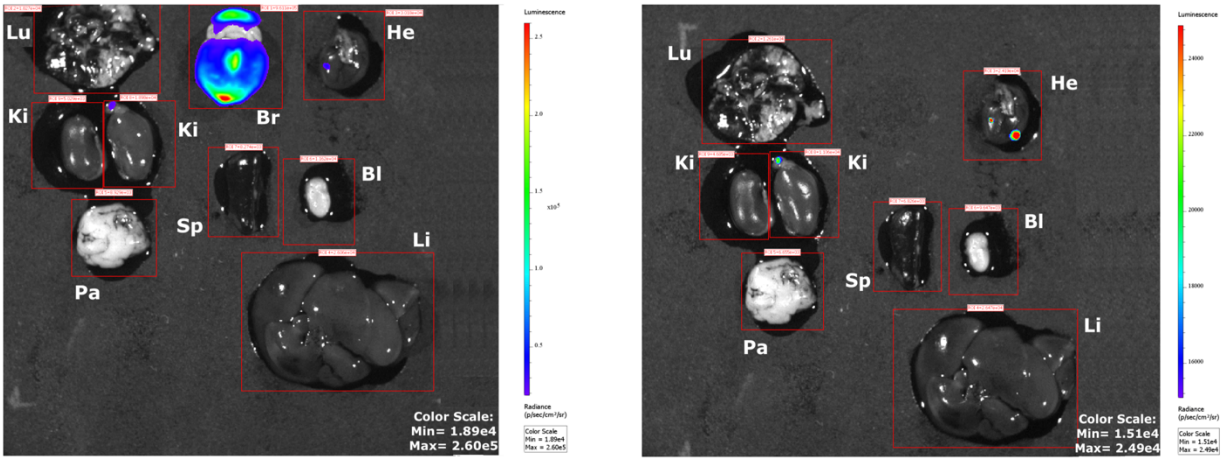

Figure 80 Left sided: Ex vivo 2D BLI organ imaging from MCT-261 of Lu= lungs, Br= brain, He= heart, Ki= kidneys, Sp= spleen, Bl= bladder, Pa= pancreas and Li= liver. Imaging was performed ten days after systemic administration of B16F10 cells, s.c. luciferine injection into the neck afterwards cervical dislocation among deep anesthesia and organ collection was done. Right sided: Ex vivo 2D BLI organ imaging from MCT-261, excluding brain with highest signal in order to visualize a potential signalizing organ which may have been overlapped by the high brain signal.

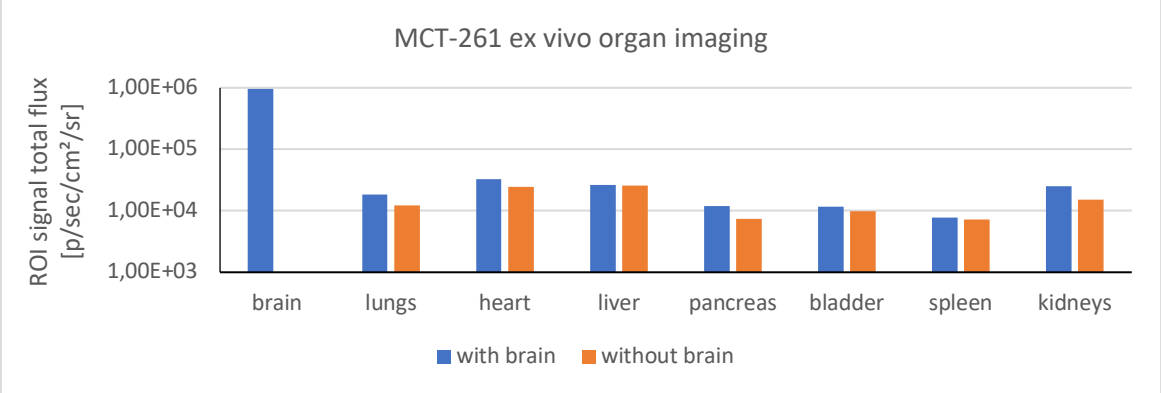

Figure 81 Diagram of exported ROI values deriving from images presented in Figure 80 comparing ex vivo 2D BLI organ imaging of all organs vs. exclusion of brain.

MCT-262

In contrast to the former presented findings, MCT-262 reveals a clear signal spot movement within the experimental time frame captured by in vivo 2D BLI whole body imaging, Figure 82. On the first day a round shaped single signal spot located in the upper lung area is visible which splits up in the following day into smaller spots located in the upper lung area, left situated and into the liver. On day seven, Figure 82 **C**, a clear single bigger round shaped signal spot is present. A signal movement from the lung area down to the liver can be witnessed which stays located in this area till the

end of the experiment. Nevertheless, the exported ROI signal values, shown in Figure 83, just point out a whole body signal enrichment on day three which decreases. The lowest signal value is captured on the seventh day, but afterwards the whole body signal intensity increases again. However just having a look at the detached signals for lungs and liver no change in signal intensity can be recorded.

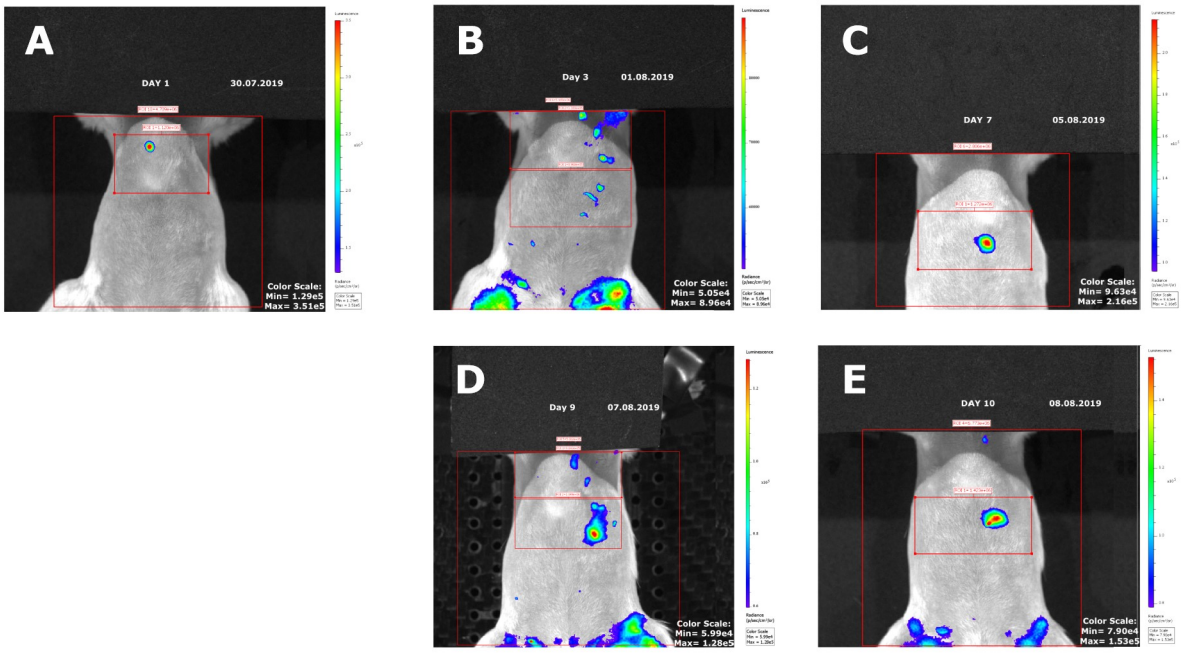

*Figure 82 In vivo 2D BLI whole body imaging in time series study mode, of MCT-262 in supine position after s.c. Luciferine injection into the neck before every imaging session. Representation of images with the highest whole-body ROI, taken from each time series study imaging on **A** day 1, **B** day 3, **C** day 7, **D** day 9 and **E** day 10 after systemic injection of the B16F10 melanoma cells. Signal location in lung area over the experimental days with a movement of the signal in direction to the left liver lobe.*

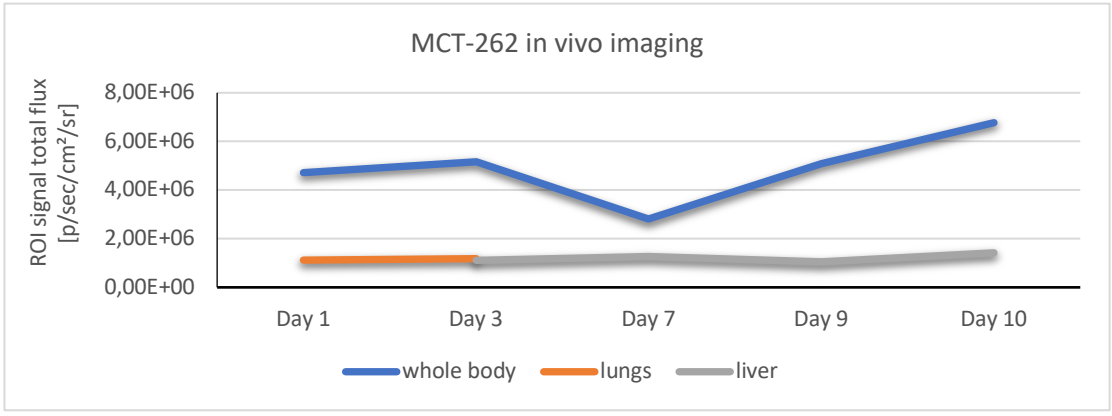

Figure 83 Diagram of exported ROI values deriving from images presented in Figure 82.

Figure 85 represents the findings from the ex vivo 2D BLI organ imaging. The cause of brain signal is the same as already explained in former mentioned mouse, MCT-261. Further, among exclusion of brain, the organ imaging points out elevated signals for kidney, liver, lungs, pancreas and heart, Figure 85.

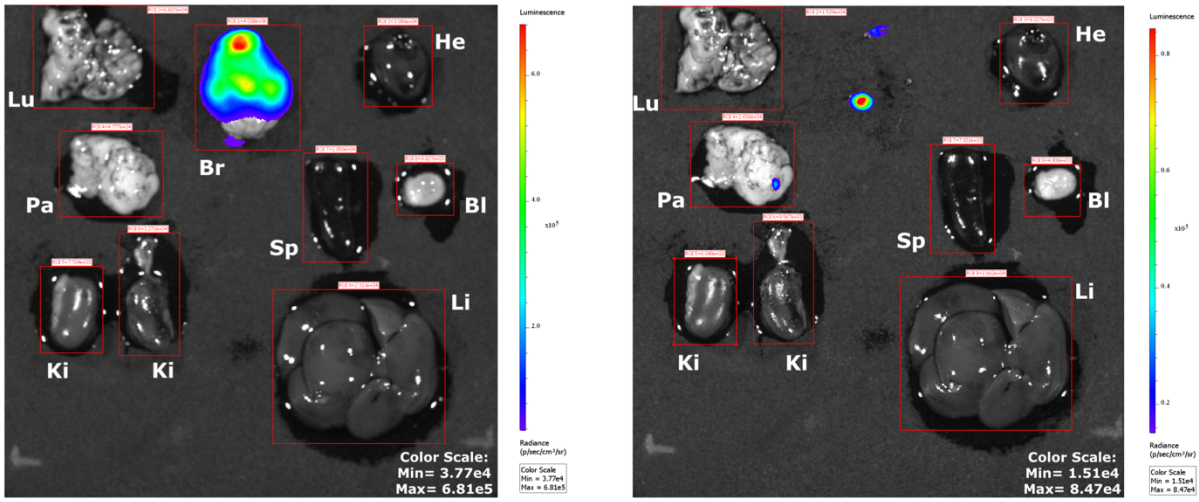

Figure 84 Left sided: Ex vivo 2D BLI organ imaging from MCT-262 of Lu= lungs, Br= brain, He= heart, Ki= kidneys, Sp= spleen, Bl= bladder, Pa= pancreas and Li= liver. Imaging was performed ten days after systemic administration of B16F10 cells, s.c. Luciferine injection into the neck afterwards cervical dislocation among deep anesthesia and organ collection was done. Right sided: Ex vivo 2D BLI organ imaging from MCT-262, excluding brain with highest signal in order to visualize a potential signalizing organ which may have been overlapped by the high brain signal.

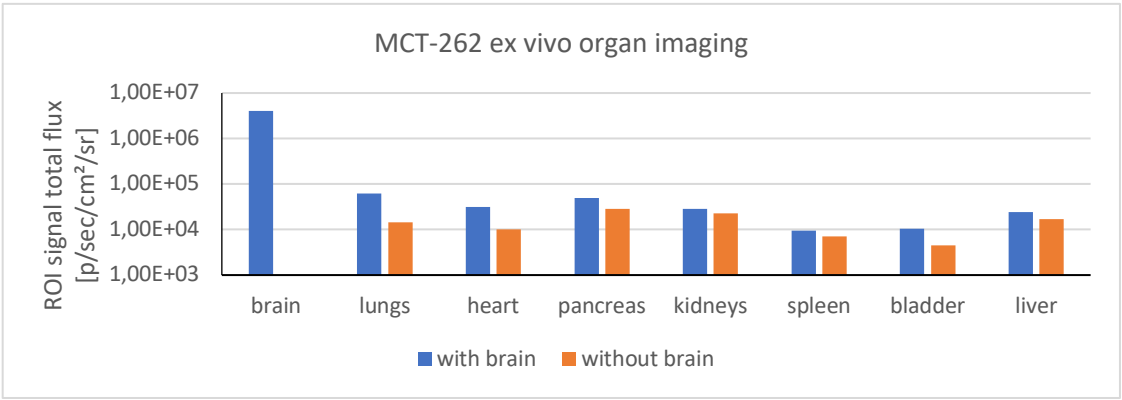

Figure 85 Diagram of exported ROI values deriving from images presented in Figure 84 comparing ex vivo 2D BLI organ imaging of all organs vs. exclusion of brain.

Studying the role of Thy-1.2. in implanted B16F10 melanoma cells and metastatic potential lead to following results. The first mouse was wrongly phenotyped as positive but during the experimental time frame the proof of negative phenotype could be shown by GIT background signal obtained from in vivo imaging. Additionally, this fact got underpinned by the lack of brain signal in organ imaging, which normally lights up in phenotypical positive Thy-1.2.-Luc mice. [53] In the other two mice signal localization in lung area on first- and third-day post injection was visible which then moved down to the liver area. Moreover, metastatic potential into lungs which is pointed out by Fu et. al [50] got underpinned. Nevertheless, the need of clarification whether metastatic potential in those areas are assumable or signal movement from lung to liver is just based on the bloodflower is outstanding. Concerning the organ imaging among exclusion of brain, as it had the highest signal, shows in both mice signal in kidneys pancreas and liver.

9 CONCLUSION

Regarding the first project on siRNA biodistribution, a renal excretion could be demonstrated after i.v. injection of the AF750 labeled NC-siRNA. The biodistribution pattern remained conserved in kidney and bladder area over the experimental time frame which underpins this excretion route and was also additionally supported by the results obtained from ex vivo 2D organ imaging.

The outcome of the systemically applied Luc-SSO and non coding-SSO cLPEI based polyplexes was investigated by whole-body BLI imaging and ex vivo BLI imaging. Whole-body BLI imaging was not able to show any splice correction as similar signal behavior was observed over time in all Luc-SSO polyplex treated animals. On the other hand, ex vivo 2D BLI organ imaging results sum up a comparable and reproducible signal pattern of splice correction in lung and bladder in case of Luc-SSO polyplex treated animals. This outcome leads to the possibility of SSO delivery and splice correction into lung and bladder tissue.

Evaluation of reporter gene activity in SpC strain mice, which undergo expression of the luciferase gene under control of the SpC promoter, could show that localization is not only restricted in lung tissue as signals were found in skin too.

Investigation of metastatic potential of B16F10 implanted melanoma cells and interplay of Thy-1 in metastatic extravasation did not lead to a clear conclusion. Although, the signal pattern was in two mice comparable the signal spot movement from lungs to liver could not be demonstrated as it is not clear whether real metastasis occurred, or this movement was just provoked by the blood flow.

10 REFERENCES

[1] M. Keyaerts, V. Caveliers, and T. Lahoutte, “Bioluminescence imaging : looking beyond the light,” *Trends Mol. Med.*, vol. 18, no. 3, pp. 164–172, 2012, doi: 10.1016/j.molmed.2012.01.005.

[2] P. Ray, “Multimodality molecular imaging of disease progression in living subjects,” vol. 36, no. August, pp. 499–504, 2011, doi: 10.1007/s12038-011-9079-0.

[3] S. W. Glasser, S. K. Eszterhas, E. A. Detmer, M. D. Maxfield, and T. R. Korfhagen, “The murine SP-C promoter directs type II cell-specific expression in transgenic-mice,” *Am. J. Physiol. - Lung Cell. Mol. Physiol.*, vol. 288, no. 4 32-4, pp. 625–632, 2005, doi: 10.1152/ajplung.00250.2004.

[4] G. Choy, P. Choyke, and S. K. Libutti, “Current Advances in Molecular Imaging : Noninvasive In Vivo Bioluminescent and Fluorescent Optical Imaging in Cancer Research,” vol. 2, no. 4, pp. 303–312, 2003.

[5] J.-C. Tseng, K. Vasquez, J. D. Peterson, and D. Ph, “Optical Imaging on the IVIS SpectrumCT System : General and Technical Considerations for 2D and 3D Imaging,” no. 1, pp. 1–18, 2015.

[6] E. McKinnon, A. Moore, S. Dicit, Z. Yun, and A.-M. Broome, *No Title*. 2017.

[7] “Luciferase Reporter.” [Online]. Available: https://www.thermofisher.com/at/en/home/life-science/protein-biology/protein-biology-learning-center/protein-biology-resource-library/pierce-protein-methods/luciferase-reporters.html. [Accessed: 30-Jul-2020].

[8] D. B. Murphy, *Fundamentals of light microscopy and electronic imaging*. 2001.

[9] C. Martelli, A. Lo Dico, C. Diceglie, G. Lucignani, and L. Ottobrini, “Optical imaging probes in oncology,” vol. 7, no. 30, 2016.

[10] “AF750, Fluorophoe information.” [Online]. Available: https://www.thermofisher.com/at/en/home/life-science/cell-analysis/fluorophores/alexa-fluor-750.html. [Accessed: 30-Jul-2020].

[11] T. Ruxana and S. and T. S. Blackwell, “Bioluminescence Imaging,” no. 28, 2005, doi: 10.1513/pats.200507-067DS.

[12] F. Khan, “The Luciferase Reporter Assay: How it works.” [Online]. Available: https://bitesizebio.com/10774/the-luciferase-reporter-assay-how-it-works/. [Accessed: 30-Jul-2020].

[13] H. Dressler, K. Economides, S. Favara, N. N. Wu, Z. Pang, and H. G. Polites, “The CRE luc Bioluminescence Transgenic Mouse Model for Detecting Ligand Activation of GPCRs,” 2015, doi: 10.1177/1087057113496465.

[14] I. Manni, L. De Latouliere, A. Gurtner, and G. Piaggio, “Transgenic Animal Models to Visualize Cancer-Related Cellular Processes by Bioluminescence Imaging,” vol. 10, no. March, pp. 1–12, 2019, doi: 10.3389/fphar.2019.00235.

[15] S. D. Patil, D. G. Rhodes, and D. J. Burgess, “DNA-based therapeutics and DNA delivery systems: A comprehensive review,” *AAPS J.*, vol. 7, no. 1, 2005, doi: 10.1208/aapsj070109.

[16] R. Kole, A. R. Krainer, and S. Altman, “RNA therapeutics: Beyond RNA interference and antisense oligonucleotides,” *Nat. Rev. Drug Discov.*, vol. 11, no. 2, pp. 125–140, 2012, doi: 10.1038/nrd3625.

[17] T. Lehto, K. Ezzat, M. J. A. Wood, and S. EL Andaloussi, “Peptides for nucleic acid delivery,” *Adv. Drug Deliv. Rev.*, vol. 106, no. 2016, pp. 172–182, 2016, doi: 10.1016/j.addr.2016.06.008.

[18] M. R. Stratton, P. J. Campbell, and P. A. Futreal, “The cancer genome,” *Nature*, vol. 458, no. 7239, pp. 719–724, 2010, doi: 10.1038/nature07943.The.
[19] A. Singh, P. Trivedi, and N. K. Jain, “Advances in siRNA delivery in cancer therapy,” *Artif. Cells, Nanomedicine Biotechnol.*, vol. 46, no. 2, pp. 274–283, 2018, doi: 10.1080/21691401.2017.1307210.
[20] D. Hassan *et al.*, “Molecular Mechanisms and Biological Functions of siRNA.,” *Int. J. Biomed. Sci.*, vol. 13, no. 2, pp. 48–57, 2017.
[21] M. Dirin and J. Winkler, “Influence of diverse chemical modifications on the ADME characteristics and toxicology of antisense oligonucleotides,” *Expert Opin. Biol. Ther.*, vol. 13, no. 6, pp. 875–888, 2013, doi: 10.1517/14712598.2013.774366.
[22] H. Hatakeyama, Y. S. Wu, S. L. Mangala, G. Lopez-Berestein, and K. A. Sood, “Assessement of in vivo siRNA delivery in cancer mouse models,” *Methods Mol Bio*, vol. 1402, no. January, pp. 119–134, 2016, doi: 10.1007/978-1-4939-3378-5.
[23] A. Geyer *et al.*, “Fluorescence- and computed tomography for assessing the biodistribution of siRNA after intratracheal application in mice,” *Int. J. Pharm.*, vol. 525, no. 2, pp. 359–366, 2017, doi: 10.1016/j.ijpharm.2017.02.025.
[24] S. Gao *et al.*, “The effect of chemical modification and nanoparticle formulation on stability and biodistribution of siRNA in mice,” *Mol. Ther.*, vol. 17, no. 7, pp. 1225–1233, 2009, doi: 10.1038/mt.2009.91.
[25] B. Haraldsson, J. Nyström, and W. M. Deen, “Properties of the glomerular barrier and mechanisms of proteinuria,” *Physiol. Rev.*, vol. 88, no. 2, pp. 451–487, 2008, doi: 10.1152/physrev.00055.2006.
[26] R. L. Juliano, “The delivery of therapeutic oligonucleotides,” *Nucleic Acids Res.*, vol. 44, no. 14, pp. 6518–6548, 2016, doi: 10.1093/nar/gkw236.
[27] D. L. Black, “Mechanisms of Alternative Pre-Messenger RNA Splicing,” *Annu. Rev. Biochem.*, vol. 72, no. 1, pp. 291–336, 2003, doi: 10.1146/annurev.biochem.72.121801.161720.
[28] M. A. Havens and M. L. Hastings, “Splice-switching antisense oligonucleotides as therapeutic drugs,” *Nucleic Acids Res.*, vol. 44, no. 14, pp. 6549–6563, 2016, doi: 10.1093/nar/gkw533.
[29] S. Resina, K. Ryszard, A. Travo, B. Lebleu, and R. A. Thierry, “Switching on transgene expression by correcting aberrant splicing using multi-targeting steric-blocking oligonucleotides,” *J. Gene Med.*, vol. 14, no. 1, pp. 44–53, 2012, doi: 10.1002/jgm.
[30] E. T. Wang *et al.*, “Alternative Isoform Regulation in Human Tissue Transcriptomes,” vol. 456, no. 7221, pp. 470–476, 2008, doi: 10.1038/nature07509.Alternative.
[31] N. López-Bigas, B. Audit, C. Ouzounis, G. Parra, and R. Guigó, “Are splicing mutations the most frequent cause of hereditary disease?,” *FEBS Lett.*, vol. 579, no. 9, pp. 1900–1903, 2005, doi: 10.1016/j.febslet.2005.02.047.
[32] S. Y. Xie, W. Li, Z. R. Ren, S. Z. Huang, F. Zeng, and Y. T. Zeng, “Correction of β654-thalassaemia mice using direct intravenous injection of siRNA and antisense RNA vectors,” *Int. J. Hematol.*, vol. 93, no. 3, pp. 301–310, 2011, doi: 10.1007/s12185-010-0727-1.
[33] J. Summerton, “Morpholinos:BBA,” *Biochim. Biophys. Acta*, vol. 1489, pp. 141–158, 1999.
[34] F. Rigo, P. P. Seht, and C. F. Bennett, *Systems Biology of RNA binding proteins*. 2014.
[35] J. M. D. and R. K. DeLong, “A High-Troughput Screening Assay for the Functional Delivery of Splice-Switching Oligonucleotides in Human Melanoma Cells,” *RNA Nanotechnol. Ther. Methods Protoc.*, pp. 1–239, 2015, doi: 10.1007/978-1-4939-2562-

9.
[36] S. Gehrig, H. Sami, and M. Ogris, “Gene Therapy and imaging in preclinical and clinical oncology: recent developments in therapy and theranostics,” *Ther. Deliv*, vol. 5, pp. 1275–1296, 2014, doi: 10.4155/tde.15.92.
[37] R. H. Waterston, K. Lindblad-Toh, E. Birney, and J. Rogers, “Initial sequencing and comparative analysis of the mouse genome,” *Nature*, vol. 420, no. 6915, pp. 520–562, 2002.
[38] D. A. Dunn, D. L. Kooyman, and C. A. Pinkert, “Foundation review: Transgenic animals and their impact on the drug discovery industry,” *Drug Discov. Today*, vol. 10, no. 11, pp. 757–767, 2005, doi: 10.1016/S1359-6446(05)03452-5.
[39] J. W. Gordon and F. H. Ruddle, “Integration and stable germ line transmission of genes injected into mouse pronuclei,” *Science (80-.).*, vol. 214, no. 4526, pp. 1244–1246, 1981, doi: 10.1126/science.6272397.
[40] J. M. Hickman-Davis and I. C. Davis, “Transgenic mice,” *Paediatr. Respir. Rev.*, vol. 7, no. 1, pp. 49–53, 2005, doi: 10.1016/j.prrv.2005.09.005.
[41] S. Pinczolits, “Optimising genotyping protocols in three novel transgenic reporter mouse strains,” Universität Wien, 2017.
[42] S. Resina *et al.*, “Lipoplex and peptide-based strategies for the delivery of steric-block oligonucleotides,” *Int. J. Pharm.*, vol. 344, no. 1–2, pp. 96–102, 2007, doi: 10.1016/j.ijpharm.2007.04.039.
[43] E. L. Rawlins and A. K. Perl, “The a"MAZE"ing world of lung-specific transgenic mice,” *Am. J. Respir. Cell Mol. Biol.*, vol. 46, no. 3, pp. 269–282, 2012, doi: 10.1165/rcmb.2011-0372PS.
[44] Y. K. Mo *et al.*, “Surfactant protein expression in human skin: Evidence and implications,” *J. Invest. Dermatol.*, vol. 127, no. 2, pp. 381–386, 2006, doi: 10.1038/sj.jid.5700561.
[45] M. Yee *et al.*, “Type II epithelial cells are critical target for hyperoxia-mediated impairment of postnatal lung development,” *Am. J. Physiol. - Lung Cell. Mol. Physiol.*, vol. 291, no. 5, pp. 1101–1111, 2006, doi: 10.1152/ajplung.00126.2006.
[46] B. A. Teicher, “Review Tumor models for efficacy determination,” vol. 5, no. October, pp. 2435–2444, 2006, doi: 10.1158/1535-7163.MCT-06-0391.
[47] J. Schrader *et al.*, “Growth and metastasis of B16-F10 melanoma cells is not critically dependent on host CD73 expression in mice,” *BMC Cancer*, vol. 14, no. 1, pp. 1–11, 2014, doi: 10.1186/1471-2407-14-898.
[48] C. Danciu *et al.*, “Behaviour of four different B16 murine melanoma cell sublines: C57BL/6J skin,” *Int. J. Exp. Pathol.*, vol. 96, no. 2, pp. 73–80, 2015, doi: 10.1111/iep.12114.
[49] M. Potez *et al.*, “Characterization of a B16-F10 melanoma model locally implanted into the ear pinnae of C57BL/6 mice,” *PLoS One*, vol. 13, no. 11, pp. 1–19, 2018, doi: 10.1371/journal.pone.0206693.
[50] Q. Fu *et al.*, “Novel murine tumour models depend on strain and route of inoculation,” *Int. J. Exp. Pathol.*, vol. 97, no. 4, pp. 351–356, 2016, doi: 10.1111/iep.12192.
[51] K. Schubert, D. Gutknecht, M. Köberle, U. Anderegg, and A. Saalbach, “Melanoma Cells Use Thy-1 (CD90) on Endothelial Cells for Metastasis Formation,” *Am. J. Pathol.*, vol. 182, no. 1, pp. 266–276, 2013, doi: 10.1016/j.ajpath.2012.10.003.
[52] S. M. M. Haeryfar and D. W. Hoskin, “Thy-1: More than a Mouse Pan-T Cell Marker,” *J. Immunol.*, vol. 173, no. 6, pp. 3581–3588, 2004, doi: 10.4049/jimmunol.173.6.3581.

[53] A. J. Bradley, G. Ramirez, and S. J. Hagood, “Roles and Regulation of Thy-1, a Context-Dependent Modulator of Cell Phenotype,” *Biofactors*, pp. 258–265, 2009, doi: 10.1016/j.gde.2016.03.011.
[54] P. Caroni, “Overexpression of growth-associated proteins in the neurons of adult transgenic mice,” *J. Neurosci. Methods*, vol. 71, no. 1, pp. 3–9, 1997, doi: 10.1016/S0165-0270(96)00121-5.